Novel Zwitterionic Copolymers to Enhance Hydrophilicity of PVDF Membranes: A Comprehensive Computational Study

A Thesis Submitted to the College of Graduate and Postdoctoral Studies
in partial fulfillment of the requirements for the degree of

Master of Science

in the Department of Chemical and Biological Engineering
University of Saskatchewan

By
Mahboobeh Maghami

PERMISSION TO USE

The author has agreed that the Libraries of the University of Saskatchewan may make this thesis freely available for inspection. Moreover, the author has agreed that permission for extensive copying of this thesis for scholarly purposes may be granted by the professor who supervised the thesis work recorded herein, by the Head of the Department of Chemical and Biological Engineering or the Dean of the College of Graduate and Postdoctoral Studies. Copying or publication or any other use of the thesis or parts thereof for financial gain without written approval by the University of Saskatchewan is prohibited. It is also understood that due recognition will be given to the author of this thesis and to the University of Saskatchewan in any use of the material of the thesis.

DISCLAIMER

Reference in this thesis/dissertation to any specific commercial products, process, or service by trade name, trademark, manufacturer, or otherwise, does not constitute or imply its endorsement, recommendation, or favoring by the University of Saskatchewan. The views and opinions of the author expressed herein do not state or reflect those of the University of Saskatchewan, and shall not be used for advertising or product endorsement purposes.

Requests for permission to copy or to make other use of material in this thesis in whole or in part should be addressed to:

Head of the Department of Chemical & Biological Engineering
University of Saskatchewan
57 Campus Drive
Saskatoon, Saskatchewan S7N 5A9, Canada

OR

Dean
College of Graduate and Postdoctoral Studies
University of Saskatchewan
116 Thorvaldson Building, 110 Science Place
Saskatoon, Saskatchewan S7N 5C9, Canada

ABSTRACT

Membrane technology covers all the engineering approaches with a key growth for large-scale industrial applications, including biotechnology, biomedical applications, food industry, and water and wastewater treatment. Poly (vinylidene fluoride) (PVDF) membrane has been gained remarkable attentions in recent years due to its excellent advantages in terms of thermal stability, chemical resistance, and high mechanical strength for water treatment. Despite its outstanding advantages, the performances of PVDF membranes are substantially limited by fouling problems. In this research study, we designed novel zwitterionic (ZW)-PVDF membranes with high hydrophilicity by employing a set of comprehensive computational methods. To achieve our goal, we first investigated the interactions occurring between water molecules and the fragments of hydrophobic and hydrophilic membrane models at the molecular level using the pair interaction energy decomposition analysis (PIEDA) as part of the fragment molecular orbital (FMO) method's framework. This research direction is critical, since a research study of the reasons behind the interactions between water molecules and membrane materials would help design ground-breaking membranes with superior hydrophilicity.

The computational studies and experimental analyses of PVDF and Polyacrylonitrile (PAN) membranes were considered as the models for hydrophobic and hydrophilic membranes, respectively. Density-functional theory (DFT), based on B3LYP functional and split-valance 6-311+G (d, p) basis sets, was used in order to optimize the geometry of PAN, PVDF, and their complexes with different numbers of water molecules. Furthermore, the functional groups of membrane surfaces were experimentally evaluated through Fourier-transform infrared spectroscopy (FTIR- ATR), ^{13}C cross polarization magic angle spinning (^{13}C CP MAS) Solid State Nuclear magnetic resonance SSNMR, and Fourier transform Raman (FT-Raman) spectroscopies. The confocal microscopic was also employed to interrogate water transport and the interactions between fluorescence particles through the membrane matrices.

The non-covalent interactions in terms of electrostatic, exchange-repulsion, and charge-transfer parameters were comprehensively investigated for the designed ZW-PVDF copolymers. The performance of ZW moieties was derived from three different anionic groups in the ZW head, specifically, carboxylate, sulfonate, and phosphate. This approach was used in addition to the inclusion of a linker between the ZW head and the PVDF backbone, such as trimethyl

ammonium groups and hydroxyl group, for an improvement of PVDF hydrophilicity. The quantum chemical calculations were conducted to examine the hydration structure of moieties. The interactions between the ZW moieties, with water molecules confirmed that it depended on the charged groups in addition to the chemical functional groups between charged groups. Furthermore, the types of anionic groups, the polar functional groups between charged groups, and the hydrophilic group, as a linker between charged groups of the ZW to the PVDF polymer backbone are the key reason for membrane hydrophilicity and the membrane water uptake. The double Zwitterionic PMAL®-C_8-CB-OH-SB-PVDF was designed through the addition of protonated carboxyl group on a backbone of copolymer PMAL®-C_8, and the protonated nitrogen atom of the amide group. This double zwitterion showed strong electrostatic interactions between individual water molecules and the secondary ammonium and the Oxygen of carboxybetaine, compared to PMAL®-C_8-OH-SB-PVDF model. Our designed hydrophilic ZW-PVDF membranes, and especially the double zwitterion membrane, are an exciting development that can be applied in a broad range of water applications.

ACKNOWLEDGEMENTS

First of all, I would like to express my gratitude to my supervisor, Dr. Amira Abdelrasoul, for giving me the chance to be a member of her research group and on top of that for her continuous support and guidance in overcoming numerous obstacles, which I have been facing through this challenging research.

Also, I would like to thank my committee members, Dr. Dalai and Dr. Lin from the Department of Chemical and Biological Engineering, for providing me with valuable advice and suggestions during the research.

I also acknowledge the University of Saskatchewan for receiving the Dean's Scholarship and the Devolved Scholarship for the financial support through my graduate studies.

I would like also to express my gratitude for the Saskatchewan Structure Science Centre for the facilities provided.

Finally, I would like to express my gratitude to all the members of the IT group, especially Sergiy Stepanenko and Juan Zuniga, for all the useful discussion and suggestions.

DEDICATION

I dedicate this thesis to the following:

- My beloved parents for their unconditional love and wholehearted support in my life.
- To my best friend and thoughtful Partner, Mehran Rezazadeh Khalkhali, behind this successful accomplishment.
- To my siblings for their diverse supports throughout my studies.

Thank you for always supporting me and encouraging me to work hard and pursue my dreams.

TABLE OF CONTENTS

CHAPTER 2

CHAPTER 3

LIST OF TABLES

LIST OF FIGURES

NOMENCLATURE

ΔE^{CT}_{IJ}	Charge transfer
ΔE^{DI}_{IJ}	Dispersion Energy
ΔE^{SOLV}_{IJ}	Solvation Energy
ΔE^{ES}_{IJ}	Electrostatic Coulomb Interaction Energy
ΔE^{ij}_{int}	Pair interaction energy between the monomer fragments i and j
$E_i^{'}$	Internal energy values of monomers
$E_i^{''}$	Internal energy values of dimers
D^{IJ}	Density matrix difference of dimer IJ
I	Fragment I
J	Fragment J
V^{IJ}	Electrostatic potential on the ith monomer
Å	Angstrom
D	Debye

LIST OF ABBREVIATIONS

B3LYP	Lee–Yang–Parr
BSA	Bovine serum albumin
CT+mix	Charge-Transfer and Mixing
^{13}C CP MAS	^{13}C Cross Polarization Magic Angle Spinning
CB	Carboxybetaine
$CaSO_4$	Calcium sulfate
DFT	Density-functional theory
ES	Electrostatic
EG	Ethylene glycol
EX	Exchange Repulsion
FMO	Fragment Molecular Orbital
FWHM	Full Width at Half Maximum
FTIR-ATR	Fourier-Transform Infrared Spectroscopy
FT-Raman	Fourier transform Raman
HF	Hatree-Fock
LY	Lysozyme
MPC	Phosphorylcholine
MD	Molecular Dynamics Simulation
MF	Microfiltration
NF	Nanofiltration
PMAL®-C_8	Poly (maleic anhydride-alt-1-decene), 3-(dimethylamino)-1-propylamine
PVDF	Poly (vinylidene fluoride)
PAN	Polyacrylonitrile
PEG	Poly (ethylene glycol)
PIEDA	Pair Interaction Energy Decomposition
PI	Polyimide
PSF	Polysulfone

PTFE	Polytetrafluoroethylene
PRO	Pressure Retarded Osmosis
PS-b-PEGMA	Polystyrene-b-poly (ethylene glycol) Methacrylate
RO	Reverse Osmosis
SBMA	Sulfobetaine methacrylate Derivative
SB2VP	Sulfobetaine 2-vinylpyridine
SA	Sulfopropyl methacrylate
SB	Sulfobetaine
SSNMR	Solid State Nuclear Magnetic Resonance
TMA	[2-(methacryloyloxy) ethyl] trimethylammonium
UF	Ultrafiltration
ZW	Zwitterion

CHAPTER 1

Introduction and Thesis Outline

1.1 Background

The demand of fresh water is continually growing over the past decades due to the population growth and expansion of industry across the world (Montgomery, 2007; Shannon, 2008). Although over 70% of the surface of the earth is covered with water, however, the access to safe drinking water has become one of the critical issue worldwide. Therefore, nowadays the shortage of fresh water is one of the most global challenges for over 2.6 billion people due to intense population growth and increased water pollution (Kevin *et al*., 2006; Gleick *et al*., 1996, Drioli *et al*., 2012). In order to reduce consumption of the global fresh water, and protect the limited worldwide fresh water resources, finding an alternative method to purify water, clean up brackish water, and remove harmful ions from contaminated water would be necessary. This can be done with membrane filtration techniques such as microfiltration, ultrafiltration, nanofiltration and reverse osmosis that have been considered as a green separation method for water treatment (Gin et al,, 2011; Ulbricht et al., 2006; Baker et al., 2004).

Although, membrane technologies have attracted a growing interest in the fields of water purification and water treatment, however, membrane fouling limits the wide application of membrane-based technologies (Laabs et al., 2006; Puro et al., 2011; Bokhary et al., 2017). Membrane fouling caused by the attachment of foulants such as proteins, bacteria, large particles, inorganic contaminants and salts on the membrane surface and inside membrane pores cause loss of membrane permeability, an increase in the cleaning frequency and decrease in membrane lifetime (Herzberg *et al*., 2007, Hoek *et al*., 2008, Antony *et al*., 2012). Hydrophobicity is the membrane characteristic that has a great influence on the membrane fouling phenomenon (Clark and Heneghan, 1991; 2005; Kwon *et al*., 2005). Hence, hydrophilizing the membrane surface to reduce the attachment of contaminants is essential (Weis *et al*., 2005; Persson *et al*., 2006). In the work of this dissertation, a number of efforts were made to overcome intrinsic hydrophobicity of PVDF membranes. A series of novel hydrophilic

zwitterionic polymer additives such as PMAL®-C_8-CB, PMAL®-C_8-SB, PMAL®-C_8-MPC, and PMAL®-C_8-OH-SB were designed in order to improve the hydrophilicity of PVDF membrane.

1.2 Membrane Technology for Water Treatment

Membrane separation processes play a key role in water and wastewater treatments compared to conventional water treatment methods such as disinfection, sand filtration, sand filtration, biological treatment and distillation (Elimelech *et al*., 2011; Misdan *et al*., 2012; Bruggen *et al*., 2003). Membrane separation has attracted research attention due to their low energy consumption and excellent separation abilities at large industrial scale.

Nanofiltration membranes have gained great research interest due to the unique combination of high-salt rejection, higher water permeability flux, low operation cost and at lower pressures requirements compared to reverse osmosis membranes (Martina *et al*., 2010). Nanofiltration membranes, designed for retaining divalent ions of the same charge with a pore size in the range of 0.5–2.0 nm (Bruggen *et al*., 1999). Nanofiltration membranes with negatively/positively charged surfaces can retain charged solutes by electrostatic interactions or the Donnan effect, whereas uncharged solutes mainly are rejected by steric hindrance or exclusion effect (Bruggen *et al*., 1999; Roy *et al*., 2017). Numerous studies have shown that commercially available charged nanofiltration membrane surfaces are able to retain different contaminants. However, the basic principles of separation in nanofiltration membranes are strongly influenced by solute size, charge and chemical interactions (Bruggen *et al*., 1999).

Examples include the removal pollutants such as pesticides, viruses and bacteria, salinity, nitrates, and arsenic from surface water and groundwater (Bruggen *et al*., 2003). Furthermore, the dye removal from dye/salt mixtures by asymmetric cellulose acetate and composite polyamide nanofiltration membranes (Yu *et al*., 2010), in addition to the retention of pharmaceuticals materials by a nanofiltration membrane (Nghiem *et al*., 2005). Therefore, nanofiltration membranes indicate good performance in removing pollutants for different applications. Nevertheless, the major challenge for existing membranes is to improve the filtration efficiency, that is permeability and selectivity, which are often considered to be inversely proportional to each other.

1.2.1 Membrane Fouling

Membrane fouling is defined as a reduction in the active area of the membrane due to the reversible or irreversible deposition or the attachment of contaminants, such as solutes, macromolecules, biological substances, colloids, particles, salts, on the membrane surface and inside its pores (Baker *et al*., 2004). As indicated in Figure 1.1, flux decline in membrane filtration is a result of the increase in the membrane resistance by the membrane pore blockage and the formation of a cake layer on the membrane surface. The pore blocking increases the membrane resistance while the cake formation creates an additional layer of resistance to the permeate flow. Pore blocking and cake formation can be considered as two essential mechanisms for membrane fouling (Li *et al*., 2008; Song *et al*., 1998). Membrane fouling reduces membrane permeability and water flux, which lead to increased energy consumptions. In addition, fouling requires cleaning frequency, declines membrane lifetime and increases energy requirements, which limits the application of membrane system at large scale (Herzberg *et al*., 2007; Hoek *et al*., 2008; Antony *et al*., 2012).

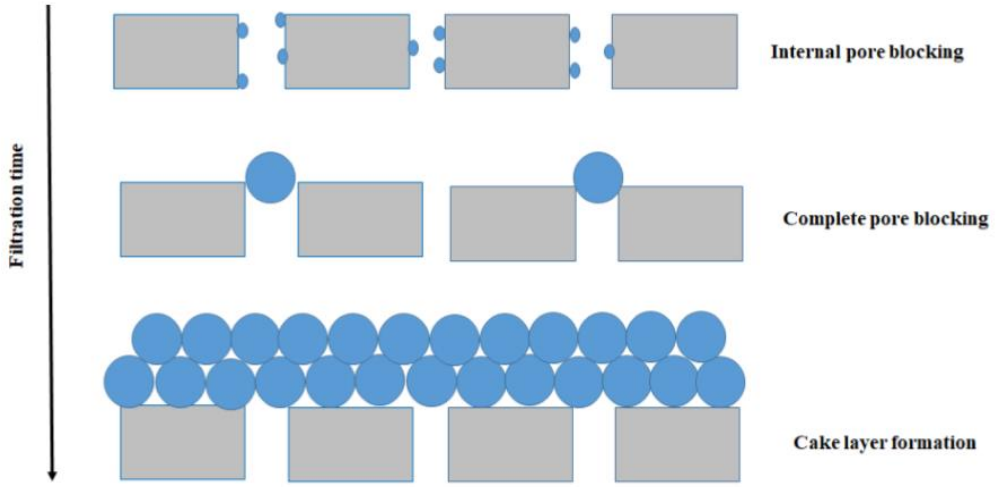

Figure 1.1. Fouling mechanisms of porous membrane.

A typical flux-time curve of ultrafiltration (UF), as shown in Figure 1.2, starts with (I) a rapid initial drop of the permeate flux due to pore blocking (II) followed by a long period of gradual flux decrease, and (III) ended with a steady-state flux due to the formation of the cake layer (Li *et al*., 2008; Song *et al*., 1998).

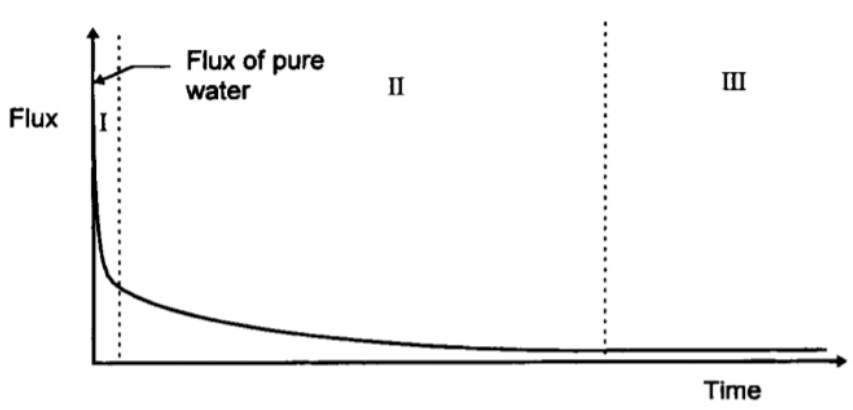

Figure 1.2. A Schematic presentation of the three stages in flux decline. Reproduced with permission from Reference (Song *et al*., 1998).

In terms of the source of foulants, fouling can be categorized as organic fouling, particulate fouling, bio-fouling, or inorganic fouling. For example, Labs, et al. (Laabs *et al*., 2006) studied fouling of MF and UF membranes with wastewater effluent and found the organic matter was primarily responsible for the flux decline. Haberkamp et al. (Haberkamp *et al*., 2008) found that both biopolymers and proteins are responsible for fouling on UF membrane surfaces. In addition, the smaller organic compounds such as humic acids, which are not rejected by the UF membrane are less problematic.

Most previous studies on biofouling and organic fouling demonstrated that flux reduction is not just related to polymers and proteins and there is the complexity of fouling in wastewater treatment due to the hydrophobicity of the membrane.

On the other hand, scaling fouling occurs when specific minerals or primary salts such as calcium sulfate ($CaSO_4$) are supersaturated at the membrane surface, which can damage the membrane and reduce membrane permeability (Kwan *et al*., 2013). The high concentration of sparingly soluble salts might increase risk of the high level of inorganic fouling. Shirazi et al. (Shirazi *et al*., 2006) performed experiments to compare fouling mechanism of $CaSO_4$ and $CaHPO_4$ on NF by observing the flux reduction behavior. They found that $CaSO_4$ fouling contributed a greater resistance than $CaHPO_4$ fouling under the same operating conditions. They showed that the flux reduction caused by $CaSO_4$ fouling was due to reversible cake formation, while the flux decline caused by $CaHPO_4$ fouling was partially irreversible by both pore/surface adsorption and cake formation.

1.2.1.1 Hydrophobicity vs Hydrophilicity

Membrane fouling in filtration systems is closely related to surface characteristics (Saqib, 2016). Among these characteristics, hydrophilic surfaces are considered the most critical characteristic (Weis *et al*., 2005; Persson *et al*., 2006; Malaeb *et al*., 2011). Membranes with hydrophilic surfaces demonstrated less fouling tendency, compared to membranes with hydrophobic surfaces. This performance is attributed to form a water layer easily on a hydrophilic surface, and consequently foulants with hydrophobic property are repellent to the surface.

Hydrophilic membranes have less tendency to fouling due to its ability to form hydrogen-bonds with water, high wettability, high surface tension as shown in Figure 1.3 (b), compared to Figure 1.3 (a). Therefore, hydrophilic membranes can limit the foulants from attaching to the surface (Li *et al*., 2008). Consequently, incorporating hydrophilic materials on the membrane surface would enhance the antifouling properties.

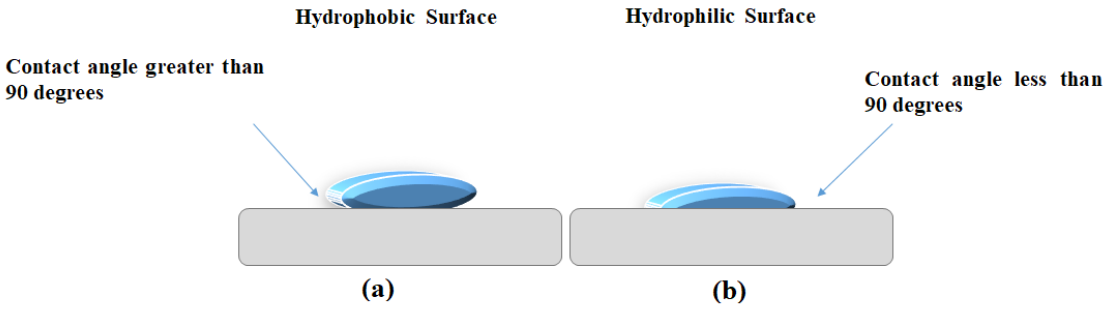

Figure 1.3. a) Hydrophobic membrane, (b) Hydrophilic membrane.

1.2.2 Polymeric membranes

Nowadays, numerous synthetic membranes for industrial applications are made from inorganic materials or organic polymers, leading into major portions on the existing membrane market, including polyamide (PA), Polyimide (PI), poly (ether sulfone) (PES), Polysulfone (PSF), polyacrylonitrile (PAN), polytetrafluoroethylene (PTFE), and poly (vinylidene fluoride) (PVDF) (Shibutani *et al*., 2011; Naomi *et al*., 1983). Although a variety of organic polymers can be used to synthesize membranes, but the selection of polymer is based on fouling tendency, in addition to chemical and thermal stability.

Therefore, the PVDF with repeating units of $–(CH_2CF_2)$ and is one of the most attractive semicrystalline polymeric membrane materials. PVDF has gained a remarkable attention, and widely applied in industrial NF membrane fields, due to its excellent advantages in terms of thermal stability, chemical resistance, and high mechanical strength for water treatment (Liu *et al*., 2011; Kang *et al*., 2014; Martins *et al*., 2014). The strong thermal stability and excellent chemical resistance of PVDF is attributed to the high electronegativity of fluorine atom in PVDF chains, resulting into increase the bond dissociation energy of C–F. Despite its outstanding advantages, the performances of PVDF membranes are substantially limited by fouling on the membrane surfaces in water treatment. Fouling affects PVDF membrane efficiency, and consequently increasing the operation cost (Jang *et al*., 2015). Therefore, to address this problem, the hydrophilic modifications of PVDF membranes are necessary to remediate fouling.

1.2.3 PVDF Surface Modifications

The intrinsic hydrophobicity of PVDF membrane is prone to fouling, such as protein attachment and deposition onto the membrane surface, which leads to serious reductions in permeation, decreases PVDF lifetime, and accordingly increases the costs of operational process (Jang *et al*., 2015)

Hence, the surface modification of PVDF membranes is necessary to improve its hydrophilicity. The hydrophilic surface, usually forms a pure water layer on the membrane surface and inner pore walls, which can prevent the adsorption and deposition of hydrophobic pollutants onto the membrane surface, thus reducing fouling (Kang and Cao, 2012). There are several promising hydrophilic, net-neutral monomers and polymers, including poly (ethylene glycol) (PEG), and zwitterions (Holmlin *et al*., 2001, Zhang *et al*., 2006).

Poly (ethylene glycol) (PEG) is a water soluble, neutrally charged polyether that has been attracting more attention due to its low fouling capability against the adhesion and accumulation of protein/cell/bacteria or other pollutants (Gudipati *et al*., 2005). PEG group enhances the formation of a strong hydration layer through hydrogen bonding that prevents pollutants from approaching the membrane surface.

Venault et al. (Venault *et al*., 2016) modified PVDF membrane surface with an amphiphilic copolymer additive: polystyrene-b-poly (ethylene glycol) methacrylate (PS-b-PEGMA) to reduce bacterial attachment. Although PEG has been a useful hydrophilic material to enhance the

hydrophilicity of membranes and reduce membrane fouling, however, it quite is susceptible to autoxidation in the presence of dioxygen, transition metal ions and enzymatic cleavage in complex media, losing the antifouling ability (Herold *et al*., 1989). Consequently, there is great interest in finding other hydrophilic alternatives to PEG, such as Zwitterions.

1.3. Antifouling Zwitterionic Polymers

Currently, numerous exploring efforts have been made for the development of zwitterionic polymers as best and latest alternative candidates for enhancing its hydrophilicity and reducing fouling (Schlenoff, 2014). The remarkable nonfouling properties of zwitterions have been inspired from the zwitterionic phosphatidylcholine head-groups existing in the phospholipid bilayer in the outside surface of cell membranes (Bretscher and Raff, 1975). For first time, Alfrey et al. (Alfrey and Morawetz, 1952) reported the successful synthesis of a zwitterionic compound in 1950. As a consequence, many of novel anti-fouling polymer material with zwitterionic head groups have been developed in recent decades. The antifouling behavior of zwitterions is attributed to its special chemical structure, which have both positively and negatively charged units in one group. Recently, zwitterionic materials such as poly (carboxybetaine methacrylate) (polyCBMA), Poly (phosphobetaine), and poly (sulfobetaine methacrylate) (polySBMA) with high hydrophilicity, neutral charge, and hydrogen bond acceptors are receiving considerable attention because they present excellent nonfouling properties (Schlenoff, 2014), as shown in Figure 1.4.

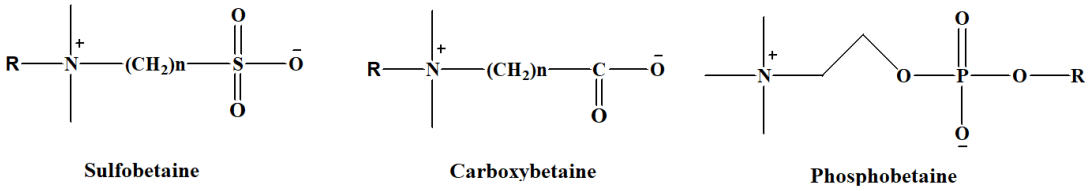

Figure 1.4. Zwitterionic functional groups.

Venault et al. (Venault, *et al*., 2014) investigated the relationship between the membrane charge and the membrane antifouling properties through modification of PVDF membranes with the copolymers of [2-(methacryloyloxy) ethyl] trimethylammonium (TMA) and sulfopropyl methacrylate (SA). As shown in Figure 1.5, there is a strong electrostatic attraction between

positively-charged membranes and negatively charged bovine serum albumin (BSA), and negatively-charged membranes and positively charged lysozyme (LY), resulting into protein adsorption. However, pseudo-zwitterionic membranes indicated excellent antifouling to different proteins, which is attributed to electrostatic repulsions of ion pairs when a charge bias is involved.

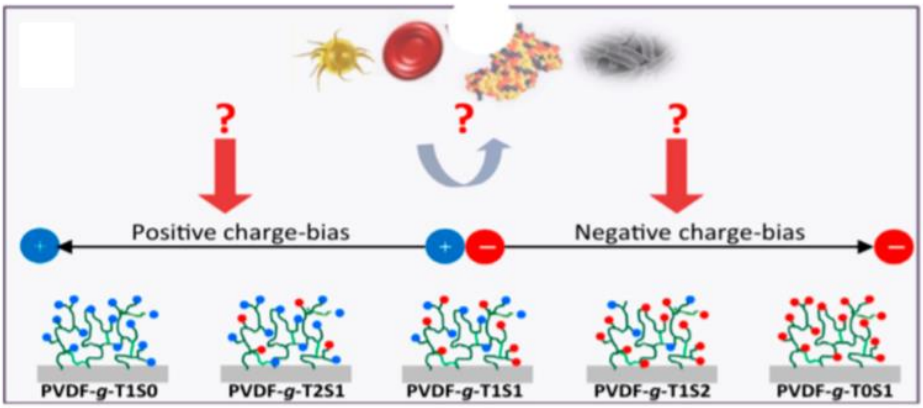

Figure 1.5. a) Scheme of polyvinylidene Fluoride (PVDF) membranes coated with [2-(methacryloyloxy) ethyl] trimethylammonium (TMA) and sulfopropyl methacrylate (SA) monomers, before undergoing plasma polymerization. Reproduced with permission from Reference (Venault *et al*., 2016).

1.3.1 The effect of zwitterions on Membrane Hydrophilicity

The strong hydration is believed to be the main source of minimizing the attachment of the contaminants and salts on membrane surfaces (Schlenoff, 2014). As mentioned before, zwitterionic and non-ionic PEG materials have shown strong hydration. However, their hydration free energy, dynamics, and structure is different, leading to different performance. Wu et al, (Wu *et al*., 2012) proved that much more water molecules surrounded zwitterionic materials than PEG using the low-field nuclear magnetic resonance tests and Molecular Dynamic Simulation studies. As indicated in Figure 1.6, the hydrophilicity of Zwitterion sulfobetaine compared to PEG indicates that water molecules interacting with the sulfobetaine unit are more tightly adhered than those on the ethylene glycol (EG). In addition, there are more water molecules adsorbed on polySBMA chains than those on PEG. Figure 1.6 showed that the EG unit includes an oxygen atom that interact with one water molecule via hydrogen bonding, while the SB unit consists of integrated positively charged group and a negatively charged group which interact with at eight water molecules via electrostatic interactions. Therefore, Zwitterions are considered as best hydrophilic materials on modification of PVDF membrane surfaces.

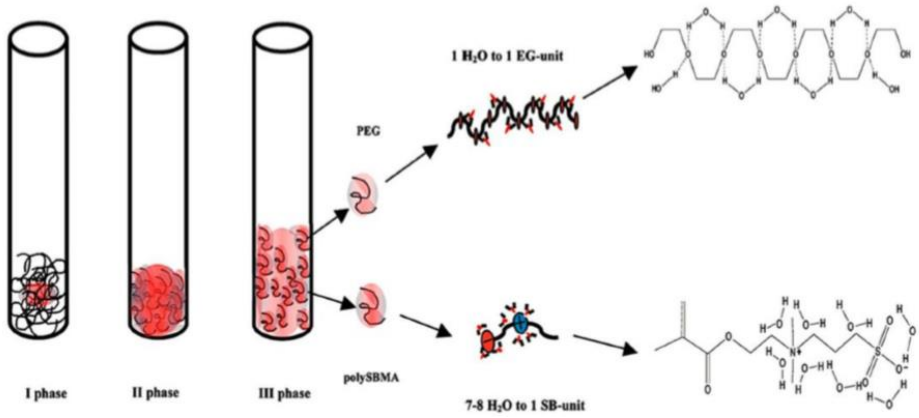

Figure 1.6. A proposed model of the hydration process of both PEG and polySBMA polymers. Reproduced with permission from Reference (Wu *et al*., 2012).

Shao et al. (Shao *et al*., 2010) calculated the hydration free energies of Carboxybetaine (CB), Sulfobetaine (SB), and Ethylene glycol (EG) moieties using the free energy perturbation method. They used CB and SB moieties, with two methylene groups between the charged groups. The hydration free energy of zwitterionic CB and SB moieties is much lower than that of non-ionic EG 4 moieties, indicating that zwitterionic materials exhibit stronger hydration. Zhao et al. (Zhao et al., 2010) grafted a zwitterionic polymer, poly (sulfobetaine methacrylate) (poly(SBMA)), onto a hydrophobic polypropylene membrane surface. The enhanced hydrophilicity is mainly due to the hydrophilic zwitterionic groups, which can bond large amounts of water through electrostatic interactions. As a result, the hydrophilicity and water permeability of membranes could be improved by incorporating zwitterions on membranes.

1.4 Pair Interaction Energy Decomposition Analysis (PIEDA)

The optimization of geometry in membranes and their different complexes with water molecules can be calculated using the adiabatic connection method-Becke three parameters and applying the density functional theory (DFT) method with Lee–Yang–Parr (B3LYP) functional and no symmetry constrains (Gordon and Schmidt, 2005). In addition, the frontier molecular orbital theory (FMO) can be used to calculate the interactions between membrane oligomers and water fragments. Monte Carlo-type global optimization followed by FMO is used to calculate the

all the possible interactions between membrane oligomers and water fragments. The pair interaction energy (PIE) occurring between any two fragments can be calculated by FMO, as a collective summation of four energy terms, specifically: exchange-repulsion, charge transfer value, dispersion, and electrostatics, which are provided using the PIEDA as the FMO-based EDA, where the bulk parameters of are being decomposed into the same components as in EDA (Kitaura and Morokuma, 1976).

1.5 Knowledge gaps

1. The intrinsic hydrophobicity PVDF membrane is dominating, which leads to severe fouling. Although many research efforts have been made to overcome this issue using surface modification techniques by adding hydrophilic materials. However, the majority of the previous studies just studied the hydration of common zwitterions including carboxybetaine, sulfobetaine, and phosphobetaine, but designing novel zwittronic materials are still lacking.

2. An in depth understanding of the reasons behind the interactions of water molecules with hydrophilic and hydrophobic membranes is lacking.

2.6 Hypotheses

1. A systematic study and an investigation of the reasons behind the hydrophobicity of PVDF membrane compared to the hydrophilic PAN membrane, as a reference, can help designing ground-breaking membranes with superior hydrophilicity.
2. Zwitterions are considered as the latest generation of hydrophilic materials for antifouling interfaces and membranes. Thus, the incorporation of zwitterion materials into PVDF membrane can improve water transport and achieve antifouling of PVDF membrane.

3. Despite most attempts on the modification of PVDF membrane with common zwitterions, computational studies to understand the influence of the chemistry of zwitterionic materials are lacking. A comprehensive computational study can be ideal for in-depth understanding of

how the zwitterion chemistry influences the hydrophilicity of the membrane and achieve novel designs.

1.7 Research Objectives

In view of the knowledge gap discussed above:

1. The primary objective of the thesis research was to investigate the interactions occurring between water molecules and the fragments of PAN and PVDF, as hydrophilic and hydrophobic membrane models, respectively, at the molecular level using the pair interaction energy decomposition analysis (PIEDA) as part of the fragment molecular orbital (FMO) method's framework.

2. Another objective of this research was to perform a systematic study with FMO-PIEDA method to overcome to the hydrophobicity of PVDF membranes through hydrophilic modifying surfaces with novel zwitterions.

1.8 Organization of the Thesis

The organization of the MSc thesis is aligned with the guidelines for manuscript-based thesis of University of Saskatchewan. In this regard, the thesis is written in the manuscript (paper) based style and the discussions have been presented as a series of journal manuscripts, and it is organized into four chapters. The work presented in this thesis resulted in two manuscripts, which are currently under review. The introduction is presented in Chapter 1, along with background of membrane technology for water treatment, antifouling zwitterionic polymers, knowledge gaps, research objectives, organization of the Thesis, and manuscript content of the thesis.

Chapter 2, contains the first manuscript which presents the computational studies and the experimental analyses of Polyvinylidene fluoride (PVDF) and Polyacrylonitrile (PAN) membranes, which were considered the models for hydrophobic and hydrophilic membranes, respectively.

The novel zwitterions to overcome to hydrophobicity PVDF membranes were designed. The performance of the designed ZW- PVDF copolymers were studied by FMO-PIEDA method, as presented in Chapter 3.

Finally, a summary of the results, conclusions and recommendations are presented in Chapter 4, followed by the list of the references, used in the thesis.

1.9 Manuscript Content of the Thesis

Membrane fouling on PVDF membrane surfaces is due to its intrinsic hydrophobicity and it is a long-term critical obstacle, especially in applications related to water and wastewater treatment. In this study, FMO approach was applied for the first time to examine the noncovalent interactions between water molecules with PAN, PVDF, and ZW-PVDF membranes for an accurate quantum chemical level analysis.

Thus, the first phase of the research focused on the quantitative analyses of the hydrophobicity of the fluorinated materials using PIEDA and spectroscopic analyses. The details of this research study, are presented in Chapter 2. (First manuscript)

Currently, numerous exploring efforts have been made on the development of zwitterionic polymers as best and latest alternative candidates for enhancing hydrophilicity and reducing fouling of the hydrophobic membrane surfaces. Thus, it was interesting to design novel ZW materials with super hydrophilicity property to enhance the hydrophilicity of PVDF membranes. The details of this study are presented in Chapter 3. (Second manuscript)

CHAPTER 2

Pair Interaction Energy Decomposition Analysis (PIEDA) and Experimental Approaches for Investigating Water Interactions with Hydrophilic and Hydrophobic Membranes

The contents of the manuscript provided in this chapter is under review in the Journal Materials Today communications, MTCOMM_2019_134.

Citation:

Maghami, M., Abdelrasoul, A., Pair Interaction Energy Decomposition Analysis (PIEDA) and Experimental Approaches for Investigating Water Interactions with Hydrophilic and Hydrophobic Membranes. Journal Materials Today communications, MTCOMM_2019_134.

Contribution of the MSc student

The inception of the project idea and the direction of the project experiments and computational calculations were planned by Dr. Amira Abdelrasoul. The experiments and computational calculations were performed by Mahboobeh Maghami, under the supervision and the guidance of Dr. Amira Abdelrasoul. The samples for PVDF and PAN and their extensive characterizations were performed by Mahboobeh Maghami with the assistance of Jason Maley at Saskatchewan Structural Sciences Centre. The collection of data, analysis and interpretations were performed by Mahboobeh Maghami with the guidance and support from Dr. Abdelrasoul. Dr. Amira Abdelrasoul supervised and provided consultation during the entire experimental period as well as computational jobs. The manuscript was written by Mahboobeh Maghami and Dr. Amira Abdelrasoul, who has also provided additional points to be discussed, editorial guidance regarding the style and content of the paper. Dr. Abdelrasoul is the corresponding author of the manuscript, in addition, she supervised and provided consultation during the thesis preparation.

Contribution of this chapter to overall study

This chapter addresses the challenge of the first objective of the project: to provide an in-depth understanding of the interactions occurring between water molecules and the fragments of 14 hydrophobic and hydrophilic membranes (PVDF and PAN) at the molecular level. We used the pair interaction energy decomposition analysis (PIEDA) as part of the fragment molecular orbital (FMO) method's framework for the first time. These types of analyses included the inter fragment interaction energy (IFIE), like the electrostatic (ES), exchange repulsion (EX), and charge-transfer and mixing term (CT+mix). Furthermore, the function groups of the membranes were examined through Fourier-transform infrared spectroscopy (FTIR- ATR), 13C cross polarization magic angle spinning (13C CP MAS) Solid State Nuclear magnetic resonance SSNMR, and Fourier transform Raman (FT-Raman) spectroscopies. Furthermore, the confocal microscopic was applied to study the interactions between fluorescence particles inside the membrane matrices.

2.1 Abstract

The origins of low and high interactions of polar groups with water molecules are still unknown and need to be further examined for effective future membrane synthesis and modification. The primary aim of this research study is to provide a comprehensive overview of the interactions at the molecular level occurring between water molecules and the fragments of hydrophobic and hydrophilic membranes based on pair interaction energy decomposition analysis (PIEDA) as part of the fragment molecular orbital (FMO) method's framework. This direction is critical, since a research study of the reasons for water and membrane interactions can help design ground-breaking membranes with superior hydrophilicity characteristics. To accomplish this, the computational studies and experimental analyses of Polyvinylidene fluoride (PVDF) and Polyacrylonitrile (PAN) membranes were considered as models for hydrophobic and hydrophilic membranes, respectively. Density-functional theory (DFT), based on B3LYP functional and split-valance 6-311+G (d,p) basis sets, was used in order to optimize the geometry of PAN, PVDF, and their complexes with different numbers of water molecules. Furthermore, fragment molecular orbit (FMO) and the Pair Interaction Energy Decomposition Analysis (PIEDA) were carefully interrogated. These types of analyses included the inter fragment

interaction energy (IFIE), like the electrostatic (ES), exchange repulsion (EX), charge-transfer and mixing term (CT+mix), and dispersion (DI) energies. Furthermore, the hydrophilicity and hydrophobicity of the origins of membrane function groups were experimentally evaluated through Fourier-transform infrared spectroscopy (FTIR- ATR), ^{13}C cross polarization magic angle spinning (^{13}C CP MAS) Solid State Nuclear magnetic resonance SSNMR, and Fourier transform Raman (FT-Raman) spectroscopies. Confocal microscopic approach was used to interrogate water transport and the interactions between fluorescence particles and membrane layers.

Keywords: hydrophilicity, interactions, hydrophobicity, Pair Interaction, fragment, DFT, hydrogen bond, electrostatic, spectroscopy.

2.2 Introduction

Membrane technology is a rapidly developing area with key growth for large-scale industrial applications, including biotechnology, biomedical applications, food industry, and water and wastewater treatment. The goal of the membrane design is to make a particular process highly efficient, cost effective, easily applicable, and sustainable. Although there have been a number of attempts to improve this technology, the understanding of membrane fouling and consequent permeate flux decline still remain a challenge (Dechnik *et al*., 2017; Qadir *et al*., 2017; Khorshidi *et al*., 2018; Zularisam *et al*., 2005, Noble and Agrawal, 2005).

PVDF is the fluorinated type of membrane and has incited more interest in research and manufacturing due to its outstanding properties (Dalvi and Rossky, 2010), including thermal and chemical stabilities that are essential for chemical cleaning, backwash, and increased membrane lifetime, in addition to offering higher mechanical strength than other membranes (Dalvi and Rossky, 2010; Rabuni *et al*., 2013). In addition, PVDF is preferred over other membranes, since it provides enhanced protein retention, strength, and chemical compatibility (Rabuni *et al*., 2013). The uses of PVDF membranes have been limited due to the issue of fouling occurring in water treatments caused by the membrane's hydrophobic property. Consequently, PVDF membrane is predisposed to the negative effects of the fouling phenomenon, which in turn leads to high operational costs, increased transmembrane pressure values, greater power consumption,

and reduced membrane lifetimes. Current research focuses on improving PVDF hydrophilicity and overcoming this phenomenon by increasing water permeability, enhancing water transport across the membrane, and facilitating a significant improvement of the membrane efficiency and stability in long term applications (Abdelrasoul *et al*., 2017; Pendergast and Hoek, 2011; Rezakazemi *et al*., 2014; Seoane *et al*., 2015). However, the investigation of the hydrophobicity of PVDF as a fluorocarbon membrane would be difficult as it consists of a simultaneous presence of the hydrophobic and hydrophilic structural components, such as CH bonds that have a hydrophobic surface and the Fluorine heteroatoms with hydrophilic centers.

In order to achieve these improvements, revolutionary advances in membrane materials are necessary since only then membrane technologies can tackle water and energy sustainability. Therefore, developments of theoretical methods that are capable of understanding the water interactions with membranes and the origins of hydrophobicity and of the origins of its interactions are essential. In fact, these methods are key to the design of novel PVDF membranes with innovative infused nanomaterials and featuring strong interactions. An appealing and efficient approach is to employ a reliable level of two novel fragmentation methods in the electronic structure program GAMESS (employing the typical atomic and molecular electronic structure), which pairs interaction energy decomposition analysis (PIEDA) (Kitaura and Morokuma, 1976; Stevens and Fink, 1987; Chen and Gordon, 1996) with the framework of the fragment molecular orbital (FMO) (Fedorov *et al*., 2012; Fedorov, Kitaura, 2007; Kitaura *et al*., 1999) method. PIEDA method relies on an investigation of the various inter- and intramolecular interactions with respect to the exchange-repulsion, electrostatic, charge transfer energies, and the added correlation (dispersion) term (Su *et al*., 2012; Morokuma, 1971; Fedorov and Kitaura, 2007). By successfully accomplishing the FMO geometry optimizations and reviewing the PIE profiles, Fujimura and Sasabuchi (Fujimura and Sasabuchi, 2010), explained the role of fluorine atoms within the fluorinated prostaglandin agonist. Looking at the relevance of the FMO in chemical medicine, Ohno et al. (Ohno *et al*., 2011) offered computational data on the binding of bisphosphates to farnesyl pyrophosphate synthase. The practical value of CH/p hydrogen bonds in rational drug design and production was likewise shown by Ozawa et al. and based on FMO calculations.

Thus, the intent of this research study is to offer a comprehensive overview of the interactions occurring between water molecules and the fragments of hydrophilic and hydrophobic

membranes based on pair interaction energy decomposition analysis (PIEDA) within the framework of the fragment molecular orbital (FMO) methodology. The correlation between water molecules and hydrophilic and hydrophobic membranes was simulated with Density-functional theory (DFT) (Gordon and Schmidt, 2005), and the Gamess interface in Avogadro and Facio (Parr and Yang, 1989), for an in depth understanding of the water interactions with the membrane oligomers. The hydrogen bonding parameters, stretching vibrational frequencies, influence of solvation, electrostatic interactions, dipole interactions, interfragment Vander Waals, charge transfers, energy level gaps, and molecular orbitals are extensively discussed and analyzed. Furthermore, the hydrophilicity and hydrophobicity of the origins of membranes function groups are examined through Fourier-transform infrared spectroscopy (FTIR- ATR), ^{13}C cross polarization magic angle spinning (^{13}C CP MAS) Solid State Nuclear magnetic resonance SSNMR, and Fourier transform Raman (FT-Raman) spectroscopies. Confocal microscopic is applied for the study of the water transport interactions between fluorescence particles and membrane layers.

2.3 Computational Analyses

2.3.1 Computational Density Functional Theory (DFT)

For the process of improving the structure of PVDF and PAN oligomers and their complexes with water, vibrational spectra, energy, fragment molecular orbital method (FMO), and molecular electrostatic potential were carefully executed with the help of GAMESS Software (Gordon and Schmidt, 2005). The optimization of geometry in both membranes and their different complexes with water molecules were completed using the adiabatic connection method-Becke three parameter and applying the density functional theory (DFT) method with Lee–Yang–Parr (B3LYP) functional and no symmetry constrains. All of these calculations were done with the standard 6-311+G (d, p) basis set so as to achieve a higher degree of accuracy during the theoretical computation of DFT level of theory. For our model, we started with a monomer, followed by dimer, trimer, and then tetramer, to ensure the accuracy of calculations. In this study, the tetramer oligomers are considered the membrane model representatives of the polymer behavior. As part of the experiment, optimizations were conducted without any symmetry constrains. For continued accuracy of the collected data, we examined the convergence of the modeled oligomers with respect to the longer chain polymer. The exact

harmonic vibrational frequency values were calculated so as to check the precise optimized geometry corresponding to the local minimum values that solely include real frequencies. Furthermore, frequency calculations at 298.15 K and 1.0 atmosphere pressure values were used to determine the thermodynamic properties for all of the experimental compounds. The collected data values for energies were zero-point (ZPE) corrected in relation to the unscaled frequencies. In order to investigate the solvent influences on the conformational equilibrium as well as the contribution to the enthalpies total, the experiment relied on the polarized continuum (overlapping spheres) mode (PCM) developed by Tomasi and coworkers, (Parr and Yang, 1989, Barone et al., 1998) at the B3LYP/6-311^{+}G (d, p) level. The specific solvation calculations were conducted for water (ε = 78.35, SCRF method) using optimized geometries. The POP was selected to equal the NBO key-word for a full natural bond orbital analysis of atomic charge assignments and spin density values (Morokuma, 1971).

2.3.2 Fragmentation and basic theory

In addition, frontier molecular orbital theory (FMO) was used to calculate the interactions between membrane oligomers and water fragments. In addition, Monte Carlo-type global optimization followed by frontier molecular orbital theory (FMO) were used to calculate the all the possible interactions between membrane oligomers and water fragments.

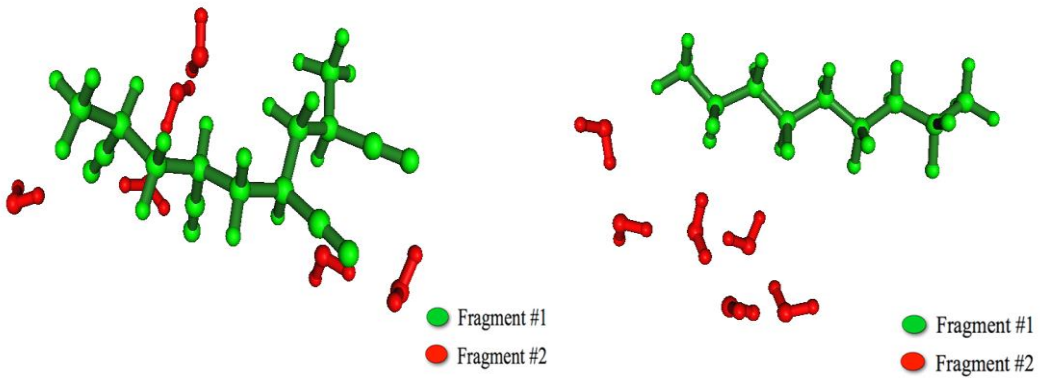

(a) **(b)**

Figure 2.1. Fragmentation of water molecules and PAN and PVDF membranes, calculated at FMO-RHF/6-31G* level (a) PAN. $6H_2O$; and (b) PVDF. $6H_2O$.

Unlike the traditional Quantum-mechanical (QM) methods (Alexeev *et al.*, 2012), the fragment molecular orbital (FMO) methodology guarantees a significant computational speed-up. A critical part of the FMO method is that it allows for a listing of the interactions being created between the water molecules and membranes, as shown in Figure 2.1.

The pair interaction energy value of the fragments is determined using Equation (2.1):

$$\Delta E_{IJ}^{int} = \left(E_{IJ}' - E_I' - E_J'\right) + Tr(\Delta D^{IJ} V^{IJ}) \quad \text{Equation (2.1)}$$

The first term stands for the pair interaction amount that occurs between the sections being polarized by the surrounding environment, while the second term is the interaction between the external Coulomb field and the relaxed density, of dimer versus the two monomers. The multiple-body polarization energy values in FMO is divided into (a) the destabilization contribution, calculated based on the variance occurring between free (unpolarized) state of fragments and their respective polarized state, based on the internal energy values; and (b) the stabilization contribution value, which in turn is part of the overall pair interaction energy (PIE), also defined as the interfragment interaction energy (IFIE).

During the molecular interaction based expression of the two-body FMO (FMO2) method, the obtained electrostatically embedded monomer E_I' and dimer E_{IJ}' energies are effectually joined. In order to describe the pair interactions in FMO, Equation (2.1) can be revised, as presented in Equation (2.2).

$$\Delta E_{IJ}^{int} = \sum_I E_I' + \sum_{I>J}[\left(E_{IJ}' - E_I' - E_J'\right) + Tr(\Delta D^{IJ} V^{IJ})] \quad \text{Equation (2.2)}$$

where E_I' and E_{IJ}' represent the internal energy values of monomers and dimers. In addition, D^{IJ} stands for the density matrix difference of dimer IJ and the sum of monomer I and J electron densities, while V^{IJ} is the electrostatic potential caused by the external fragments influence on the dimer IJ. When it comes to the dimers where the interfragment distance amount is greater, the third term in Equation (2.2) is relatively smaller while the second term can be estimated with the aid of the electrostatic interactions happening between fragments I and J.

2.3.3 Pair Interaction Energy Decomposition Analysis (PIEDA)

The pair interaction energy (PIE) occurring between any two fragments was calculated by FMO as a collective summation of four energy terms, specifically: exchange-repulsion, charge transfer value, dispersion, and electrostatics, as presented in Equation (2.3), which are provided

using the pair interaction energy decomposition analysis (PIEDA) as the FMO-based EDA, where the bulk parameters of ΔE_{IJ}^{int} are being decomposed into the same components as in EDA. In order to show the applications of FMO, we apply the gas phase PIEDA to the PAN and PVDF with six water molecules, at the hf/6-31G* level, and implementing the default parameters in GAMESS.

$$\Delta E_{IJ}^{int} = \Delta E_{IJ}^{ES} + \Delta E_{IJ}^{EX} + \Delta E^{CT+mix}_{IJ} + \Delta E_{IJ}^{DI} + \Delta E^{SOLV}_{IJ} \quad \text{Equation (2.3)}$$

where ΔE_{IJ}^{ES} is the electrostatic Coulomb interaction occurring between the fragments' polarized charge distributions; and ΔE_{IJ}^{EX} *is* the exchange repulsion between fragments located close to each other. This repulsion is caused by the Pauli repulsion forces and is directly linked to the overlap between two occupied orbitals. In addition, ΔE_{IJ}^{CT} *is* the charge transfer comes from the interactions between the unoccupied orbitals of an acceptor and the occupied orbitals of a donor, adding to the mixed higher order terms.

The ΔE_{IJ}^{DI} *is* dispersion develops as the process appearing between instantaneous dipole moments of two fragments; while ΔE^{SOLV}_{IJ} represents the energy contribution due to solvation provided by PIEDA/ PCM designates the solvent screening for the pair interaction energies, a correlation that is vital for a more comprehensive examination of these interactions. Within the scope of this research study, we studied exchange-repulsion (EX), electrostatics (ES), charge-transfer plus mixed (higher order) terms for the interactions occurring between water and the PAN and PVDF membranes.

It is important to mention that the charge transfer values and electrostatic terminology is relevant to polar interactions and hydrogen bonds, while the dispersion terminology can be considered as hydrophobic. Finally, the exchange-repulsion keyword defines the steric repulsion force between electrons that in turn ensures that the atoms do not collapse into each other.

2.4 Materials and Methods

Polyvinylidene fluoride (PVDF) (Koch Membrane Systems, molecular weight cut off MWCO of 100, 000 Da) and Polyacrylonitrile (PAN) (GE Water and Process Technologies, MWCO of 100,000 Da) membranes were used for the experimental analyses, as hydrophobic and hydrophilic membranes, respectively. Figure 2.2 represents the scanning electron microscopy (SEM) of PVD and PAN membrane surfaces at a magnification of 100. The zeta potential of

PVDF and PAN are -2.5 mV and – 41.5 mV respectively. The membrane surfaces' zeta potential value was calculated with the help of zeta potential analyzer (Zetasizer Nano Series, Malvern Instruments Ltd., U.K., ±0.01 mV). The surface energy of PVDF and PAN was found to be 29.8 mJ/m^2 and 54.1 mJ/m^2, respectively. A contact angle meter (CAM-PLUS, Cheminstruments) was employed to measure the surface energy values.

The spectroscopies analyses were used, not only to obtain a deeper understanding of the specificity of more polymeric membrane interactions with water, but also for tracking structural changes in the membranes that occur during various phase states. The FTIR-ATR spectra were documented through a Nicolet IR 560 spectrometer with horizontal ATR accessory equipped with a ZnSe crystal. Raman spectra data was recorded with the aid of a Dilor Labram spectrometer, featuring a confocal microscope (Olympus BX40) for the purposes of collection of the scattered light as well as sample illumination. A He-Ne laser (wavelength 632.8 nm) was applied for the excitation during the experiment. Throughout testing, a 1800 lines per mm grating was used together with a Peltier cooled CCD camera for the Raman scattered light detection. During all the measurements the spectral resolution was kept at 2 cm^{-1}.

In this case, the perfect depth resolution system value was ascertained in relation to the full width at half maximum (FWHM) of the intensity response of the silicon mode at 520.7 cm^{-1}. This occurred when the focal point of the objective was carefully scanned through a silicon surface and was determined to be 2 mm for a 100 objective (NA 0.9, confocal hole 200 mm) and 4 mm using a 80 objective (NA 0.75, confocal hole 120 mm).

Moreover, the PAN, PVDF virgin samples, as well as their respective complexes with water were quantitatively assessed through the ^{13}C ssNMR technique, including the one dimensional (1D) ^{13}C direct polarization/magic-angle spinning method. This research suggests that the combination of a selectively ^{13}C-labeled technique and high spinning speed of 20 kHz in magic-angle spinning (MAS) NMR experiment can noticeably improve the detection sensitivity. Specifically, the data shows an improvement by nearly 2 orders of magnitude, and provides a clear Solid-state (ssNMR) spectra with little peak overlaps. This research is critical for the discovery of the water reactions with hydrophilic and hydrophobic membranes with higher performances. During this experimental setup, all ^{13}C ssNMR spectra were completed on a Bruker AV III 400WB spectrometer functioning at a ^{13}C resonance frequency of 100.6 MHz.

The detailed steps about ^{13}C ssNMR spectra technique was reported in another study (Mowery *et al*., 2007).

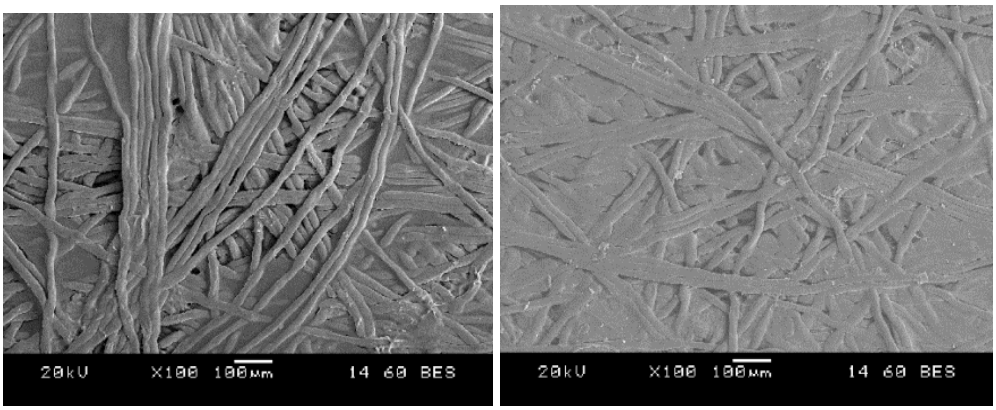

(a) **(b)**

Figure 2.2. SEM at a magnification of 100 of the membrane surface of (a) PAN; (b) PVDF.

2.5 Result and discussion

2.5.1 DFT Theoretical Analysis

2.5.1.1 Geometry optimization of PVDF and PAN membranes

The structure of PVDF and PAN membranes were likewise optimized with B3LYP approach and implementing a 6-311+G*basis set, without initial symmetry restrictions and with the assumption of C1 point group, as outlined in Figure 2.3. In this case, the energy gape of the two frontier orbitals of PAN and PVDF are -211.01 and – 224.42 eV, respectively.

The PVDF has different possible conformations including α-phase and β-phase with C–F bonds polar bond that features the highest dipole moment. The data indicates that the polymer's dipole alignment is in the identical direction as in β-phase of PVDF, while they are in opposite directions in α-phase of PVDF, as shown in Figure 2.4 (Fedorov *et al*., 2007). In this study the α-phase of the PVDF was used since it has marked properties in terms of chemical resistance, thermal stability, and process ability for forming membranes (Fujimura et al., 2010, Ohno *et al*., 2011, Gordon *et al*., 2005, Parr *et al*., 1989). Ligand's optimized geometry in the gas phase was again re-optimized with the polarized continuum model (PCM) by incorporating the solvent effect (e = 78.35).

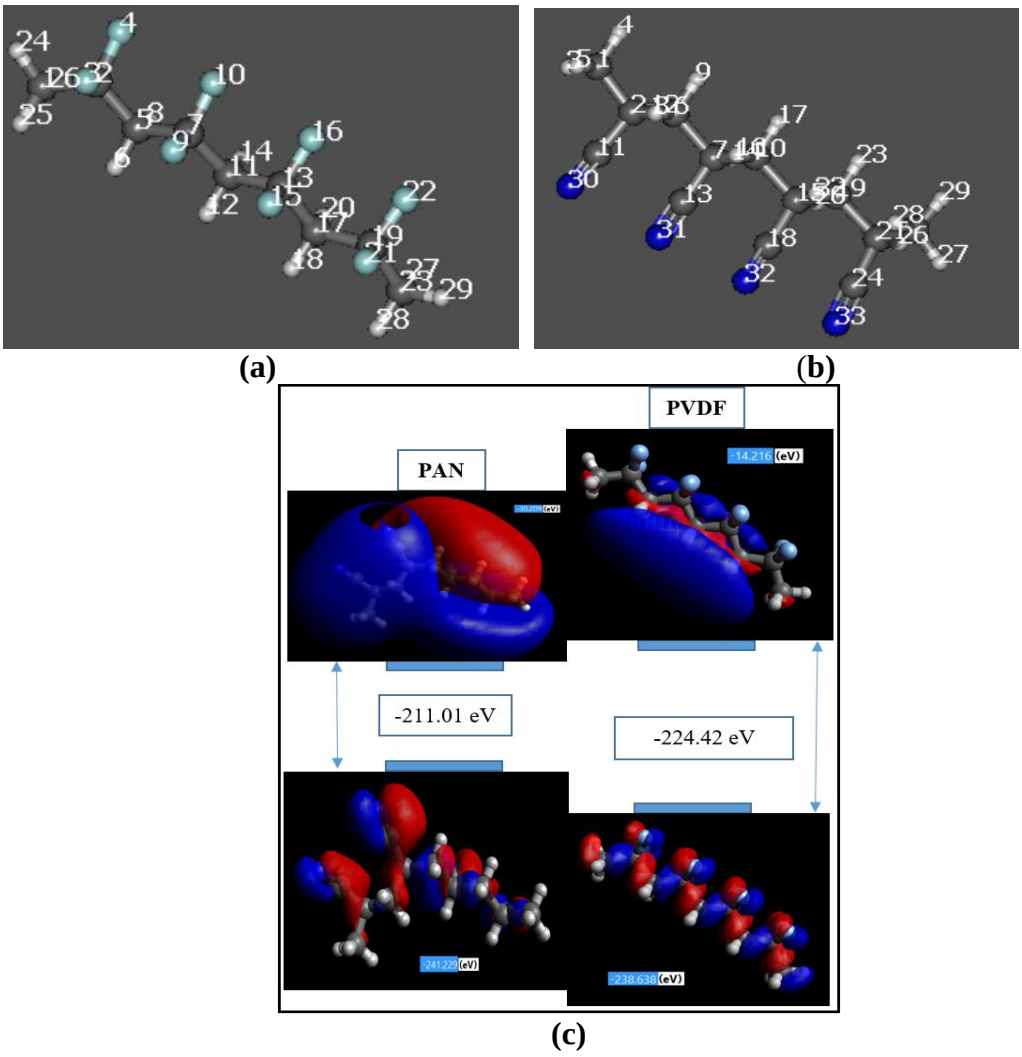

Figure 2.3. (a) Optimized structure of PVDF; (b) Optimized structure of PAN (Carbon in grey, Hydrogen in white, Nitrogen in blue, and Fluorine in green) with atom numbering; and (c) level of energy gap between HOMO and LUMO of membrane oligomers.

Within this dynamic, Tomasi's polarized continuum model describes such type of cavity as the union of a series of interlocking atomic spheres. The corresponding outcome of the solvent continuum polarization is characterized numerically.

2.5.1.2 Influence of Solvation Model of PAN and PVDF Oligomers

The interactions between hydrophilic and hydrophobic membranes and water molecules can lead to either a presence of dissolution or an absence of dissolution in water, respectively. During modeling complexes, the setup took into account that oligomers can be both a donor and an

acceptor of protons. First we calculated the complexes of PVDF and PAN with one water molecule (1:1). The hydrogen bonding formed between the hydrophilic part of oligomers and the water molecules is presented in Figure 2.5 The C≡N and C-F function group created a hydrogen bond with one water molecule as shown in Figure 2.5. However, the hydrogen bond was stronger in the case of PAN compared to PVDF with an interfragment distance of 2.3 and 2.43 angstrom, respectively.

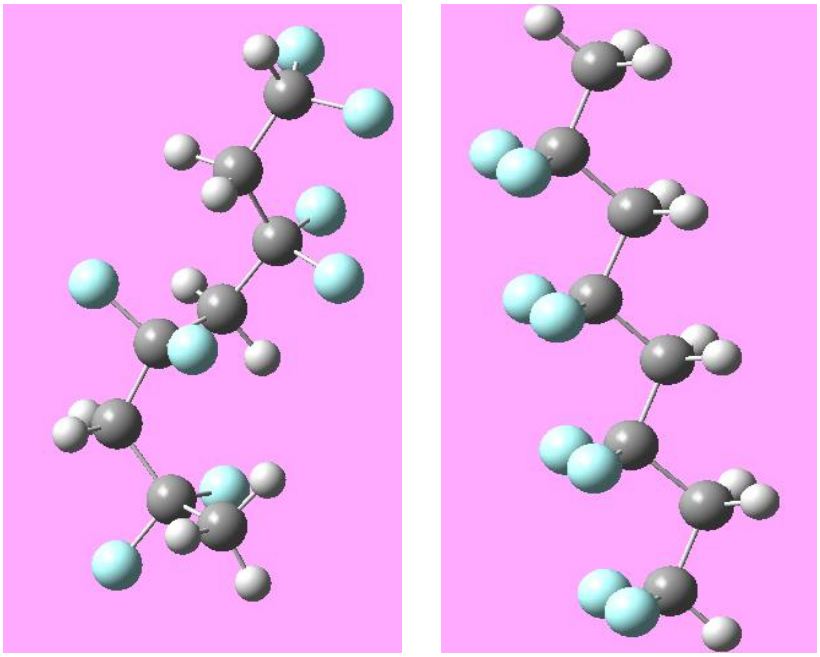

Figure 2.4. Schematic structure of the polymeric PVDF membrane (a) α-phase; and (b) β-phase.

This can be attributed to the fact that the hydrophilic C≡N of PAN has thermodynamically favorable interactions and features the formation of strong hydrogen bonds with water more than C-F, as shown in Table 2.1. PAN and PVDF optimized structures have energies of interaction -3029.23 and -4808.5 kJ/mol, respectively, and suggest that PVDF has a lower tendency to interact with water molecules. In addition, the energy gap level occurring between the highest occupied molecular orbital (HOMO) of PAN containing electrons and the lowest unoccupied molecular orbital (LUMO) that does not contain electrons are: -241.22 eV and -30.21 eV, respectively. Notably, the HOMO and LUMO of PVDF were -238.64 eV and -14.216 eV, respectively. Therefore, the energy gap of the two frontier orbitals of PAN and PVDF are -

211.01 eV and -224.42 eV, respectively, as illustrated in Figure 2.3 (c), reflects the higher kinetic stability and lower chemical reactivity of transition complexes of PVDF when compared to PAN. It was essential to experimentally increase the number of water molecules gradually to 2, 4, and 6 water molecules so as to investigate how the water molecules will be able to form hydrogen bonds with each function polar group of the membrane oligomers.

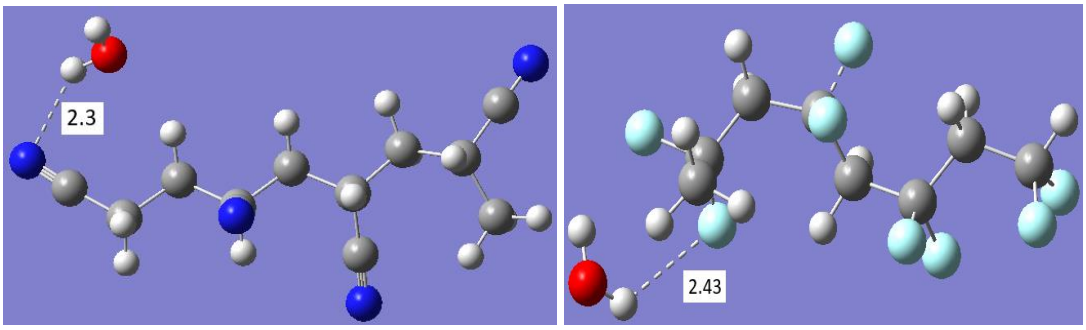

(a) **(b)**

Figure 2.5. Complexes with water (1:1) (a) PAN. H_2O; and (b) PVDF. H_2O

A comparative assessment of ΔG (298 K) and ΔH (298 K) interactions between the PVDF.4H_2O and PAN.4H_2O models in gas phase and solvent phase at B3LYP/6-311G* basis set level of theory was presented in Table 2.1. The free energy and enthalpy of interactions happening between solute and solvent have been assessed for the PAN.4H_2O and PVDF.4H_2O models in solvent phase and then related to the free energy and enthalpy of interaction in a model with the same PVDF.4H_2O and PAN.4H_2O complexes in gas phase. This comparison shows that the variance in enthalpy and Gibbs free energy between the PVDF.4H_2O solvent phase model and PVDF.4H_2O gas phase model were insignificant, further indicating that there are supplementary direct H-bond interactions in the PVDF.4H_2O model. These extra direct H-bond interactions are caused by the water molecules situated above and below the plane and demarcated by the PVDF.4H_2O model. On the other hand, the significant increase in the enthalpy and Gibbs free energy indicates a destabilization of the system from the PVDF.4H_2O in gas phase to the PVDF.4H_2O model in solvent phase. This escalation outlines the hydrophobic interactions between the PVDF and solvent, in comparison to PAN.

As part of the experiment, the once optimized ligand geometry in the gas phase was then re-optimized by carefully examining the solvent's effect (ε = 78.35) with the help of polarized continuum model (PCM). As noted earlier, polarized continuum model developed by Tomasi

sums up the cavity as a collection of interlocking atomic spheres. In this case, the consequences of solvent continuum polarization process are represented numerically.

Table 2.1. Comparison of ΔG (298 K) and ΔH (298 K) of interactions between the PVDF.4H_2O and PAN.4H_2O models in gas phase and solvent phase at B3LYP/6-311G^+ level of theory.

	ΔG(kJ/mol, 298 K)	**ΔH(kJ/mol, 298 K)**
PVDF.4H_2O (Gas)	28.06	179.40
PVDF.4H_2O (solvent)	27.98	122.56
PAN. 4H_2O (Gas)	300.46	167.35
PAN.4 H_2O (Solvent)	-205526.92	-205643.26

The specific configuration change in solute molecule of the PVDF·4H_2O complex is made available in Figure 2.6 (a). As the figure indicates, there is a small change in conformation when examining solvent effects for PVDF, and a slight change when adding interacting water molecules, a dynamic that will be considered in the hydrophobic polymeric membranes study. PAN exhibited a substantial conformation of the configuration PAN.4H_2O complex interacting with water molecules, in comparison to PAN in gas phase and solvent as shown in Figure 2.6 (b). This is a substantial change in conformation, and will be established in relation to hydrophilicity of PAN membranes and their tendency to water transport.

2.5.1.3 Membrane Oligomers Interactions with Water Molecules

Table 2.2 included only the hydrogen bonding parameters between membrane model and water molecules, and not the water cluster, in order to emphasize the difference between the interactions occurring within the function groups of the oligomers and water molecules. According to the GAMESS computations performed, the PAN complex with one water molecule has a bond length (N_{30}…HOw) of 2.30 Å and the angle φ (N_{30}…HOw) is 140.01˚, while the hydrogen bond lengths (F_3…HOw) of complex PVDF with one water molecule is 2.43 Å and angle is (F_3…HOw) 118.09˚, as indicated in Table 2. The optimized structures of PAN and PVDF complexes with 2, 4, and 6 water molecules are included in Figure 2.7 and Figure 2.8 respectively, while the calculations of hydrogen bridge parameters for the oligomer complexes are presented in Table 2.2. When the number of water molecules was increased in PVDF oligomer model the number of hydrogen bonds was amplified, but to a lesser extent than in PAN.

The hydrogen bonding between N and H_2O are stronger compared to PVDF with the average hydrogen bonding length varying from 2.10 Å to 2.47 Å, respectively.

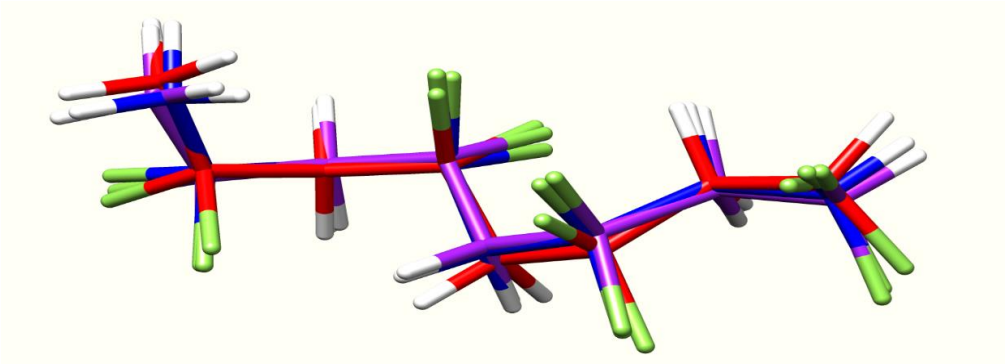

(a)

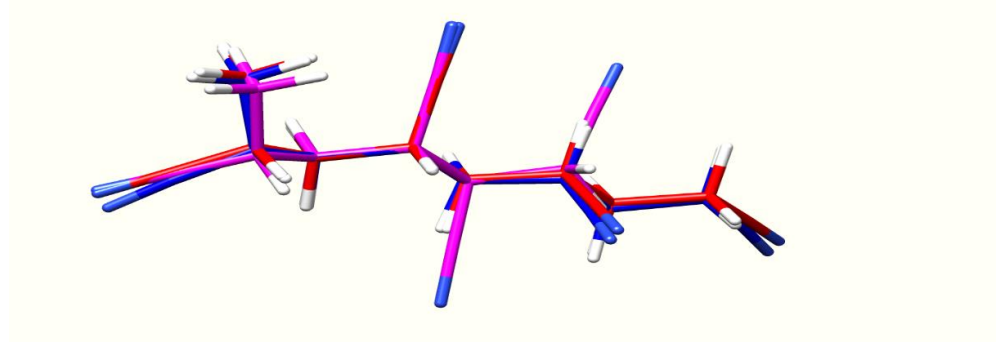

(b)

Figure 2.6. Change in conformation (a) PVDF between the gas phase calculation (blue), solvent effect (purple), and interaction with four water molecules (using polarized continuum model (PCM) (red); (b) PAN between the gas phase calculation (blue), solvent effect (red), and interaction with four water molecules (using polarized continuum model (PCM) (purple).

This data is connected to the subsequent creation of hydrogen bonds between water and PAN molecule, since after breaking hydrogen bonds between the water molecules the conditions become energetically favorable. The calculations showed that the most stable complex turns out to be the PAN complex that forms hydrogen between N and water molecule bonds N_{30}…HOw (O_w of water), as outlined in Figure 2.7.

The reason for hydrogen bond stability can be linked to the lower energy of this bond if compared to the other hydrogen bond CH_{14}…Ow (CH of PAN and O_w of water). As a consequence, the influence of water solution leads to a change in the lengths of hydrogen bridges. It should be noted that, the interaction of PAN with water led to the creation of stable

water clusters formed between PAN and water molecules, which played an important role in their activity. On the other hand, in case of PVDF oligomer model, the angle decreases from 134.51° to 131.17 °, for PVDF complexes with four and six water molecules, respectively. These changes in the hydrogen bridge parameters can be facilitated by the favorable interactions between the six water molecules, and that in turn lead to the formation of water cluster instead of attaching themselves to fluorine atoms (Figure 2.8(b) and Figure 2.8(c)). This switch to a weaker hydrogen bond was confirmed by the calculation results of the PVDF hydrogen bridge parameters with six water molecules.

Thus, PVDF indicated hydrophobic properties through the favorable water cluster formation, which improved the interaction of water molecules with PVDF. Therefore, the angular component of the hydrogen bridge, φ, was decreased when PVDF interacted with six water molecules instead of four. In addition, the hydrogen bond lengths for PVDF complexes with water molecules are greater than those occurring in PAN complexes with water molecules. The investigation of PVDF hydrophobicity proved difficult since it involved a simultaneous presence of the hydrophobic and hydrophilic structural components, such as CH bonds which are a hydrophobic surface and the hydrophilic centers that are the Fluorine heteroatoms. Fluorinated compounds showed negative entropies of aqueous solvation because of the water molecule's predisposition toward structuring the hydrophobic portions of the PVDF (Barone et al., 1998; Alexeev *et al*., 2012). It was determined that PVDF polar fluorinated hydrocarbons in the gas phase function as hydrogen-bond acceptors, while forming hydrogen bonds that are around half the strength potential of hydrogen bonds created using water molecules from the same proton donor (Abboud *et al*., 1994). The hydrophobic property of PVDF is thus related to the properties of the hydrate shell effect (Kobayashi *et al*., 1975).

The overall energy of hydrogen bond F…OH and N…OH is shown in Table 2.3. It shows specific energy values for the hydrogen bond OH…N and F…OH as being 42.36 kcal/mol and 259.63 kcal/mol. The hydrogen bond energy value between F and water molecule of PVDF was larger, compared to the hydrogen bond energy occurring between N and water molecule of PAN. The specific hydrogen bond energy interacting with the four water molecules was calculated as follows: ΔE_{HB} PAN. $4H_2O$ = EPAN. H_2O –$4EH_2O$-EPAN and ΔE_{HB} PVDF.$4H_2O$ = EPVDF.H_2O – $4EH_2O$ – EPVDF, for PAN and PVDF respectively.

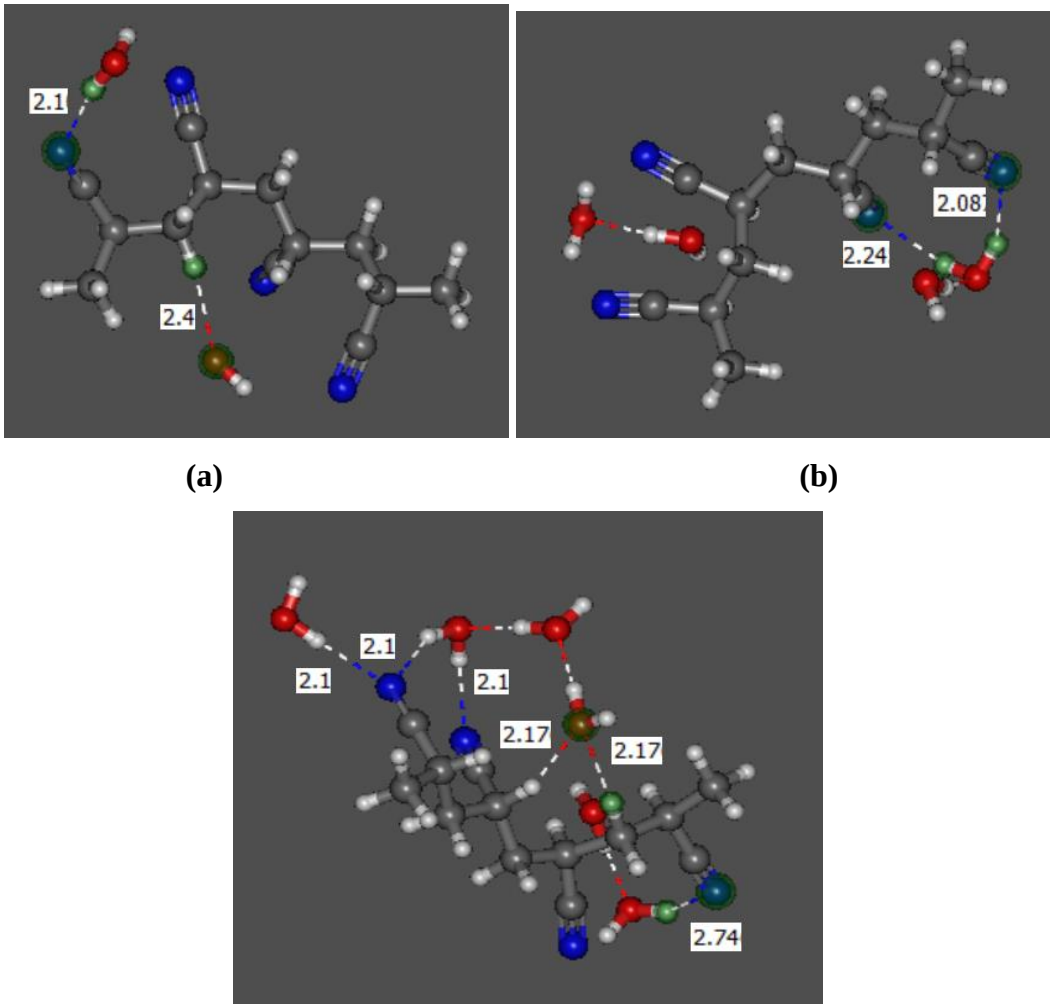

(a) **(b)**

(c)

Figure 2.7. Structural schemes of PAN complexes with water molecules at the B3LYP/6-311+G* level of theory: (a) two molecules of water; (b) four molecules of water; and (c) six molecules of water.

The energy values collected suggest that the PAN.4H_2O complexes are relatively more stable than the water complexes with PVDF, and as a consequence these PAN.4H_2O complexes are favored during the interactions with water. Once the number of water molecules was added around PAN, the interaction with water was easier to achieve than the higher values of energy in PVDF. This can be attributed to the significant increase in energy ΔE_{HB} PAN. 4H_2O compared to ΔE_{HB} PAN. On the other hand, PVDF showed a limited increase in energy ΔE_{HB} PVDF. 4H_2O compared to ΔE_{HB} PVDF. The substantial increase of PAN energy with water complexes is a sufficient signal that there is an ongoing formation of a strong hydrogen bond with water molecules, in turn confirming the hydrophilicity of PAN during the interactions with water. It

should be pointed out that in addition to the strength of hydrogen bond, the increase in the number of water molecules did not significantly amplify the number of hydrogen bonds in PAN compared to PVDF, as shown in Table 2.2.

Table 2.2. Comparison of Energy (kcal/mol), hydrogen bond, length (*l*, Å), angle (φ, deg) of hydrogen bridges and dipole moment (μ, D) in polymeric PAN and PVDF complexes

	Hydrogen bond between Membrane Model and Water Molecules		**Energy [kcal/mol]**		**Parameters of Hydrogen bridge**				**Dipole moment μ [D]**	
	PAN	PVDF	PAN	PVDF	PAN		PVDF		PAN	PVDF
					l [Å]	Φ [°]	*l* (Å)	Φ [°]		
1	N_{30}…HOw	F_3…HOw	12.77	231.04	2.30	140.01	2.43	118.09	12.6	14.2
2	N_{30}…How	F_3…HOw	17.01	240.63	2.1	144.27	2.37	126.69	13.1	15.2
	CH_{14}…Ow	F_{10}…HOw			2.4	172.07	2.47	135.53		
4	N_{30}…How	F_3…HOw	42.36	259.63	2.08	156.17	3.09	134.51	13.7	17.6
	N_{31}…HOw	F_{15}…HOw			2.24	153.02	2.29	158.45		
6	N_{30}…HOw	F_{16}…HOw	49.86	254.11	2.10	168.15	2.27	131.76	15.2	17.6
	N_{30}…How	F_{21}…HOw			2.10	147.57	2.27	142.03		
	N_{31}…HOw	CH_{29}…Ow			2.1	170.94	2.1	166.95		
	CH_{14}…Ow				2.17					
	CH_{23}…Ow				2.17					
	N_{33}…HOw				2.74					

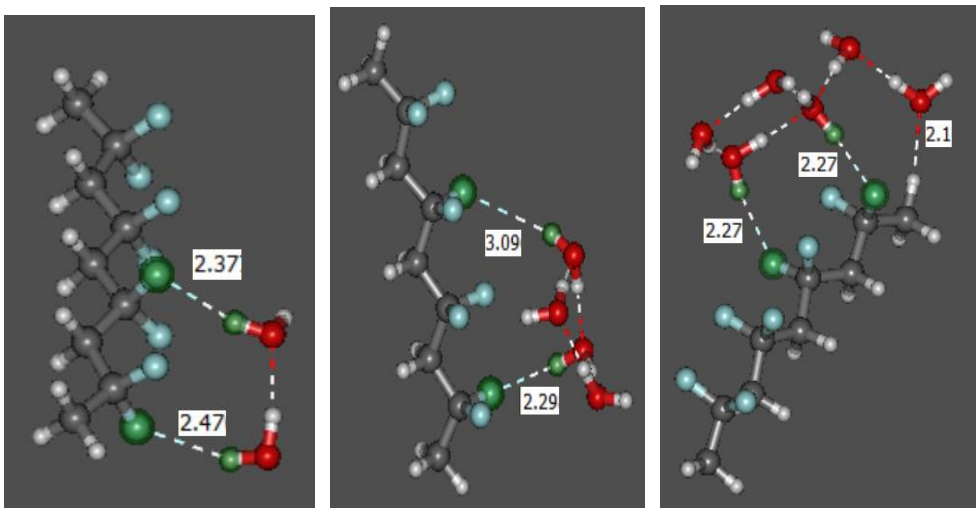

(a) **(b)** **(c)**

Figure 2.8. Structural schemes of PVDF complexes with water molecules at the B3LYP/6-311G* level of theory: (a) two molecules of water; (b) four molecules of water; and (c) six molecules of water.

Furthermore, as indicated in Table 2.2, electronegative atoms of nitrogen in PAN are disposed in a manner such that the dipole moment of complex surrounding PAN with water molecules changes substantially. For the isolated PAN, the value of dipole moment, μ, was 11.5 D. Therefore, the respective values of dipole moments for complexes 1:1, 1:2, 1:4, and 1:6 were 12.6, 13.1, 13.7 and 15.2 (Table 2).

An additional increase in the water molecules practically changed the size of the complex dipole moment. In fact, the dipole moment is connected with a definite orientation of dipoles near the electronegative atoms of PAN and the structure of hydrogen bonds. The direction of the water molecules displacement surrounding PAN favors pulling the PAN molecules into the water solution and, as a result, is determined to have high hydrophilicity at room temperature. On the other hand, the results of PVDF dipole moments show that the C–F bond is non-polarized. Consequently, the C–F bonds reduced the molecular polarizabilities by improving the carbon framework's hardness characteristic. Therefore, the C–F bond of PVDF is considered as a hard Lewis base. Furthermore, an increase of the number of water molecules in complexes with PVDF leads to an insignificant dipole moment change. The isolated PVDF value of the dipole moment, μ, was 14.2 D. When one water molecule was added (1:1), the dipole moments did not show any change and remained at the same value of 14.2 D. A small increase occurred from 15.2 D and 17.6 D for complexes 1:2, 1:4, respectively.

However, during the dipole moment of the complex for 6 the water remained the same as water for 4 at 17.6 D. The insignificant change in the increase of water molecules led to the formation of water clusters instead of interactions with fluorine atoms of PVDF. In this dynamic, the peculiarity of hydrophilic centers disposition in a PVDF molecule does not intend to drag water molecules, determining the low hydrophilicity of PVDF at room temperature.

2.5.1.5 PIEDA Analysis for PAN Hydrophobicity

The goal of PIEDA Analysis is to comprehensively define intramolecular non-covalent interactions in PAN and PVDF membranes with water molecules, as well as provide a reference for an improved understanding PVDF hydrophobicity, compared with PAN by using FMO and PIEDA. The non-covalent interactions are generally assumed to be composed of polarization, charge-transfer, Coulomb, and dispersion attractive forces, which are in turn countered by a repulsive force rising because of the electronic wave functions and its quantum nature. In order to have consistently accurate results and an improved understanding of the types of interactions occurring between PVDF and PAN with water, geometry optimizations were performed with standard FMO, for PAN and PVDF with six water molecules with FMO-RHF/6-31+G* level of theory by GAMESS and Gabedit viewer, as presented in Figure 2.9. Both PAN and PVDF structures showed the same number of hydrogen bonding with water molecules. The interactions were noncovalent in nature for all of the experimental fragmentation schemes. The results indicated that the interactions between PVDF and water molecules are much stronger in terms of bond length than in PAN interactions with the water environment. PAN showed bond lengths of 1.96, 2.12, and 2.46, while PVDF indicated bond lengths of 1.89, 1.98, and 2.07. These results confirmed that PVDF does have hydrogen bonding and interactions with water, however the data also raises questions about the types of interactions that can occur between PVDF and water molecules.

We selected water clusters $(H_2O)_n$ because they offer greater charge transfer, interaction, and coupling terms (n = 2, 4, 6). Due to the fact that the EDA application in GAMESS involves Cartesian d-functions (6d), we likewise applied cluster n=6 during the PIEDA calculations. In order to enable an effective comparative analysis with PIEDA we turned off all FMO approximations, and the resulting data is available in Table 2.3. Figure 2.10 shows that the

interactions between water molecules and the PAN and PVDF membranes are decomposed by PIEDA.

Each pair interaction was labeled based on its primary attractive force interaction component, electrostatic (E), charge transfer (C), or exchange-repulsion (E). The relevant data on PAN and PVDF membranes and their respective interactions with water molecules are provided in Table 3, and it should be noted that only major interactions are included.

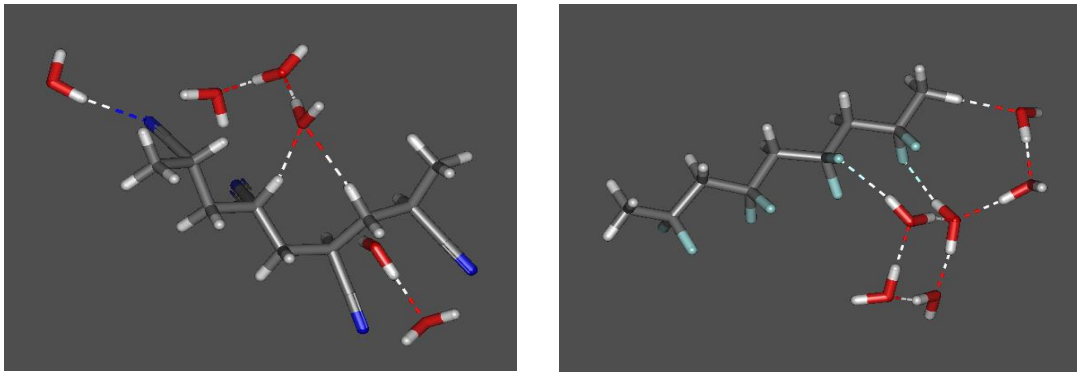

(a) **(b)**

Figure 2.9. FMO optimization of a) PAN and b) PVDF with six water molecules, calculated with FMO-RHF/6-31+G* level of theory.

Once a comparison between PVDF and PAN engaging in interactions with water environment was conducted, we realized that PAN shows 3 usual and 2 distorted hydrogen bonds with six water molecules which are supplemented by several sizable electrostatic interactions (-33.192), as shown in Table 2.3.

Some hydrogen bond energies obtained were strong. Alternatively, in the case of PVDF, 3 usual, and 6 distorted hydrogen bonds were accompanied by electrostatic interactions (-20.066), with the results that are lower than for PAN. The main influence on the interaction energy for PAN and PVDF is the electrostatic term that controls the sign and magnitude values of the overall interaction energy. Specifically, the total interaction energy for PAN with six water molecules was greater than that of PVDF, -31.58, -18.85 kcal/mol respectively, resulting in more interactions between water and PAN. However, the other contributions to the PAN and PVDF interactions, such as charge-transfer and exchange, are likewise notable. Robust electrostatic interaction for PAN can be facilitated by the process of hydrogen bonding occurring between PAN and water.

It is curious to note that, despite a more dipole moment of PVDF and polar groups, electrostatic interactions in Figure 2.10 (b) and table 3 are showing lower attraction, or even repulsion for PVDF, thus indicating that at least some electrostatic repulsion is happening between PVDF and water molecules. The exact charge transfer amount value is within the typical range for hydrogen bonding, between 0.02–0.03 a.u. Charge transfer between PAN and water is more than the charge transfer occurring with PVDF. There is no significant difference between charge transfer for PAN (-15.269) and PVDF (-12.175), while the energy charge transfer for PVDF is noteworthy and can be attributed to polar groups in PVDF.

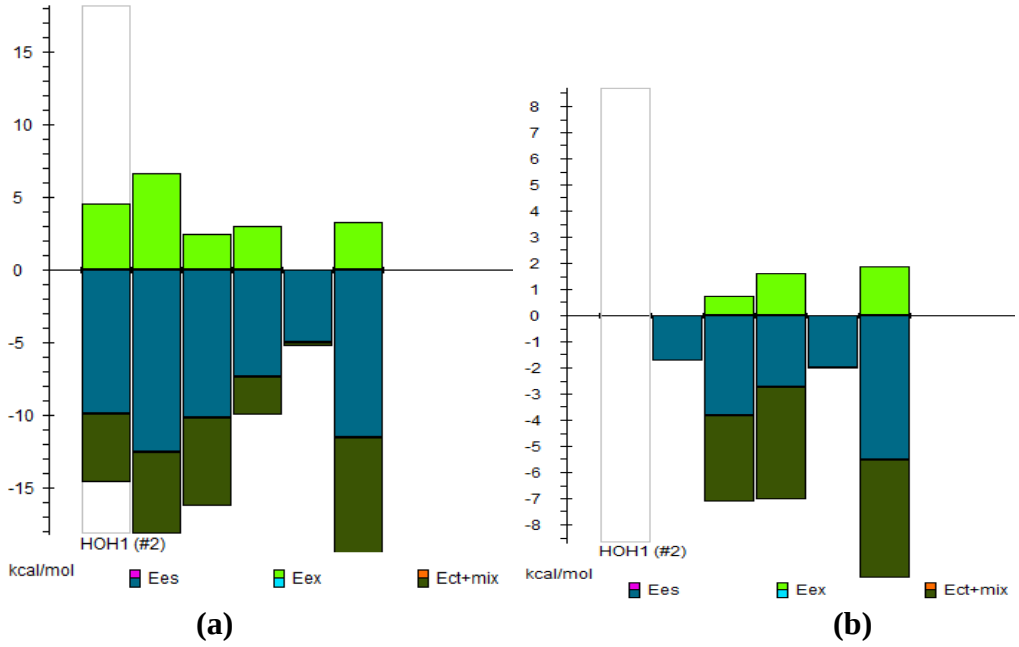

Figure 2.10 Energy contributions (PIEDA) of each intermolecular interaction for a) PAN and b) PVDF with six water molecules, calculated with PIEDA/6-31G*. The pair interaction energy is separated into the electrostatic (ES), exchange-repulsion (EX), and charge-transfer plus higher order mixed terms (CT+mix) contributions.

To properly interrogate the relative stabilities of PAN and PVDF, we compared energy values of Exchange-repulsion as given in Table 2.3. The pair interactions in PAN -33.19 kcal/mol, compared with -20.06 kcal/mol in PVDF that show more hydrogen bonding sites, suggests that there is a tendency in PAN to favor water more (by 13.3 kcal/mol). The dipole moment for PVDF, compared with PAN, indicates that the electrostatic interaction is anticipated to be greater in the PVDF, because it has more fragment dipole instances and provides the shortest distances

between its fragments. Remarkably, PAN offers a more widespread hydrogen bonding and as such augments the electrostatic, charge transfer energy, and exchange potential. Experimental results of the exchange-repulsion energy confirmed that the interaction between PAN and water is more stable. Summing up the collected research data and its implications, PAN and PVDF result in the following relative stabilities. The PVDF structure is more destabilized by exchange-repulsion energy (4.18 kcal/ mol). The electrostatic gain due to the intramolecular interactions is greater by -33.19 kcal/mol, the exchange value is larger by 10.82 kcal/mol, and the charge transfer energy gain is bigger by -15.27 kcal/mol for PAN with six water molecules. In fact, the PVDF features a large charge transfer that can be attributed to the polar groups and extensive hydrogen bonding in its structure.

The results also showed electrostatic interaction that can be related to van der Waals interactions with water. As a result, the Fluorine has much greater electronegativity than C, N or even O, but the covalent bond of C-F is stronger than C-N, which is harder to break and interact with water. The energy of the polar covalent bond of C-F and C-N is 485 kJ/mol and 293 kJ/mol. Consequently, the water prefers to cluster together with hydrogen bonding instead of breaking the C-F polar covalent bond as shown in Figure 2.11.

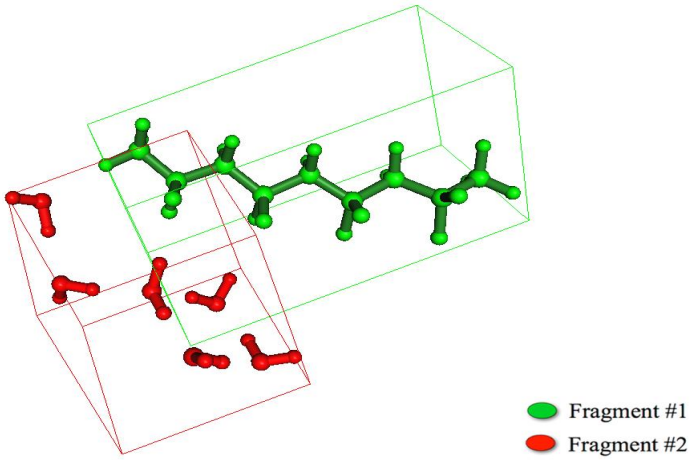

Figure 2.11. Fragmentation of water molecules interacted with PVDF membranes, calculated at FMO-RHF/6-31G* level

In cases where solutions are involved experimentally, the additional work of cavities forming, in order to adapt to the needs of fluorocarbon, and in comparison to a hydrocarbon, is not balanced out though the enhanced energy interactions with water. In particular, the better hydrophobicity of fluorinated surfaces occurs because of the fluorocarbons being packed less

densely on the surfaces and thus causing lower number of van der Waals interactions with water. Our research indicates that the interactions between water and a hydrophobic solute or surface are primarily dependent on the van der Waals interactions and as a result are mostly independent from electrostatic interactions. Such independence is triggered by the tendency of room temperature water to keep its hydrogen bonding network structure whenever the interface lacks hydrophilic sites.

Our research suggests that the reason behind higher hydrophobicity of fluorocarbons versus hydrocarbons is determined across geometries by their sizes. The dispersion forces linked to fluorocarbons are lower than might be anticipated due to the atomic size. This effectually implies that the free energy of hydration located on these surfaces is more receptive to alterations in Lennard-Jones interactions, than it might be to the electrostatic interactions.

Table 2.3. Comparison of PIEDA output analysis for the system of PAN and PVDF membranes interacting with six water molecules (b) calculated at FMO-RHF/6-31G* level (Energies in kcal/mol).

Membranes with six Fragments	**E (total pair interaction)**	**ES**	**EX**	**CT+mix**	**E_{ij}-E_i-E_j**	**dD_{ij}*V_{ij}**
PAN	-33.192	-28.739	10.818	-15.269	-31.58	-1.611
PVDF	-20.066	-12.078	4.188	-12.175	-18.855	-1.211

Table 4 represents Merz-Kollman charges (MK) calculated for PAN and PVDF membranes. PAN showed an increase in the charge distribution due to HB between N and water molecules, compared to PVDF which had a weaker interaction between F and water molecules. In addition, the Solvation Accessible Surface (SAS) was compared for PVDF and PVDF in interaction with water and PAN and PAN in interaction with water, it was found that SAS of PDVF was decreased in value from -0.169 to -0.385, due to the hydrophobicity nature, while it was increased for PAN from -0.128 to -0.09.

The greatest occupied molecular orbital (HOMO) of PAN in interaction with water containing electrons and the lowest type of unoccupied molecular orbital (LUMO) that does not have electrons are -11.18 eV and -23.69 eV, respectively. While the HOMO and LUMO of PVDF in interaction with water were -218.87 eV and -9.4 eV. As a result, the energy gap between the two

frontier orbitals of PAN and PVDF are -12.51 eV and -209.47 eV, respectively. This data reflects the higher kinetic stability and lower chemical reactivity of PVDF transition complexes if compared to PAN, as shown in Figure 2.12. Furthermore, the energy gap of PVDF before interaction with water molecules, and PVDF after interaction with water molecules, had insignificant change from -224.42 eV to -209.47 eV, as shown in Figure 2.3 and Figure 2.12, respectively. On the other hand, the energy gap of PAN before interaction with water molecules, and PAN after interaction with water molecules had a significant change from -211.01 eV to -12.51 eV, as shown in Figure 2.2 and Figure 2.12, respectively. This attributed to the high charge transfer in case of PAN (–CN), compared to PVDF (–CF).

Table 2.4. Merz-Kollman charges (MK) calculated for PAN and PVDF membranes

Atom	**PAN**	**PAN.6H_2O**	**Atom**	**PVDF**	**PVDF.6H_2O**
N2	-0.284657	-0.338484	F7	-0.320915	-0.334552
N15	-0.255477	-0.349620	F13	-0.316132	-0.316132
N30	-0.262619	-0.344861	F19	-0.287512	-0.338479
			F25	-0.291548	-0.305826
			F26	-0.291736	-0.333560

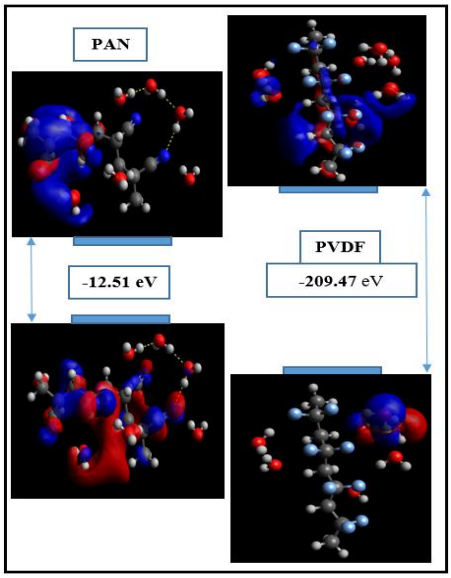

Figure 2.12. Presentation of the energy levels gaps, HOMO–LUMO, of PAN and PVDF

2.5.2 Experimental Analysis

2.5.2.1 Confocal Microscope Analysis

Figure 2.13 represents the confocal microscope images of PAN and PVDF using fluorescent latex beads during the filtration process. The fluorescent latex beads had a zeta potential value of -28.85 mv, that resulted in a greater repulsion force with the hydrophilic PAN membrane featuring zeta potential of -41.5 mv. As a consequence, the fluorescent beads passed through the membrane matrix without significant deposition, as noted in Figure 2.13 (a). On the other hand, the fluorescent latex beads experienced a higher attraction force with the PVDF membrane with the zeta potential of -2.5 mv. A significant deposition of fluorescent latex beads was detected in PVDF membrane displayed in Figure 2.13 (b).

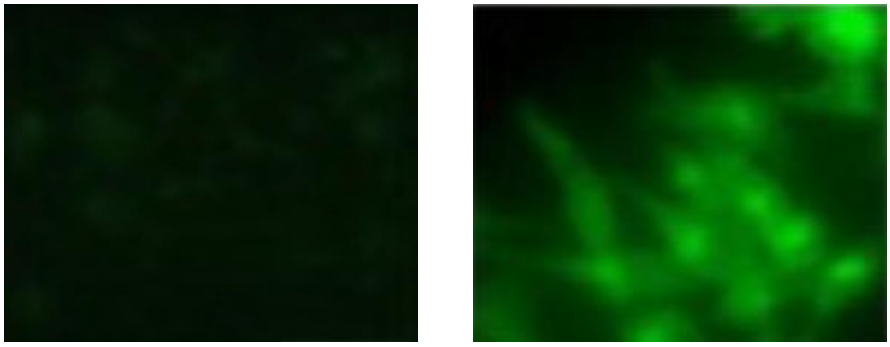

(a) **(b)**

Figure 2.13. Confocal Microspcope images after UF with flurosene latex beads (a) PAN; (b) PVDF

2.5.2.2 FTIR-ATR spectra

Further analysis included experimental FTIR-ATR spectra of PVDF and PVDF with water and also PAN and PAN with water. Figure 2.14 (a) portrays the experimental FTIR-ATR absorption spectra values of PAN and PAN with H_2O complex. Pure PAN membranes displayed the standard nitrile (C≡N) peak at 2269 cm^{-1}, C–H stretching at 2930 cm^{-1} (Hannon *et al*., 1969). The C≡N peak indicated a substantial change in PAN.H_2O, caused by the stronger hydrogen bonding between PAN and water molecules. The manifested hump at 3239 cm^{-1} in the PAN.H_2O membrane can be connected to the OH groups occurring in water molecule and the high water and PAN interaction. It is shown that hydrogen bond interactions occurring between hydroxyl and nitrile functional groups by tracing a change in the nitrile peak, which provides critical data for proving that there is hydrogen bonding happening between OH and C≡N groups.

This bonding impacts the movement of C-C bonds in the PAN because of the CH interactions between CH-groups of the polymer and oxygen atoms of the H_2O. As a result, the detected peak shifts may be connected to the CH–interaction between PAN and water. The experimental FTIR-ATR was conducted to demonstrate the interaction of PVDF with water molecules and compared to pure PVDF. As shown in Figure 2.14 (b), primary typical spectra of the PVDF membrane peaks were located at 2956, 1342, and 1175 cm^{-1}. This data may be explained by the stretching as well as deformation vibrations of C–H and the C–F stretching vibrations (Hannon *et al*., 1969).

The most prominent feature of water spectrum was the adsorption peak at 3317 cm^{-1}, which corresponded to the O–H stretching vibrations. The peaks at 2911 and 2876 cm^{-1} were linked to the presence of C–H bond. In most cases, the band of C–F stretch at 1237 cm^{-1} was shifted to a lower frequency when PVDF interacted with water. These experimental observations directly indicate that there are weak hydrogen bonding interactions happening between water molecules and PVDF. Compared to pure PVDF membrane, the PVDF.H_2O complex indicated that the broad absorption from 3483 to 3218 cm^{-1} is due to the H-bonded between O–H groups of water and F of PVDF. When comparing experimental FTIR spectroscopy results for PVDF and PAN membranes, PAN allowed for intense and wide peaks at 3400 cm^{-1}, shown in Figure 2.14, which suggest that the surface hydrophilicity was perceptibly improved.

In our case, the smallest frequency value can be caused by the H-bonded to O–H group of water cluster, rather than C-F. This group incites broad stretching bands from 3218 to 3500 cm^{-1} due to the relative confusion in the H-bonded structures created and the adsorption of water molecule clusters. In addition, the data shows a less intense band around 1638 cm^{-1} caused by the H–O–H bending. It should be noted that the experimental spectra for either the PAN or PVDF in interaction with water is not comparable with the theoretical one because the theoretical only used a specific number with water which is not the same in the experimental case. However, the theoretical spectra do allow us to become aware of the influences each water molecule makes during the interaction with the polymer functional group. The sturdy and wide bands were noted in case of the hydrophilic CN-PAN with water, while the more fragile and thin bands were present in the hydrophobic CF–PVDF with water. This can correlation can be clarified by the fact that the O–H···N hydrogen bond in hydrophilic PAN is frequently tougher than the analogous O–H···O and C–H···F hydrogen bonds in hydrophobic PVDF.

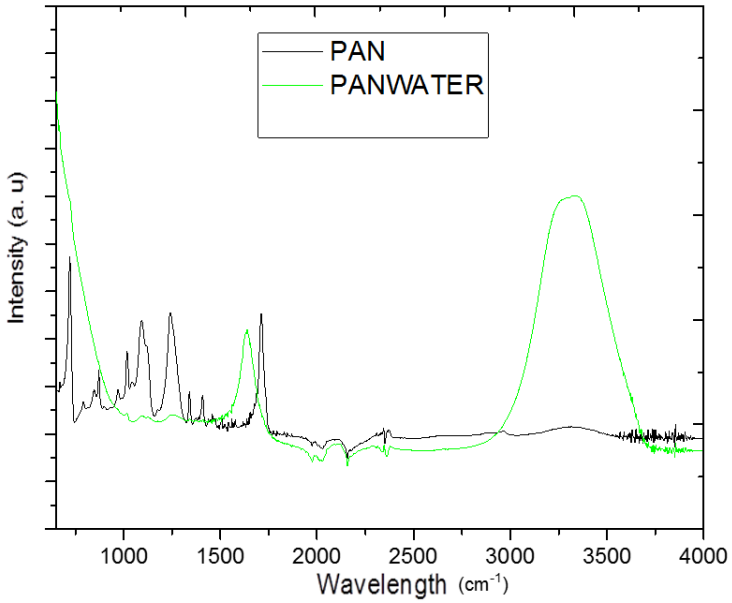

(a)

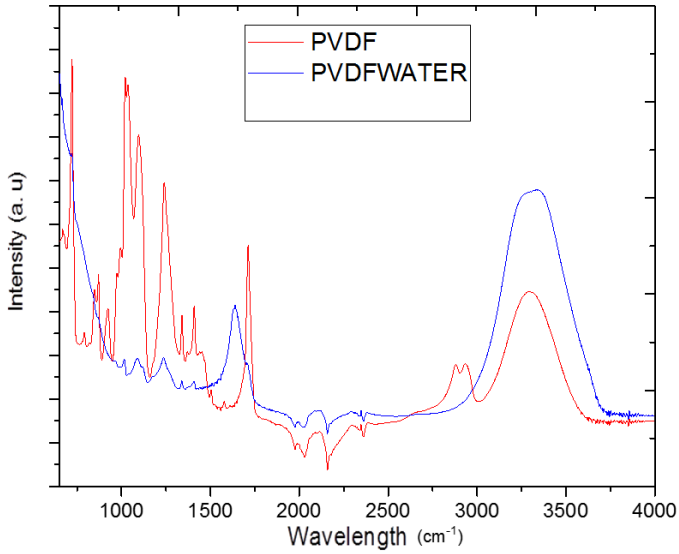

(b)

Figure. 2.14. FTIR-ATR spectra of (a) PAN and PAN.H_2O membranes; (b) PVDF, and PVDF.H_2O membranes.

2.5.2.3 Raman Vibrational Spectroscopy

Detailed information about the conjugated structure and chain skeleton of polymers can be obtained using Raman spectroscopy method. During this experiment, we measured the FT-Raman spectra of polymer-mixed water systems so as to inspect the interaction between PVDF chain and water molecules. From Figure 2.15 (a) we can obtain the data showcasing

gradual changes of the Raman spectra values when the PVDF interacted with water. Figure 2.15 (a) likewise outlines the Raman spectra of PVDF and PVDF/H_2O membranes.

By focusing on the modes at 537, 612, and 854 cm^{-1}, we can then determine that the modes at 537 and 612 can be caused by the CF_2 bending vibration and a combination of CF_2 bending with a CF_2 wagging in phase (Hannon *et al*., 1969; Koening, 1999). Meanwhile the 854 cm^{-1} mode can be defined as an out-of-phase combination of CH_2 rocking and CF_2 stretching type vibrations (Parr et al., 1989). Through a comparative analysis with the pure PVDF membrane spectrum, our experimental results show two new bands (1167 and 1528 cm^{-1}) appearing in the PVDF/H_2O membrane spectrum. The slight decrease of the peaks at 2966 and 1464 cm^{-1} is another instance of spectra change, distinctive of CH_2 bending vibration and CH stretching vibration modes. These changes indicate that there is hydrogen bonding between CH_2 when water molecules attack the PVDF chain structure.

In FT-Raman spectra of PVDF/water there is an outstanding increase in the band growth at 854 cm^{-1} connected to CH_2 rocking, and alternatively the bands at 2972 and 2985 cm^{-1} are assigned to CH_2 symmetric stretching, with their intensities reduced. FT-Raman spectra data reported here allow us to analyze the PVDF-solvent interactions and identify a weak dynamic between hydrogen in the PVDF polymer's methylene group and oxygen in the water molecules. Thus, the existence of hydrophobic PVDF membrane properties in reaction with water was confirmed by Raman spectroscopy.

In Raman spectra Figure 2.15 (b), a PAN-based polymer shows significant changes in Raman shift and intensity, when compared to PVDF engagement with the water molecules. It has been confirmed that PAN not only acts as a polymer matrix maintaining the frame of a polymer, but also participates in water transport. From their vibrational spectroscopic data, water molecules interact with CN groups of PAN chains as well as with other water solution molecules.

Figure 2.15 (b) includes the FT-Raman spectra values of the CN groups stretching mode in the PAN-based fibrous membrane. The CN peaks at around 2275 cm^{-1} in the pure polymer were shifted up to about 2235 cm^{-1} due to the activities between water molecules and the CN groups of PAN.6. The water molecules increased, shown in Figure 2.15 (b), by forming broad band of 2945 cm^{-1}, wave number band connected to the growth of strong hydrogen bonds between water molecules and CN group. Our data reflects that their intensities and positions varied according to the composition of the PAN-based polymer.

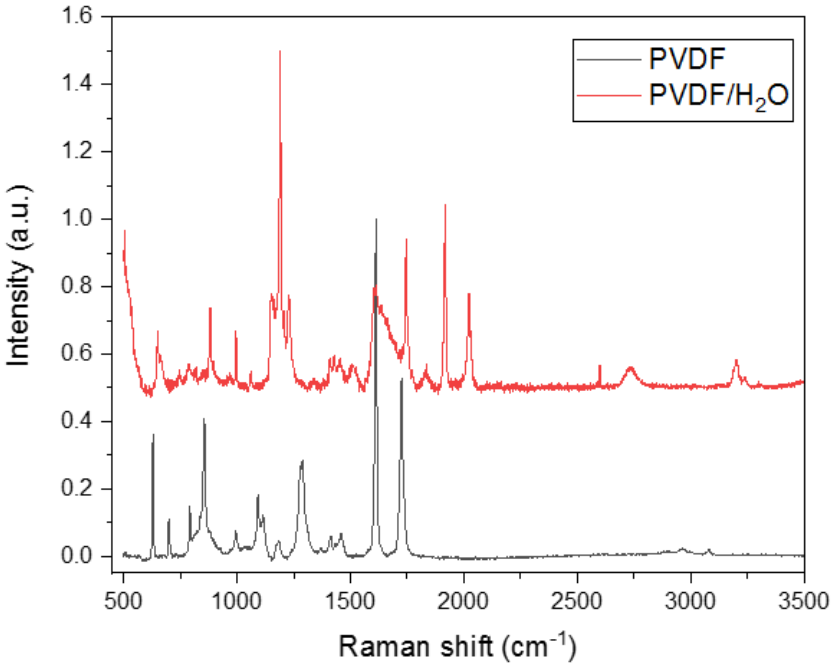

(a)

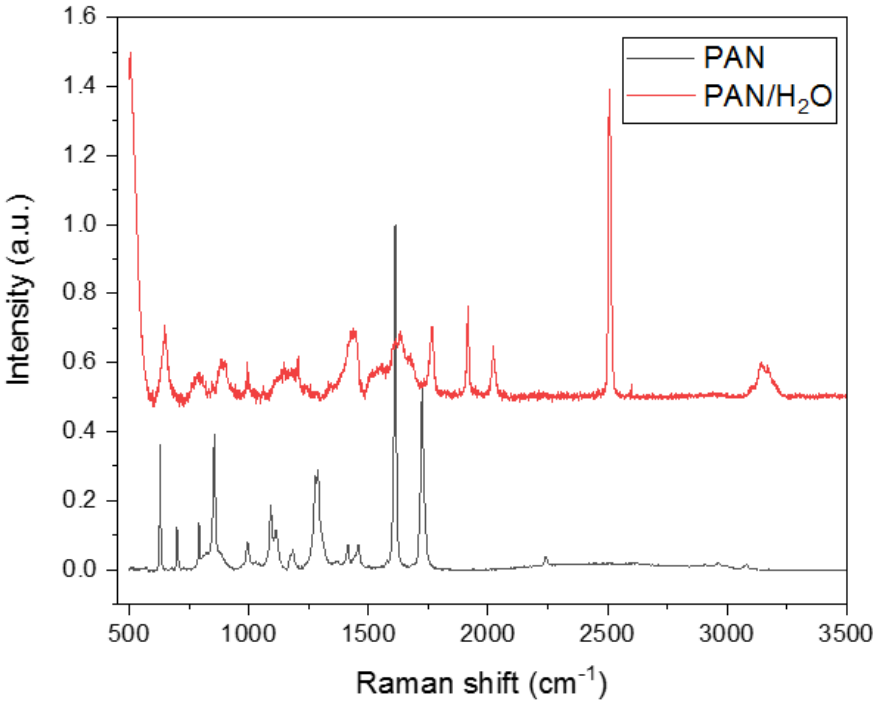

(b)

Figure. 2.15. FT-Raman spectra of (a) PVDF and PVDF-water membranes; (b) PAN and PAN-water membranes.

A PAN-solvent complex was formed from the dipolar interaction between the CN groups of PAN and hydrogen groups of water molecules. When the nitrogen atom of the CN group of PAN attacked the hydrogen atom in water molecules, the electron density around the carbon was enhanced and the CN-H bonding became stronger (Alexeev *et al*., 2012). Moreover, the related vibrational band shifted to a higher-frequency region. Figure 2.15 (b) distinctly showcases strong hydrogen bonding caused by the interactions of water molecules and -CN group of PAN.

2.5.2.4 Solid State NMR study

The solid state NMR technology is frequently used in order to identify and define the interactional behavior between polymers and water molecules. The polymorphism of PVDF, PAN, and their interactions with water were examined with the aid of solid-state nuclear magnetic resonance spectroscopy (Figure 2.16). During the process, the ^{13}C cross polarization magic angle spinning (^{13}C CP MAS) NMR spectra values were documented through the method of simultaneous high power decoupling applied to the proton and fluorine channels. Data shows that there was only one peak happening at 129.3 ppm due to the CF_2 resonance. As indicated in Figure 2.16 (a), two high intensity resonance lines occurred at 129.3 ppm and 42.85 ppm in the CP spectra when decoupling was used for Fluorine and proton.

As a result, these two chemical shifts are assigned to CF_2 and CH_2 resonances. Decoupled cross polarization experiments can be successfully applied to identify Carbon bonded to protons. In this case, two primary resonances for the CF_2 and the CH_2 groups were noted for PVDF. H_2O showed no chemical shift, other than the intensity variations (Mowery *et al*., 2007). There is no difference in the spectra (Figure 2.16 (a)) for neat PVDF and its complex with water, in instances when one decoupling was applied to Fluorine or to Proton for both $^{19}F \rightarrow {}^{13}C$ or $^{1}H \rightarrow {}^{13}C$ CP experiments. Only one peak at 62.73 ppm disappeared after the interaction with water.

Figure 2.16 (b) lists the ^{13}C CP/MAS spectra values of PAN samples C(all), C (1), C (2), and C (3). The first peak for C (1), at 120.25 ppm, as presented in Figure 2.16, is related to the ^{13}C atom on the nitrile group (−CN) (Kobayashi, 1975). Analogously, the peaks at 28.99 ppm for C (2) and at 60.77 ppm for C (3), is connected to the resonance values of the ^{13}C atom in the methylene ($-CH_2-$) and methine (−CH<) groups. The ssNMR spectrum of sample C (all), seen in Figure 16 (b), can be validated by a clear decrease of the relative intensity of peak e (120.25 ppm, corresponding to the unreacted −C≡N groups). This confirms that the majority of the −C≡N

groups on PAN main chain have incited a reaction during their interactions with water. Similarly, at 65 ppm and 105 ppm peaks can be observed declining in Figure 2.16 (b). A sharp peak located at 62 ppm can be clearly differentiated during an interaction with water.

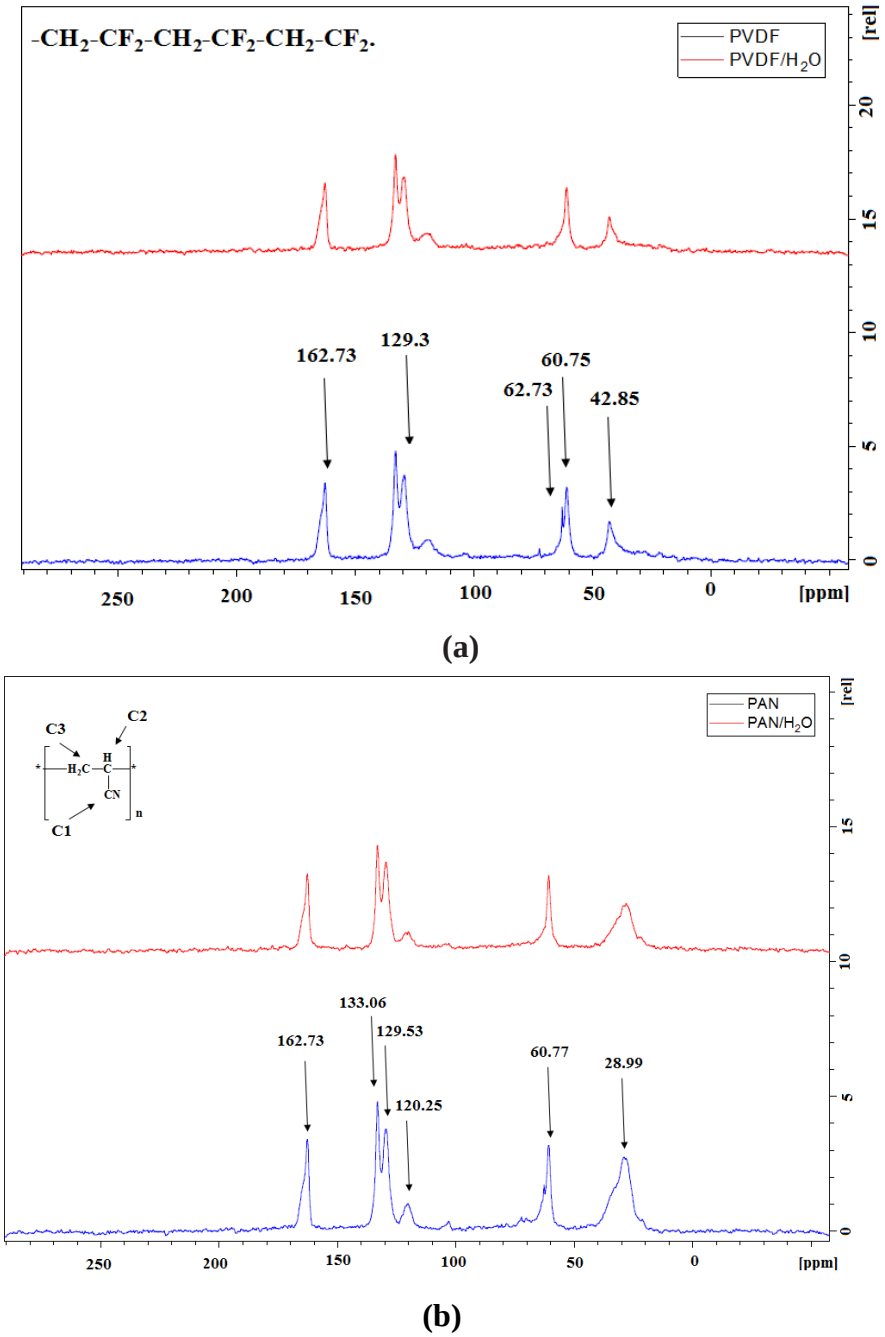

Figure. 2.16. ^{13}C NMR spectra CP MAS experiment decouple for: (a) PVDF and PVDF.H_2O; (b) PAN and PAN.H_2O.

2.6 Conclusion

This study provides an innovative direction, for a more complete, multi-scaling modelling that can open up new avenues for a closer structural examination of PVDF and its characteristics in terms of hydrophobicity during interactions with water molecules. This approach was applied in order to investigate the selectivity and binding of PVDF with water, in comparison to hydrophilic PAN membranes at the molecular level. Within the scope of this study, pair interaction energy decomposition analysis (PIEDA) was used for the FMO calculation program GAMESS and the Facio Viewer. This is one of the first instances when FMO-PIEDA calculations have been implemented for the investigation of non-covalent interactions and hydrophobicity of PVDF, with hydrogen abstraction at a range of sites with water molecules, and in comparison to PAN. Such an improvement permits researchers to better describe non-covalent interactions, when it comes to terms of electrostatic, charge-transfer, exchange-repulsion, dispersion, and optional polarization. This approach also helps to comparatively analyze the interaction energies of hydrophobic PVDF and hydrophilic PAN membranes engaging with water molecules.

The PIEDA results suggest that PAN fragment offers greater charge transfer, exchange repulsion, electrostatic, and interaction energy when interacting with six water molecules. The PVDF likewise indicated a substantial charge transfer that can be linked to a greater polar group and PVDF dipole moment. The FMO optimization revealed that the PVDF allows for hydrogen bonding, however this bonding cannot be a function linked to electrostatic interactions. This study determined that the interactions of water with a hydrophobic solute or surface is directly correlated to the van der Waals interactions, while at the same time independent of the effects of electrostatic interactions. This relative independence is primarily facilitated by higher propensity of water at room temperatures to maintain its hydrogen bonding network configuration when there is an interface without enough hydrophilic sites. In this study, the interactions between PVDF, PAN, and water molecules were experimentally analyzed with the aid of Raman and confocal microscopic spectroscopies, the data indicating that there are more interactions between the CN group compared to CF and hydrophobicity of PVDF. Overall, there was a reasonable correlation between theoretical and experimental data. Building on this successful study, our future work aims to transform the surface of PVDF membranes using hydrophilic materials in

order to resolve the fouling problems that make applications of PVDF membranes in water treatment processes difficult.

In addition, the interactions between PVDF, PAN, and water molecules were experimentally analyzed in agreement with the theoretical results using Fourier-transform infrared spectroscopy (FTIR- ATR), RAMAN, and SSNMR spectroscopies, suggesting that more interactions between the CN group compared to CF. Although Fluorine has a much higher electronegativity than nitrogen, the covalent bond of C-F is stronger than C-N, and is harder to break during interactions with water. The energy of the polar covalent bond of C-F is higher than the C-N to be broken for interaction with water. Therefore, water molecules prefer to cluster together with hydrogen bonding instead of breaking the C-F polar covalent bond. To overcome this problem, a PVDF modification needs to be added that will enhance its interactions with water molecules (our ongoing study). This improvement can be achieved during PVDF synthesis by blending hydrophilic inorganic particles in order to enhance its hydrophilicity and its ability to interact with water molecules, and with the aim of reducing fouling phenomenon for several diversified applications.

2.7 Acknowledgements

The authors would like to acknowledge the Department of Chemical and Biological Engineering at the University of Saskatchewan for the generous support provided. The authors would also like to thank the High Performance Computing Research Facility (HPCRF) and Saskatchewan Structure Science Centre (SSSC) at the University of Saskatchewan for the services and facilities provided.

CHAPTER 3

A Comprehensive Computational Study of Innovative Zwitterionic Materials for Enhanced Poly (Vinylidene Fluoride) (PVDF) Membrane Hydrophilicity

The contents of the manuscript provided in this chapter is under review in the Journal Applied Surface Science, APSUSC-D-19-03612.

Citation:

Maghami, M., Abdelrasoul, A., A Comprehensive Computational Study of Innovative Zwitterionic Materials for Enhanced Poly (Vinylidene Fluoride) (PVDF) Membrane Hydrophilicity, Journal Applied Surface Science, APSUSC-D-19-03612.

Contribution of the MSc student

The design of novel zwitterions and computational calculations were planned by Mahboobeh Maghami under supervision and guidance of Dr. Amira Abdelrasoul. The theoretical software runs were submitted by Mahboobeh Maghami with the assistance of HPC at U of S. The collection of data, analysis and interpretations were performed by Mahboobeh Maghami under supervision and guidance from Dr. Amira Abdelrasoul. Dr. Amira Abdelrasoul supervised and provided consultation during the entire computational calculations as well as molecular dynamics simulations. The manuscript was written by Mahboobeh Maghami and Dr. Amira Abdelrasoul, who has also provided additional points to be discussed, editorial guidance regarding the style and content of the paper. Dr. Abdelrasoul is the corresponding author of the manuscript, in addition, she supervised and provided consultation during the thesis preparation.

Contribution of this chapter to overall study

Zwitterions are considered as the latest generation of materials for enhancing hydrophilicity of hydrophobic materials and enhance performance of membranes. Thus, it was interesting to address the hydrophobicity problem of PVDF using super novel hydrophilic zwitterions. This chapter provides the details of the designed novel zwitterionic copolymers with different anionic heads such as carboxybetaine, sulfobetaine, and phosphobetaine, chemical groups between charged groups of sulfobetaine, and more polar and functional groups on the backbone of copolymer as a linker between zwitterionic heads and PVDF membrane. The performance of the new designed ZW-PVDF copolymers in terms of the hydrophilicity was investigated using FMO-PIEDA method. In addition, the performance the designed ZW materials were compared with the commercially zwitterions such as SBMA and SB2VP.

3.1 Abstract

The goal of this study is to design a novel zwitterionic (ZW)-poly (vinylidene fluoride) (PVDF) membrane with high hydrophilicity potential using the pair interaction energy decomposition analysis (PIEDA) within the framework of the fragment molecular orbital (FMO) method. PIEDA method allows for the analysis of non-covalent interactions in terms of electrostatic, exchange-repulsion, and charge-transfer parameters. Within this study computational methods were applied to investigate the performance of zwitterionic moieties derived from three different anionic groups in the ZW head, specifically, carboxylate, sulfonate, and phosphate. This approach was used in addition to the inclusion of a linker between the ZW head and the PVDF backbone, such as trimethyl ammonium groups and hydroxyl group for an increase in PVDF membrane hydrophilicity. The quantum chemical calculations were employed to examine the hydration structure of moieties, the number of hydrogen bonding instances, and hydration free energy. The interactions between the ZW moieties on PVDF membranes with water molecules confirmed that they depended on the charged groups and the chemical groups between charged groups. The results pointed to differences in hydrophilicity, membrane water uptake due to their structural properties depending on the types of anionic groups involved, polar groups between charged groups, and the hydrophilic groups as a linker between charged groups of the zwitterions to the PVDF polymer backbone. The double zwitterionic PMAL®-C_8-CB-OH-

SB-PVDF was formed through protonated carboxyl group on backbone of copolymer PMAL®-C_8, and protonated nitrogen atom of amide group. This double zwitterion showed strong electrostatic interactions between individual water and secondary ammonium and Oxygen of carboxybetaine, compared to PMAL®-C_8-OH-SB-PVDF model. Our designed hydrophilic zwitterion PVDF membrane, and especially the double zwitterion membrane, is an exciting development that can be used in a wide range of water applications.

Keywords: Zwitterions, PVDF, Hydrophilicity, Hydrophobicity, FMO, PIEDA, charged groups, double zwitterion, hydration

3.2 Introduction

Within the current context, water pollution is becoming a serious global issue. Therefore, water treatment methods based on advanced technologies is necessary for addressing severe water shortages in current and future applications. Membrane technology plays a key role in wastewater treatments as well as production of drinking water, due to its favorable energy efficiency when compared to other types of technologies (Zhu *et al*., 2013, Elimelech *et al*., 2011, Pendergast *et al*., 2011).

Poly (vinylidene fluoride) (PVDF) and PVDF-based membranes are one of the most popular membrane materials for various types of filtration operations including water treatment and membrane distillation (Kang and Cao, 2014). This popularity is due to their advantageous characteristics such as excellent controlled porosity, mechanical properties, chemical resistance to abrasion, acids, alkalis, and microbial corrosion, as well as outstanding thermal stability (Kang and Cao, 2014; Liu *et al*., 2011; Lang *et al*., 2007). However, due to its intrinsic hydrophobicity the PVDF membrane is prone to the effects of fouling caused by adhesion and accumulation of feed components, including pollutants and biomolecules, on the membrane surface. Fouling causes serious reduction in flux, salt rejection impairment, and separation performance within a membrane system (Fane *et al*., 2011). Surface modifications are necessary in order to improve hydrophilicity and antifouling ability of PVDF membranes (Kang and Cao, 2014).

A number of research studies have shown that when it comes to controlling and reducing membrane fouling, hydrophilic materials are considered as promising antifouling materials, including poly (ethylene glycol) (PEG) (Sin *et al*., 2014) and zwitterions (Shen *et al*., 2016;

Lewis *et al*., 2000). These types of materials show a higher tendency to absorb water and as a consequence can become mechanically weak. Therefore, a way to counter these negative effects is to implement a combination of hydrophilic materials with hydrophobic PVDF membranes that can allow them to maintain their mechanical properties. Polymeric segments of poly (ethylene glycol) (PEG) have shown drawbacks in terms of readily subjecting to oxidative degradation and enzymatic cleavage in the presence of oxygen and transition metal ions, especially in the biological media (Shen *et al*., 2002, Zhang *et al*., 2006). As an innovative alternative, Zwitterions are considered to be the latest generation of materials capable of improving the hydrophilicity and antifouling properties of membranes due to strong hydrogen bonding with water molecules, derived from robust electrostatic interactions. Zwitterionic materials are defined as materials that have moieties with both cationic and anionic groups and with overall charge being neutral, as a consequence offering a high dipole moment (Bretscher *et al*., 1975).

The majority of the previous studies on zwitterion chemistry were comparing the same two common monomers, carboxybetaine and sulfobetaine (Zhang *et al*., 2006), or phosphobetaine-PVDF and sulfobetaine-PVDF membranes (Bengani-Lutz *et al*., 2017). An in-depth comparative analysis of common zwitterionic head groups with new zwitterionic materials on membranes are lacking. Computational methods can be applied to further the understanding of the relationships between zwitterionic membranes' structure and water at the molecular level. The fragment molecular orbital (FMO) computation is considered as a fragment-based method to perform ab initio calculations of fragments and their dimers (Kitaura *et al*., 1999; Gordon *et al*., 2012). The pair interaction energy (PIEDA) between any two fragments calculated using FMO includes electrostatics, exchange-repulsion, and charge transfer energies, provided by PIEDA (Fedorov *et al*., 2012; Kitaura *et al*., 1999; Fedorov *et al*., 2007). In the previous studies, FMO have been employed only for the analysis of solvent effects on biomolecules and the design of new highly efficient drug due to a substantial relationship between FMO energy terms and protein–ligand binding (Komeiji *et al*., 2009; Fedorov *et al*., 2007). This study is the first application of FMO and PIEDA methods for the analysis and hydration of Zwitterion membranes and interactions with water molecules and evaluating their ability to enhance hydrophilicity of hydrophobic PVDF membranes.

The primary goal of this study was to design novel zwitterionic copolymers with different structures. In addition, the hydration of all strong, weak, and repulsive interactions between

water molecules around zwitterionic moieties on hydrophobic PVDF membranes will be analyzed using FMO and PIEDA methods. In this work, we examined the performance of all new zwitterionic copolymers attached to PVDF membrane surface as they interact with water molecules, compared to commercial zwitterions, SBMA, and SB2VP, (Kaner *et al*., 2017) shown in Figure 3.1.

3.3 Computational Methods

3.3.1 ZW Molecular Optimized Models

As part of this research study we designed new and highly polar zwitterion groups that are more functional than commonly used simple zwitterions, such as the commercial type references of SBMA and SB2VP. These zwitterions-based modules will include positive or negative charge modules to modulate overall charge and increase hydrophilicity on the PVDF membrane surfaces. It is important to use theoretical methods that are capable of investigating solvent effects and their interaction with ZW-PVDF membranes for the accurate prediction of hydrophilicity.

All ab initio calculations were conducted with the help of Avogadro and GAMESS electronic structure package software. The structures of the four zwitterionic molecules with different head groups, including PMAL®-C_8-CB, PMAL®-C_8-SB, PMAL®-C_8-MPC, PMAL®-C_8-OH-SB, and two previous common zwitterions for reference purposes (SBMA and SB2VP), are shown in Figure 3.1. The zwitterionic modules that were incorporated into the PVDF membrane backbone were optimized (DFT/6-31+G*). All of the structural calculations of the Zwitterionic copolymers, Zwitterion-PVDF membranes, and their interactions with water molecules were completed using GAMESS electronic structure package software (Schmidt *et al*., 1993, Gordon *et al*., 2005). Full optimizations were performed with the application of DFT theory with the 6-31+G*split valence basis set and using GAMESS (Schmidt et al., 1993; Gordon *et al*., 2005; Parr *et al*., 1989). Water molecules were then added to the B3LYP/6-31+G* minimum energy structures to assess hydrogen bond formation with zwitterionic head groups, cationic groups (quaternary ammonium), hydrophilic linker between zwitterionic types and PVDF membranes. Geometry optimizations of zwitterionic PVDF membranes and water molecules are calculated at the HF/6-31+G* levels of theory, outlined in Figure 3.2.

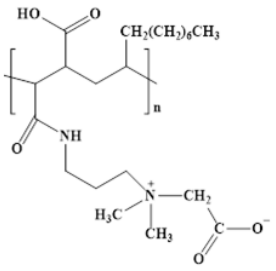

PMAL®-C_8-CB (a)

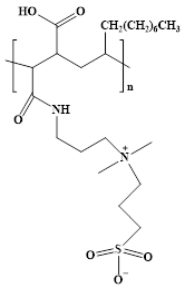

PMAL®-C_8-SB (b)

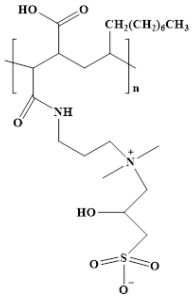

PMAL®-C_8-OH-SB (c)

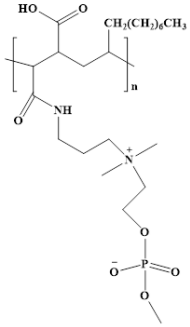

PMAL®-C_8-PBC (d)

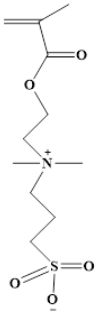

SBMA (e)

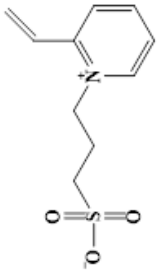

SB2VP (f)

Figure 3.1. Molecular structure of novel Zwitterion series researched in this study.

3.3.2 Partial Charge Calculation and Dipole Moment Distribution

The analyses of zwitterionic molecules, their properties of interest such as partial charges, and dipoles of the carboxybetaine, sulfobetaine, and phosphobetaine, were performed ab initio single point calculations with DFT/6-31+G* and the help of GAMESS Software, found an MDM of 33, 29, 27, 22, 22, 17 D for PMAL®-C_8-OH-SBM, PMAL®-C_8-SBMA, SBMA, PMAL®-C_8-MPC, SB2VP, and PMAL®-C_8-CBMA, respectively, in the gas phase. All relevant data with respect to charges and dipole moments are reported in Table 3.1 and Figure 3.2. It was shown in previous

studies that the SBMA zwitterion is highly polarized when compared to other zwitterions such as SB2VP. Although SB2VP copolymer has a zwitterionic sulfobetaine group like SBMA and novel sulfobetaine head groups, it showed less hydrophilic attachment than SBMA due to the pyridine-containing functional group (Kaner, 2017). As a result, it reduces hydration of SB2VP on PVDF membranes and showed less dipole moment (22 D) compared to SBMA (27 D) in Table 3.1. According to the dipole moments reported in Table 3.1, for all optimized structures of zwitterions, PMAL®-C_8-OH-SB indicated greater dipole moment (33 Debye) than other designed zwitterions and two commercial zwitterions, SBMA and SB2VP.

Table 3.1. Partial Charges of atoms of the six zwitterionic moieties and Dipole Moments μ in Debye.

Zwitterion	**Charge**	**μ(D)**		**Charge**	**μ(D)**		**Charge**	**μ(D)**
PMAL®-C_8-OH-SB	q(e)	33 D	**PMAL®-C_8-SB**	q(e)	29 D	**PMAL®-C_8-CB**	q(e)	17 D
N	-0.298		N	-0.304		N	-0.307	
H(CH3)	0.207		H(CH3)	0.206		H(CH3)	0.207	
C(CH3)	-0.291		C(CH3)	-0.298		C(CH3)	-0.289	
H(CH2)	0.199		H(CH2)	0.194		H(CH2)	0.205	
C(CH2)	-0.447		C(CH2)	-0.447		C(CH2)	-0.198	
H(CH)	0.184		H(CH2)	0.185		C	0.139	
C(CH2)	-0.058		C(CH2)	-0.331		O	-0.450	
O(OH)	-0.500		H(CH2)	0.223		O	-0.503	
H(OH)	0.327		C(CH2)	-0.222				
H(CH2)	0.218		S	1.488				
C(CH2)	-0.215		O	-0.793				
S	1.500		O	-0.736				
O	-0.730		O	-0.782				
O	-0.803							
O1	-0.736							
PMAL®-C_8-MPC		22 D	**SBMA**		27 D	**SB2VP**		22 D
N	-0.300		N	-0.305		N	-0.139	
H(CH3)	0.205		H(CH3)	0.211		H(CH)	0.231	
C(CH3)	-0.301		C(CH3)	-0.289		C(CH)	-0.033	
H(CH2)	0.183		H(CH2)	0.191		H(CH2)	0.191	
C(CH2)	-0.117		C(CH2)	-0.455		C(CH2)	-0.456	
C(CH2)	-0.226		H(CH2)	0.205		H(CH2)	0.206	
H(CH2)	0.225		C(CH2)	-0.341		C(CH2)	-0.309	
C(CH3)	-0.196		H(CH2)	0.208		H(CH2)	0.201	
H(CH3)	0.167		C(CH2)	-0.222		C(CH2)	-0.180	
P	1.367		S	1.494		S	1.495	
O1	-0.606		O	-0.741		O	-0.779	
O2	-0.586		O	-0.777		O	-0.769	
O	-0.816		O	-0.780		O	-0.739	
O	-0.764							

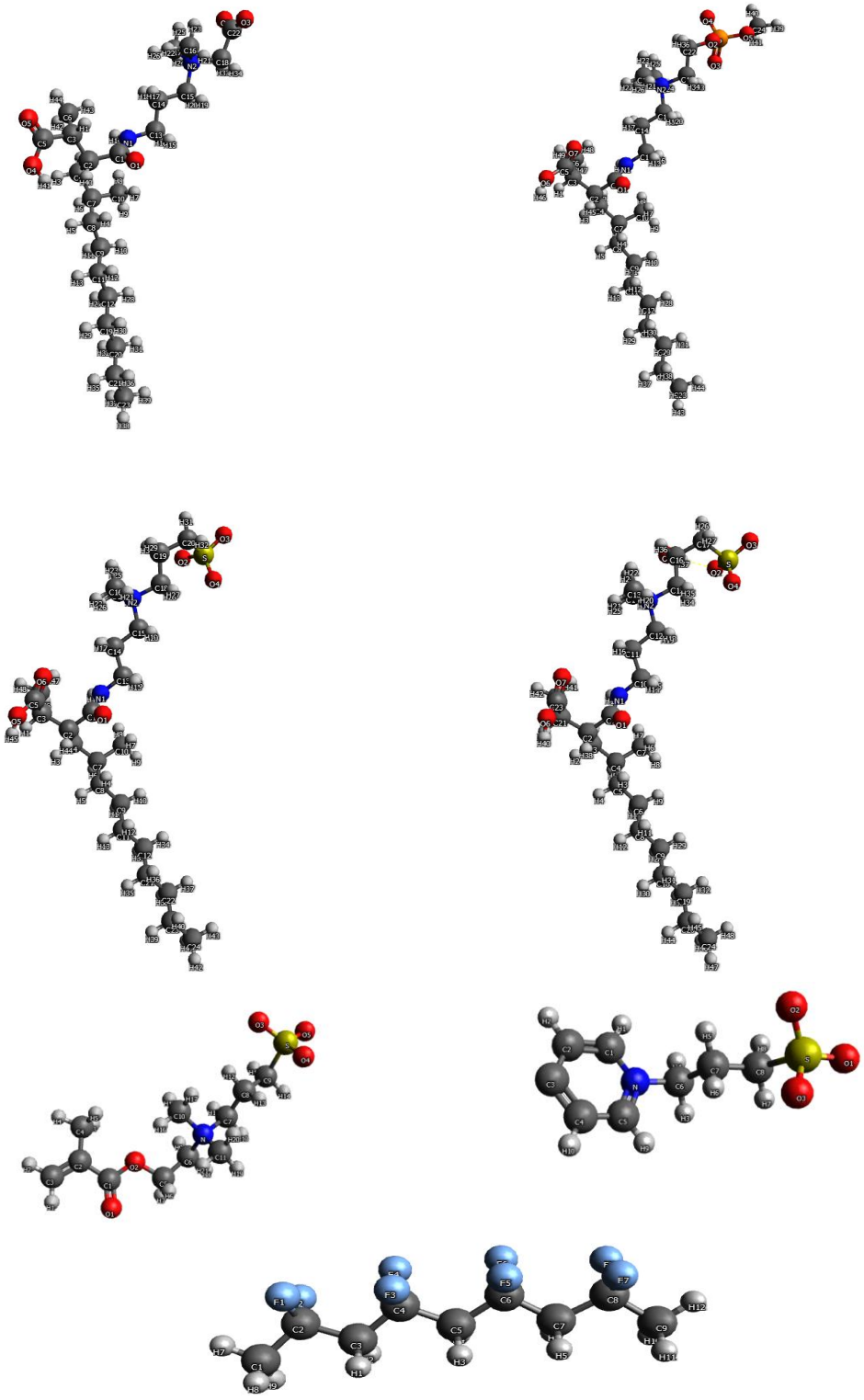

Figure 3.2. Optimized molecular structures of (a) carboxybetaine, (b) phosphobetaine, (c) sulfobetaine, (d) OH-sulfobetaine, (e) SBMA, (f) SB2VP, as references, and (g) hydrophobic PVDF membrane.

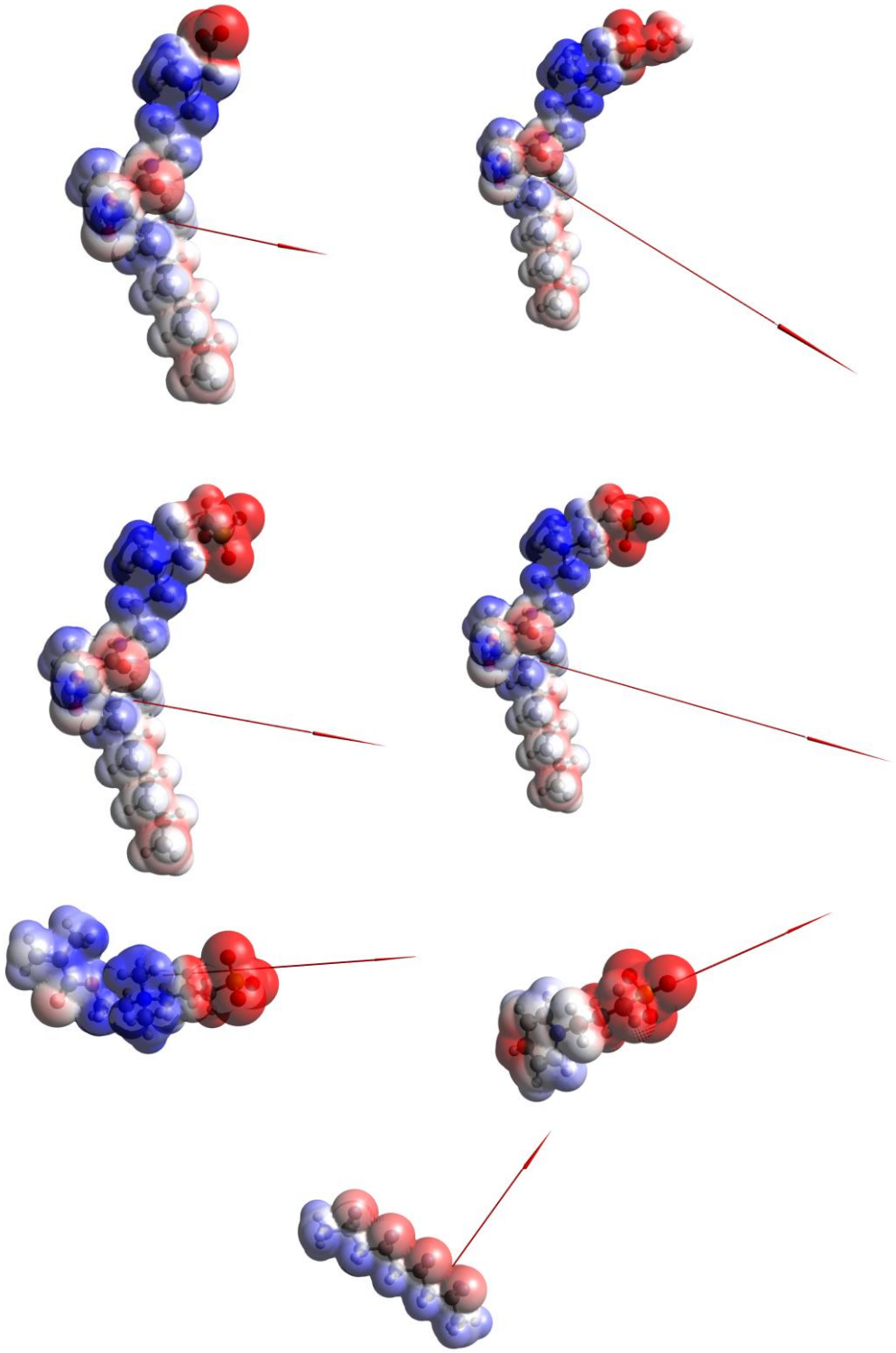

Figure 3.3. Dipole moment and electrostatic potential of PVDF, SBMA, SB2VP, PMAL®-C_8-OH-SBM, PMAL®-C_8-SBMA, SBMA, PMAL®-C_8-MPC, and PMAL®-C_8-CBMA.

All oxygen atoms in zwitterionic head groups have a very high negative charge (Table 1) and a significant molecular dipole moment due to positively charged quaternary ammonium groups located on the opposite side of zwitterionic heads, as shown in Figure 3.3 and Table 3.1.

3.3.3 Fragment Molecular Orbital (FMO)

In order to understand the affinity of Zwitterionic PVDF membranes to water molecules, this study applied the FMO approach to perform ab initio electronic structure calculations using the electronic structure package GAMESS. In this study, FMO approach was applied for first time to examine non-covalent interactions between Zwitterionic PVDF membranes and water molecules at a more accurate quantum chemical level and at a faster rate than the MD results reported by other research groups. The FMO method can be useful for obtaining accurate estimations of energy values at lower computational costs, compared with the post-Hartree−Fock methods. The FMO calculations were performed at a two-body expansion level (FMO2) with the Hartree−Fock (HF) and basis sets 6-31+G*. Hydrogen bonding was considered to be a significant molecular recognition in water-solvated ZW-PVDF complex models. Each water molecule and zwitterionic PVDF models were considered to be a monomer fragment and their dimer interactions were calculated based on FMO2 method (Schmidt *et al*., 1993), as shown in Figure 3.4.

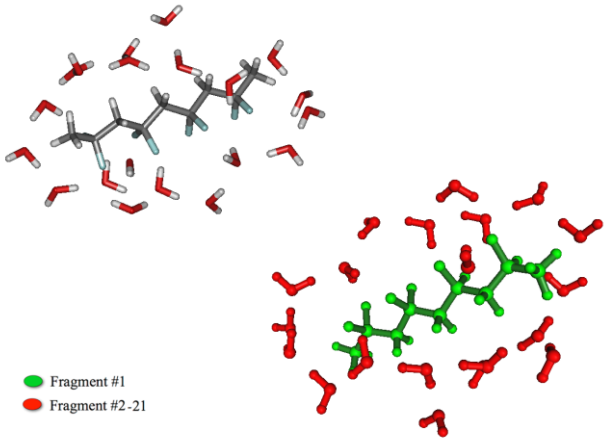

Figure 3.4. Fragmentation of water molecules and PVDF membrane, calculated at FMO-RHF/6-31+G* level.

The total FMO2 energy for this study, with monomers i and dimers ij considered, is indicated as follows:

$$E = \sum_i E_i + \sum_i \sum_{j<i} [E_{ij} - E_i - E_j]$$

Equation (3.1)

Where Ei and Eij are represented as the energy of a monomer fragment i, and the energy of a dimer fragment ij, respectively. All results obtained from FMO calculations were explained in terms of pair interaction energy decomposition analysis (PIEDA) so as to offer a better understanding of the interactions and bindings between Zwitterion-PVDF membranes and water molecules. For the analysis of the pair interaction energy, the FMO2 energy Equation (3.1) can be rewritten:

$$\Delta E_{IJ}^{int} = \sum_I E_I' + \sum_{I>J}[(E_{IJ}' - E_I' - E_J') + Tr(\Delta D^{IJ} V^{IJ})]$$

Equation (3.2)

In Equation 3.2, ΔE^{ij}_{int} is the pair interaction energy between the monomer fragments i and j, Di is the electron density of the ith monomer, and V^i is the potential on the ith monomer from all other monomer fragments. PIEDA provides energy contributions from electrostatic(ES), exchange−repulsion(EX), and charge transfer energy(CT) terms for each pair of FMO2 fragments, as indicated in Equation (3.3):

$$\Delta E_{ij}^{\text{int}} = \Delta E_{ij}^{\text{ES}} + \Delta E_{ij}^{\text{EX}} + \Delta E_{ij}^{\text{CT}}$$

Equation (3.3)

All these PIEDA energies were calculated with the aid of GAMESS software package and based on equations reported by Fedorov and Kitaura (Fedorov *et al*., 2012, Kitaura *et al*., 1999, Fedorov *et al*., 2007), at the same level of FMO method theory. The Facio 16.4 program (Schmidt *et al*., 1993), was used to split Zwitterionic PVDF membranes and water molecules into fragments and to provide the FMO parameters. Ab initio optimization of geometries and single-point energy calculations were then performed for the water-solvated ZW-PVDF complex models using GAMESS. The results were compared with two common ZW-PVDF models, SBMA-PVDF and SB2VP-PVDF, as references. All energy interactions for all water-solvated ZW-PVDF complex models were analyzed in Table 3.3.

3.4 Results and Discussions

3.4.1 Polarity of ZW Modules

Polyzwitterions indicated a range of standard dipole moments from 20- 30 D at neutral pH (Galin *et al*., 1993). A significant molecular dipole moment enhancement of more than 30 D for zwitterions is not unknown in the literature. In this study, all of zwitterions showed high dipole moments in the range between 17-29 D, as shown in Table 3.1. However, PMAL®-C_8-OH-SB zwitterion had a very high dipole moment of 33 D, which could be explained by more polar groups, especially hydroxyl group between charged groups of PMAL®-C_8-OH-SB. This high dipole moment can likewise stem from a much stronger hydrogen bond between hydroxyl group's charge groups on zwitterion and negatively O atom on sulfobetaine head group of this zwitterion. The large dipole moment of PMAL®-C_8-OH-SB can contribute to stronger hydrogen bonds between zwitterions and water molecules, that is intermolecular interactions, which have larger space separation within the molecule. While PMAL®-C_8-OH-SB showed a greater dipole moment than PMAL®-C_8-SB, 29 D, it has the same structure in terms of zwitterionic head and hydrophilic backbone. Therefore, the larger the difference in electronegativity, the larger the dipole moment, and consequently the higher is the polarity value. PMAL®-C_8-2-hydroxyl-SB showed higher dipole moment, resulting in more polarity due to hydroxyl functional group and sulfobetaine group. Both zwitterions, PMAL®-C_8-OH-SB and PMAL®-C_8-SB, showcased greater dipole moments when compared to SBMA and SB2VP, 27D and 22D, respectively. This correlation can be attributed to a larger hydrophilic area in the backbone of novel zwitterions as well as sulfobetaine head group. The result for PVDF model was noteworthy since it confirmed hydrophobicity of PVDF membrane with lower dipole moment (14 D). Conclusion can thus be drawn that any changes between charged and positive charges on zwitterions have an effect on performance of zwitterions in terms of hydrophilicity.

3.4.2 Hydration of Zwitterionic Moieties in water-solvated ZW-PVDF complex model

To assess the zwitterions in terms of hydrophilicity and permeability of PVDF membranes, they must be inserted into PVDF membranes and then tested in a water environment using computational method. The focus of this work was to study the PVDF membrane at a greater depth. The optimization of Zwitterion-PVDF membranes was carried out with HF/6-31+G* level of theory (Figure 3.5).

In this work, as outlined in Figure 3.1, we studied the hydration structure and hydration free energy around all water-solvated zwitterion-PVDF complex models, and in particular around three different anionic groups of carboxybetaine (COO^-) (a), sulfobetaine (SO_3^-) (b), and phosphobetaine (OPO_3^-) (d). The positively charged group, $N^+(CH_3)_3$, is same for all designed zwitterionic copolymers.

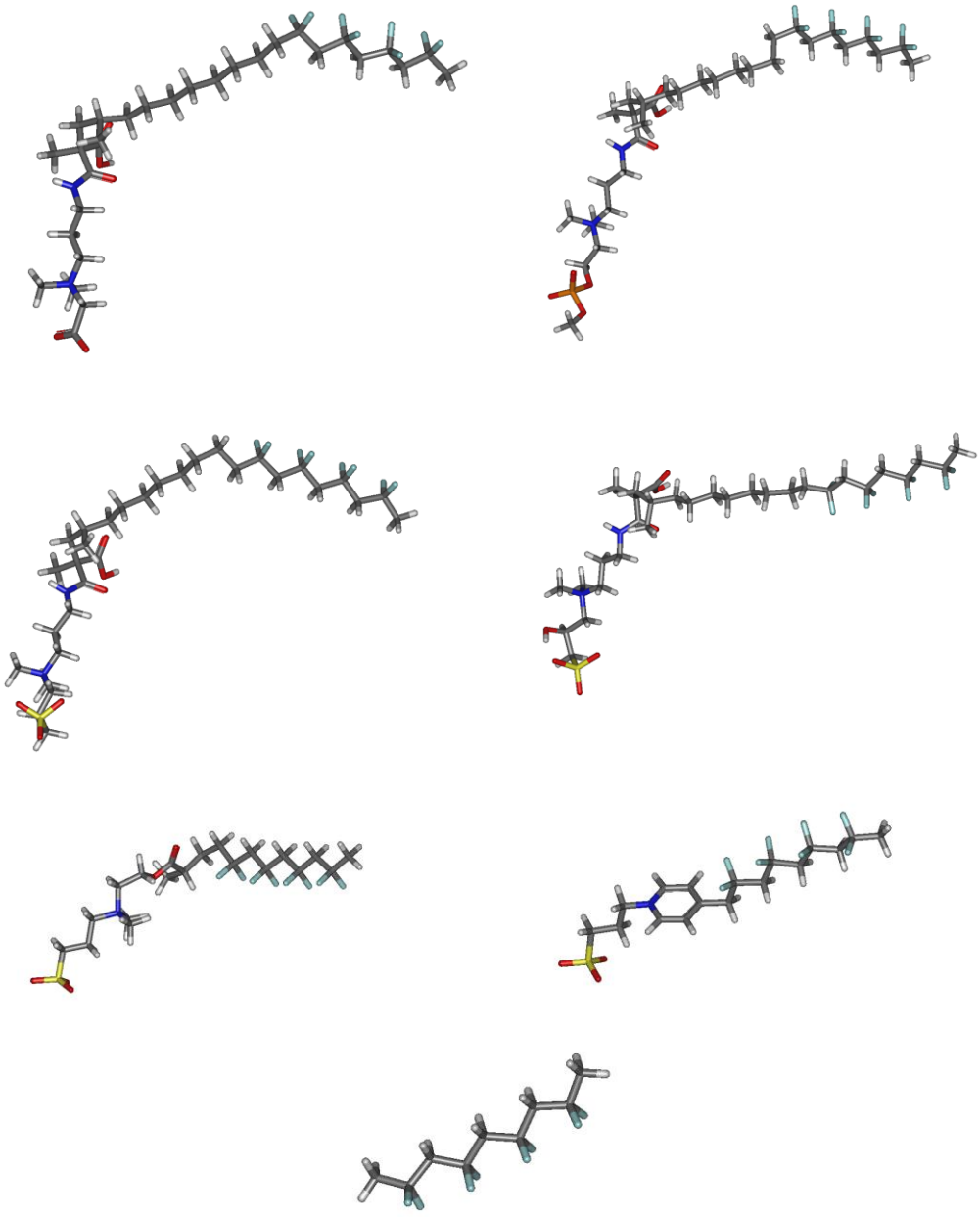

Figure 3.5. Optimization of various Zwitterion-PVDF with HF/6-31+G*, compared to pure PVDF and two commercial zwitterions.

We also focus on hydration of hydroxyl group between sulfobetaine (SO_3^-), and the linker between zwitterionic moieties and PVDF polymer(c). Hydration of these novel zwitterions in PVDF membranes was then compared to hydrophobic PVDF and two commercial zwitterions, as referenced using FMO method. Figure 3.5 presents the interactions between optimized Zwitterion-PVDF membranes and water molecules, using FMO-RHF/6-31+G* level of theory by GAMESS. This data provides a qualitative prediction of the hydration around these zwitterion-PVDF membranes through FMO dimer interactions. The interactions occurring between ZW-PVDF membrane and water are considered as hydrogen bonding. Therefore, water-ZW-PVDF distance is crucial to showing strong hydration. Each water molecule and zwitterionic PVDF models were considered to be a monomer fragment, and dimer interactions were studied using the FMO2 method, as shown in Figure 3.6.

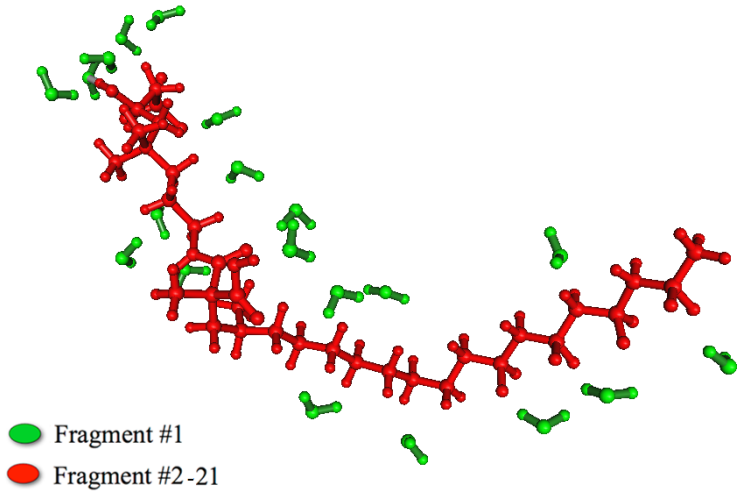

Figure 3.6. Fragmentation of water molecules and PMAL®-C_8-OH-SB-PVDF membranes calculated at FMO-RHF/6-31+G* level.

Hydration around three parts of ZW-PVDF models, anionic zwitterionic heads, positively charged groups, hydrophilic and polar groups on copolymer backbone, and PVDF were studied through controlled investigations of the hydration free energy around zwitterionic copolymers and PVDF membranes, attached to these copolymers in water-solvated ZW-PVDF complex models. All zwitterionic copolymers indicated strong hydration, but the strength of hydration around them could change depending on the types of anionic groups and cationic groups involved in these copolymers.

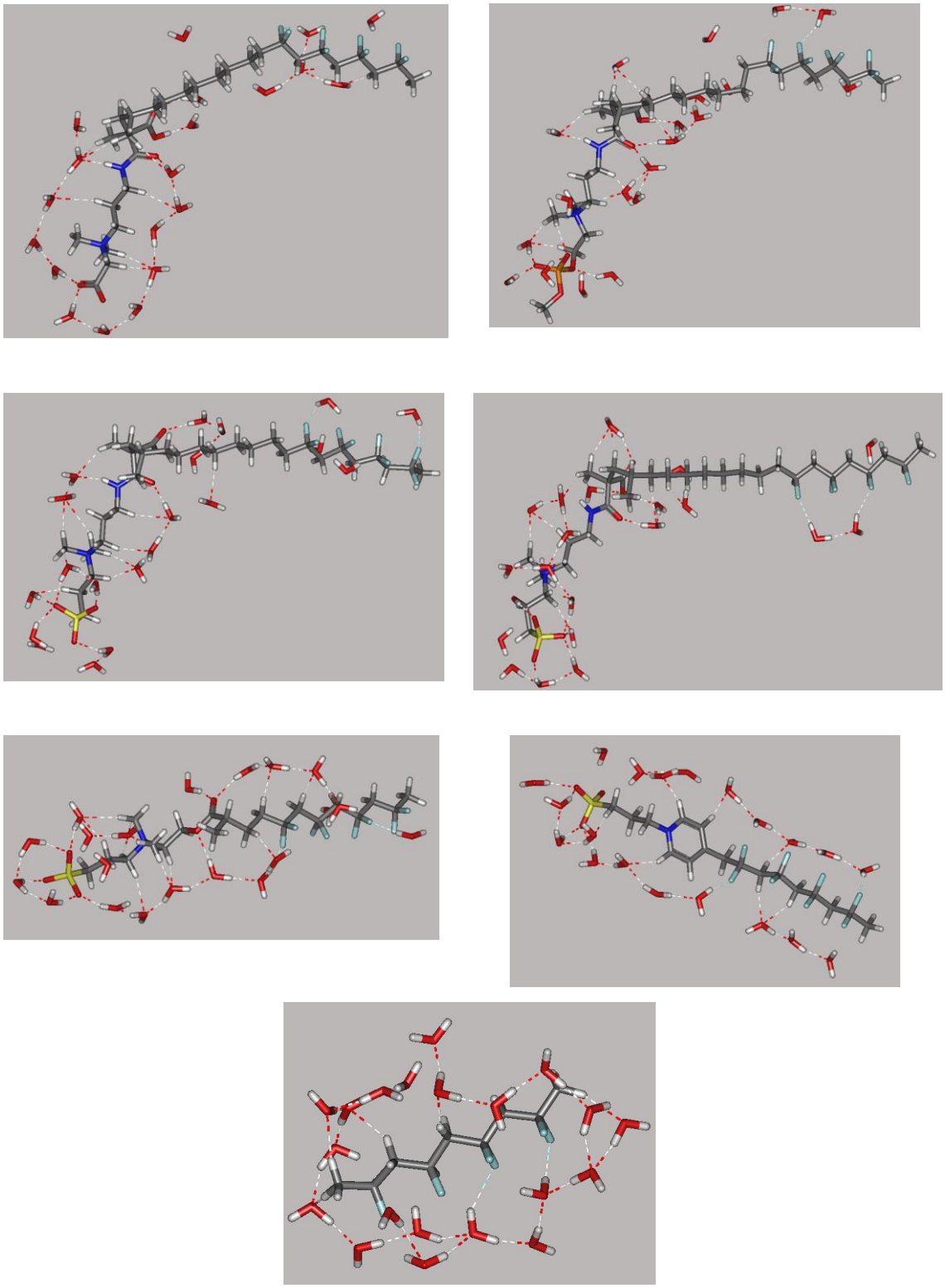

Figure 3.7. Fully FMO optimization of water-solvated ZW-PVDF complex models (a-f) and (g) hydrophobic water-solvated PVDF membranes, calculated at FMO-RHF/6-31+G* level of theory.

As shown in Figure 3.7, CB (a), SB (b), and MPC moieties have strong hydration in designed zwitterionic copolymers and commercial zwitterions used as references in this study. Although all of the zwitterionic copolymers showed more tendencies to absorb water, they had differences in hydration, in particular around the negatively charged groups of the betaine molecules. Due to their higher charge densities, the charged groups are more prone to hydration.

Therefore, a charged group with a higher charge density can have greater and stronger interactions with water molecules, consequently increasing hydration energy of zwitterionic moieties (Shao et al., 2014).

As can be observed in Table 3.1, group charge densities were found to follow the following order PO_3> SO_3 > CO_2. The cationic group, quaternary ammonium is considered the same for all zwitterions and its charge density is same for all zwitterions. Phosphobetaine showed higher charge density compared to sulfobetaine and carboxybetaine due to extra oxygen atoms on this moiety, however, because of the steric hindrance of Methyl group it had lower hydration free energy compared to sulfobetaine groups. Among all water-solvated ZW-PVDF membranes with sulfobetaine zwitterionic heads, copolymers PMAL®-C_8-SB ($-N^+(CH_2\text{-}CH_2(OH)\text{-}CH2)\ SO_3^-$) (b), PMAL®-$C_8$-OH-SB($-N^+(CH_2\text{-}CH_2\text{-}CH_2)\ SO_3^-$) (c), and SBMA($-N^+(CH_2\text{-}CH_2\text{-}CH_2)\ SO_3^-$) (e) models, incorporated into PVDF membranes allowed for strong hydration through hydrogen bonding with water molecules. This lead to an increase in hydration free energy, compared to carboxybetaine and phosphobetaine zwitterionic heads and water-solvated PVDF model. Our results were in good agreement with simulation findings available in other works examining excellent hydration properties of polySBMA (Shao *et al*., 2010, Zheng *et al*., 2005). Among these three sulfonate zwitterionic moieties have an SO_3 group and a cationic quaternary ammonium group, which is same for all zwitterions. In this case the $-N^+(CH_2\text{-}CH_2(OH)\text{-}CH_2)\ SO_3^-$ of PMAL®-C_8-OH-SB has the lowest charge density due to the lesser hydration free energy. As a result, it features stronger hydrogen bonding with water molecules.

The study also investigated structural hydration of the charged groups of zwitterionic moieties and quaternary ammonium cationic group. The numbers of water molecules and hydrogen bond strengths in the coordination shell were investigated around the cationic and anionic of ZW, hydrophilic and polar groups on backbone of copolymers, added hydroxyl group, PVDF, and two commercial zwitterions, SBMA and SB_2VP, as outlined in Table 3.2.

Based on Figure 3.7 and Table 3.2, we found that the number of water molecules around zwitterionic moieties on the copolymers and commercial zwitterions is higher than around other parts of copolymers and PVDF in all water-solvated ZW-PVDF complex models.

Table 3.2. Hydrogen bonds length (Å) for water-solvated ZW-PVDF complex models, calculated at FMO-RHF/6-31+G* level of theory.

ZW	Hydrogen Bonds(HBs)		Parameters of HB(Å)			Hydrogen Bonds(HBs)		HB(Å)	
SB	F(16)-H(77)	O(40)-H(79)	1.98	1.79	**PM-SB2VP**	F(42)-H(111)	O(76)-H(19)	1.87	2.01
	O(120)-H(8)	O(42)-H(74)	2.22	1.92		O(97)-H(27)		2.22	
	O(114)-H(65)	O(41)-H(85)	2.12	1.97		O(13)-H(75)		1.85	
	O(117)-H(68)	O(41)-H(70)	2.18	1.76		O(52)-H(34)		2.24	
	F(3)-H(88)	O(69)-H(55)	1.88	2.06		O(52)-H(28)		2.17	
	O(99)-H(45)	O(108)-H(52)	2.54	2.42		F(26)-H(105)		1.97	
	O(32)-H(100)	O(69)-H(62)	2.00	2.43		O(85)-H(49)		2.09	
	O(31)-H(95)	O(108)-H(50)	1.91	2.34		O(94)-H(48)		2.03	
	O(31)-H(113)	O(40)-H(128)	2.00	1.72		O(64)-H(50)		2.24	
	O(102)-H(51)	O(123)-H(53)	2.03	2.45		O(11)-H(68)		1.85	
	O(102)-H(60)		2.06			O(11)-H(80)		1.90	
						O(13)-H(92)		1.85	
PM-OH-SB	O(110)-H(95)	O(116)-H(41)	2.24	2.18	**PM-CB**	O(135)-H(86)	O(147)-H(37)	2.50	2.94
	O(110)-H(89)	O(116)-H(49)	2.15	3.63		O(132)-H(80)	O(129)-H(23)	3.08	2.87
	F(80)-H(142)	O(158)-H(48)	2.00	3.06		O(132)-H(74)	O(129)-H(10)	2.97	2.65
	O(113)-H(72)	O(137)-H(46)	2.78	2.19		F(71)-H(125)	O(129)-H(31)	1.86	1.79
	O(113)-H(65)	O(125)-H(74)	2.37	2.12		O(11)-H(119)		1.76	
	O(113)-H(150)	O(60)-H(127)	2.63	1.67		O(114)-H(50)		1.50	
		O(59)-H(133)	2.20	1.79		O(111)-H(22)		2.64	
	O(149)-H(30)	O(58)-H(129)	2.04	1.73		O(3)-H(113)		1.62	
	O(11)-H(63)	O(116)-H(47)	1.67	2.31		O(144)-H(33)		2.50	
	O(3)-H(124)	O(52)-H(159)	2.22	1.83		O(108)-H(62)		2.14	
	O(152)-H(33)	O(52)-H(138)	2.43	1.71		O(108)-H(44)		2.44	
	O(146)-H(10)	O(155)-H(55)	1.86	2.28		O(63)-H(104)		1.68	
	O(146)-H(31)		2.48			O(63)-H(106)		1.66	
	O(119)-H(35)								
PM-SB	F(97)-H(125)	O(62)-H(137)	2.01	1.67	**PM-MPC**	F(99)-H(121)	O(132)-H(64)	1.95	2.06
	F(79)-H(153)	O(61)-H(104)	2.09	1.94		F(88)-H(137)	O(69)-H(133)	1.89	1.62
	O(11)-H(150)	O(60)-H(156)	1.75	1.92		O(162)-H(28)	O(68)-H(47)	2.20	2.42
	O(130)-H(66)	O(60)-H(111)	2.33	1.78		O(117)-H(26)	O(65)-H(125)	2.48	1.80
	O(115)-H(10)	O(109)-H(55)	2.37	2.04		O(117)-H(21)	O(105)-H(44)	2.47	2.44
	O(115)-H(31)	O(60)-H(159)	1.86	1.85		O(108)-H(10)		2.48	
	O(3)-H(120)	O(157)-H(53)	1.63	2.23		O(108)-H(31)		1.85	
	O(118)-H(33)	O(157)-H(47)	2.51	2.01		O(114)-H(17)		3.00	
	O(145)-H(33)		2.23			O(126)-H(51)		1.58	
	O(112)-H(51)		2.25			O(3)-H(116)		1.84	
	O(112)-H(44)		2.11			O(3)-H(113)		1.76	
	O(142)-H(45)		2.90			O(147)-H(33)		2.32	
	O(142)-H(49)		2.53			O(132)-H(48)		1.98	

By comparing different zwitterionic moieties, we found that sulfobetaine zwitterionic heads are surrounded with a greater number of water molecules than carboxybetaine and phosphobetaine in all ZW-PVDF models. As noted in Table 3, the number of water molecules around zwitterions with sulfobetaine heads, PMAL®-C_8-OH-SB-PVDF, PMAL®-C_8-SB-PVDF,

and SBMA is 25, 22, and 21, respectively. They showed higher number of hydrogen bonding with water molecules compared to PMAL®-C_8-CB-PVDF and PMAL®-C_8-PC-PVDF, 18 and 17, respectively. As suggested in Table 3.2, the interaction between PVDF and water is governed by 8 hydrogen bonds. The hydrogen bond lengths of PVDF with water molecules were calculated to be 1.85–3.02 Å. Apart from the PVDF which did not produce good results, PMAL®-C_8-CB-PVDF and PMAL®-C_8-PC-PVDF showed almost an equal number of hydrogen bonds with water molecules. Both of them resulted in 17 and 18 instance of hydrogen bonding with water molecules, calculated to be 1.50-3.08 Å and 1.58-3.00 Å, respectively. PMAL®-C_8-OH-SB is governed around 25 hydrogen bonds, 23 strong hydrogen bonding distances and 2 weak hydrogen bonding distances, calculated to be 1.67-3.63 Å, whereas PMAL®-C_8-SB-PVDF had 21 hydrogen bonds, calculated to be 1.63-2.90 Å. The number of water molecules around carboxylate and phosphate groups, PMAL®-C_8-CB-PVDF and PMAL®-C_8-PC-PVDF, are always less than those around the sulfonate group, PMAL®-C_8-OH-SB-PVDF, PMAL®-C_8-SB-PVDF, and SBMA. These results were in good agreement with data from the previous reported studies (Suenaga *et al.*, 2005). The increase in number of water molecules around the negatively charged group of sulfobetaine moiety can be attributed to its extra oxygen atom, if compared to carboxybetaine, and a lack of steric hindrance of methyl group, when compared to phosphobetaine moiety. However, the number of water molecules in positively charged groups of the three zwitterionic moieties are nearly the same for all zwitterionic copolymers and are higher than in the negatively charged groups. As shown in Figure 3.7 and Table 3.2, hydrogen bond lengths between hydrogen of methyl group of the $N(CH_3)_3^+$ group and the oxygen atoms of water molecules, 2.44Å, the C1-H…Ow, is significantly larger than that of hydrogen bonds between oxygen atom of carboxybetaine, 1.66 Å, phosphobetaine, 1.62Å, and sulfobetaines, 1.67Å. It was determined that water molecules have stronger interactions with the negatively charged groups of carboxybetaine, phosphobetaine, and sulfobetaine than the positively charged group due to their higher partial charges.

Based on Table 3.2, the number of water molecules around phosphobetaine moiety of PMAL®-C_8-MPC-PVDF are lower than carboxybetaine and sulfobetaine, but the shortest value of hydrogen bonding observed for oxygen atom of phosphobetaine moiety of novel zwitterionic copolymers confirmed larger hydration strength due to higher charge density and greater number of oxygen atoms. As a result, partial charge contributes to the strength of hydrogen bonding

between betaine moieties, water, and shell volume around negative and positive charges, leading to greater number of water molecules around them and more hydrogen bonding.

Figure 3.7 shows that, although positively charged groups are surrounded by a higher number of water molecules, they have lower strength interactions with water molecules due to the random orientation of the water molecules (White *et al*., 2011). The negatively charged groups indicated stronger interactions with the water molecules due to orienting higher orders of water molecules around them, when compared to the positively charged group.

Therefore, strong electrostatic interactions between sulfobetaine zwitterionic head and water molecules, greater number of water molecules (more hydrogen bonding) around anionic groups, and the quaternary ammonium in a $-N^{+}(CH_2\text{-}CH_2(OH)\text{-}CH_2)\ SO_3^{-}$ sulfobetaine, are the primary reasons when it comes to confirming higher hydrophilicity of PVDF membranes prepared using the copolymer with PMAL®-C_8-OH-SB (Figures 8). For this comparison the study relied on similar zwitterionic copolymer PMAL®-C_8-SB-PVDF, SBMA-PVDF, and SB_2VP-PVDF, as references. The best performance of PMAL®-C_8-OH-SB-PVDF compared to PMAL®-C_8-SB-PVDF, can be attributed to additional hydroxyl group between charged groups on PMAL®-C_8-OH-SB. The PMAL®-C_8-OH-SB-PVDF with more polar groups, such as amide and carboxylic groups on backbone of copolymer PMAL®-C_8. These membranes were more hydrophilic than membranes with ester-based (SBMA-PVDF) and pyridinium-based (SB_2VP-PVDF) zwitterions due to the number of water molecules, hydrogen bond strength, and hydration free energy. The obtained results confirmed observations from the previous section on hydration free energy for novel types of zwitterions. As a result, for the hydrophilic head, and hydrophilic part of copolymer PMAL®-C_8, the structural specifics have a lot of significance. Based on hydrogen bonding between zwitterionic head groups and water molecules, we found that zwitterionic sulfobetaine head offered better performance compared to carboxybetaine and phosphobetaine. Although SB_2VP has a sulfobetaine head in its structure, these results indicated that hydrophobicity of Pyridinium on zwitterionic moiety of SB_2VP-PVDF can reduce hydrophilicity, when compared to other sulfobetaine zwitterions, SBMA-PVDF, PMAL®-C_8-OH-SB, and PMAL®-C_8-SB-PVDF that point to more hydrophilic zwitterions.

The results suggest that the hydrophilic part of backbone of new types of zwitterions has a higher number of water molecules and stronger hydrogen bonding than the commercial references such as SBMA and SB_2VP. Among the four novel zwitterionic copolymers,

carboxybetaine or phosphobetaine exhibited greater number of water molecules around amide-group and carboxylic-group on the backbone of their copolymer compared to backbone sulfobetaine copolymers, whereas the sulfobetaine head groups had more water molecules around them.

3.4.3 Non-covalent Interactions Between ZW-PVDF Models and Water

It is critical to employ theoretical methods that can provide a better understanding of non-covalent interactions between water and membranes when it comes to accurate prediction of hydrophilicity. Based on the FMO results, we analyzed interactions decomposed into ZW-PVDF and water using PIEDA. All these PIEDA energies were calculated with the aid of FMO calculation program GAMESS and Facio Viewer. The PIEDA method allows for the analysis of the inter fragment interaction energy between water and ZW-PVDF membranes in terms of the electrostatic, exchange-repulsion, and charge transfer energies. In order to determine the types of the interactions occurring between water molecules and ZW-PVDF complex models, hydrophilic, and hydrophobic regains within copolymer zwitterion-PVDF, PIEDA analysis was performed. In this study, we focused specifically on the electrostatic (ES), exchange repulsion (EX), and charge-transfer between ZW-PVDF membranes and water molecules. To obtain these results we implemented FMO-optimized water-solvated ZW-PVDF complex models. In this section, we applied FMO-based PIEDA energy decomposition analysis on the binding of water molecules with Zwitterion-PVDF models. Table 3.3 shows the results of the FMO2-PIEDA calculations using the HF method (FMO-RHF/6-31G* level). As discussed in previous section in this study, the strongest interactions between water molecules and ZW-PVDF membranes, especially zwitterionic heads and polar groups on zwitterionic copolymers, are hydrogen bonds. The study's interaction analysis indicated that they have more continuation in terms of the electrostatic and charge transfer when it comes to total pair interaction energies.

Based on PIEDA analyses, presented in Table 3.3, PMAL®-C_8-OH -SB-PVDF shows high hydrophilicity due to the strong interaction between sulfobetaine moiety and hydrophilic parts, such as amide and carboxylic groups with water molecules, when compared to original PVDF, commercial SBMA and SB_2VP zwitterions, and other designed zwitterions. Water molecules showed stronger electrostatic interactions with PMAL®-C_8-OH-SB. Energy of electrostatic

interactions between PMAL®-C_8-OH-SB and water is around -212.55 kcal/mol, whereas for the two commercial zwitterions, SBMA and SB2VP, electrostatic interaction values are -202.672 and -140.85 kcal/mol, respectively.

Table 3.3. Comparison of PIEDA analysis output for PVDF membrane, and ZW-PVDF membranes with 20 water molecules, calculated at FMO-RHF/6-31G* level (Energies in kcal/mol).

PIEDA	PVDF	SB2VP-PVDF	PMAL®-C8-SCA-PVDF	PMAL®-C8-PC-PVDF	SBMA-PVDF	PMAL®-C8-SB-PVDF	PMAL®-C_8-OH-SB-PVDF	double PMAL®-C_8-OH-SB-PVDF
E_{tot}	-53.741	-167.632	-154.204	-154.658	-197.857	-222.758	-232.547	-244.09
E_{es}	-35.644	-140.847	-160.314	-159.42	-202.672	-203.546	-212.55	-235.728
E_{ex}	24.61	52.073	83.572	108.154	91.788	97.055	171.976	112.41
E_{ct}	-42.702	-78.86	-77.46	-103.117	-116.27	-121.663	-157.279	-120.773
Eij-Ei-Ej	-43.397	-167.808	-148.229	-150.366	-193.72	-222.683	-235.742	-242.422

The electrostatic interaction energy for PMAL®-C_8-OH-SB is close to PMAL®-C_8-SB. The difference of around -10kcal/mol can be attributed to the only variance between these zwitterions, that is the added hydroxyl group between negative and positive charges on sulfobetaine in PMAL®-C_8-OH-SB. This hydroxyl group has two hydrogen bonds with water molecules and this strong hydrogen bonding potential increases the amount of electrostatic interaction energy to around -64 kcal/mol more than in PMAL®-C_8-SB. Figures 3.7 A and B show a PIEDA diagram, with specific colors assigned to show the more substantial energy components for PMAL®-C_8-OH-SB–PVDF and PVDF interactions with each water fragment, respectively. In this case, the green color represents exchange repulsion, dark green color stands for charge transfer, and blue color shows electrostatic interactions between ZW-PVDF models and water as fragments on color-coded PIEDA diagram. Based on the results included in Table 3.3 and Figure 3.8, original PVDF indicated small charge transfer of around -41 kcal/mol in comparison to PMAL®-C_8-OH-SB-PVDF. Although the original PVDF showed good interaction and charge transfer (-41 kcal/mol) with water molecules, there are several repulsive pair interactions, identified in purple color in Figure 8B, that can confirm PVDF hydrophobicity in water the system. This suggests that PMAL®-C_8-OH-SB-PVDF has stronger hydrogen bonds with water molecules compared to original PVDF, which can lead to higher electrostatic

interaction energy, charge transfer, and exchange repulsion energy. The PIEDA application suggests that PMAL®-C_8-OH-SB and PMAL®-C_8-SB had stronger electrostatic energy around sulfobetaine groups and polar groups, such as amide and carboxyl groups, than other betaine copolymers and SBMA.

In Table 3.3, the ES interactions forming hydrogen bonds between PMAL®-C_8-OH-SB – PVDF and PMAL®-C_8-SB-PVDF with the water were the strongest, at –212 kcal/mol and –203 kcal/mol, respectively. The obtained results indicated that amide and carboxylate groups on PMAL®-C_8-OH-SB and PMAL®-C_8-SB, have stronger electrostatic interaction energy of around -60 kcal/mol, compared to ester group on SBMA-PVDF of approximately -47 kcal/mol. Although ester group in SBMA played a role in attracting water molecules, the PMAL®-C_8-OH-SB can be identified as the best zwitterionic copolymer with stronger hydrogen bonds electrostatic interactions than other sulfobetaine zwitterions, a characteristic attributed to more charges on sulfobetaine head and higher polarization of polar groups (amide and carboxyl groups) on the copolymer backbone.

This study's results confirmed that the electrostatic interaction energy had contributed more total pair interaction energy for all novel zwitterions and commercial zwitterions with hydrophilic parts than the original PVDF model.

Charge transfer term can be described as the energy that contributes to net pair interaction energies and in this study is defined as a flow of charges between water molecules and ZW-PVDF membrane fragments. The novel zwitterion, PMAL®-C_8-OH-SB, showcased higher charge transfer energy between water molecules and ZW-PVDF membrane. This suggests that the charge transfer from the interaction between occupied orbitals of a donor (water molecules) and unoccupied orbitals of an acceptor (PMAL®-C_8-OH-SB) is greater than occurring in other zwitterions including commercial ones. PMAL®-C_8-OH-SB-PVDF indicated charge transfer energy of -157.28 kcal/mol, compared with charge transfer of previous zwitterions, SBMA and SB2VP, -121.663 and -78.86 kcal/mol, respectively.

Higher electrostatic interaction energy and charge transfer energy of PMAL®-C_8-OH-SB during contact with water molecules can be attributed to the greater number of polar groups on this zwitterion compared to two commercial zwitterions with the same zwitterionic head groups. In this case, novel PMAL®-C_8-OH-SB zwitterion, commercial zwitterions, and SBMA, feature the same zwitterionic head group. However, they are differentiated in terms of Ees, Ect, and Eex

during interaction with water molecules, between zwitterions, and previous ZWs, since more polar groups are located on the backbone of novel copolymer zwitterion and between the charges of the zwitterionic head group.

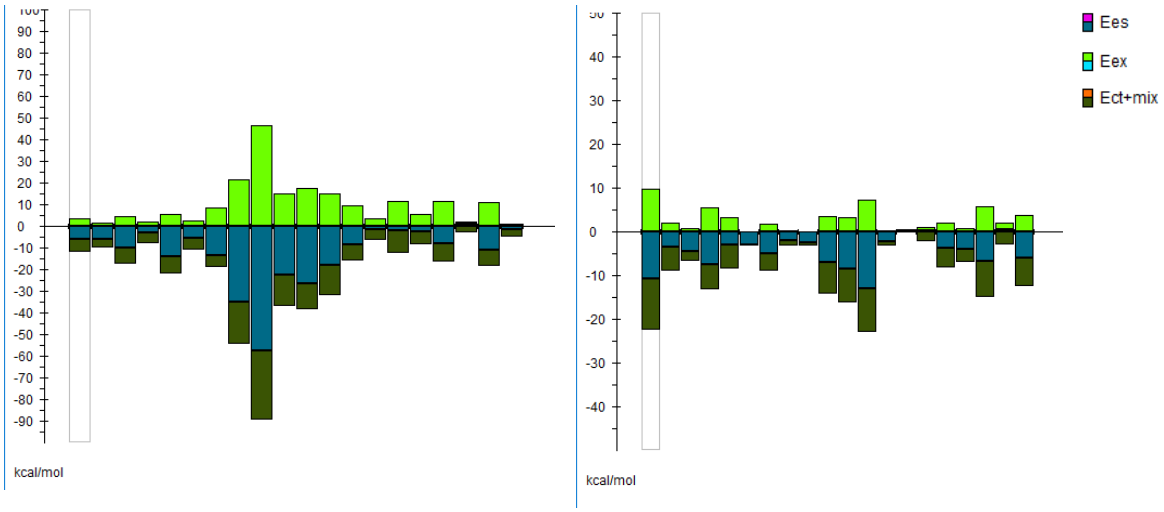

(a) **(b)**

Figure 3.8. Energy contributions (PIEDA) of each intermolecular interaction for a) PMAL®-C_8-2-hydroxyl-SB-PVDF, b) Pure PVDF with 20 water molecules, calculated with PIEDA/6-31G*. The pair interaction energy is divided into the electrostatic (ES), exchange-repulsion (EX), and charge-transfer with higher order mixed terms (CT+mix) contributions. Relevant PIEDA terms including electrostatics, charge-transfer, and exchange-repulsion are color-coded in dark blue, green, and dark green, respectively. Repulsive electrostatic is identified with purple color.

The data presented in Table 3.3 confirm the FMO results that zwitterions with sulfobetaine group, except SB_2VP, displayed better hydrophilicity compared with other zwitterions featuring carboxybetaine and phosphobetaine heads. The charge transfer energy for the hydrogen bonds in the PMAL®-C_8-OH -SB-PVDF is relatively large at -157 kcal/mol. There is a significant difference between charge transfers occurring in this zwitterion with water and other types of zwitterions. Among sulfobetaine zwitterions reported in this study, PMAL®-C_8-OH-SB-PVDF showed noticeably stronger electrostatic interaction energy, charge transfer energy, and exchange energy, as presented in Table 3.3.

It can be concluded that the charge transfer energy is considerably larger in PMAL®-C_8-OH-SB-PVDF due to more functional groups on copolymer, which have a tendency towards

hydrogen bonding. In addition to the charge transfer, the amount of the exchange repulsion energy (171kcal/mol) is higher in this zwitterion than other types of zwitterions. The exchange repulsion energy describes the interaction of exchange between the undistorted monomer charge distributions on zwitterions and water molecules. Other research groups reported results suggesting that SBMA is better than SB2VP experimentally for water treatments, and our results are in good agreement with previous data for SBMA and SB_2VP.

Based on Table 3.3, exchange repulsion energy for SB_2VP is less than for SBMA, at 52 kcal/mol and 91 kcal/mol, respectively. These resulted confirmed previous studies related to SB2VP in so far as it is reactively hydrophobic in comparison to SBMA. Charge transfer for PMAL®-C_8-CB-PVDF and PMAL®-C_8-MPC-PVDF were not consistent with their electrostatic interaction energies at -77 kcal/mol and -103 kcal/mol, respectively. Specifically, phosphobetaine showed higher charge transfer than carboxybetaine in these zwitterion-PVDF membranes, a correlation that can be attributed to a large charge transfer occurring between phosphoryl group and water molecules with extra oxygen atom on phosphobetaine head.

Two-dimensional (2D) maps of total fragment pair interaction energy (PIE) including electrostatics, exchange repulsion, and charge transfer of the best performing water-solvated PMAL®-C_8-OH -SB-PVDF complex model were obtained using ab initio FMO-HF calculations and are shown in Figure 3.9 (a−d).

The color-coded maps represent the primary components of pair interaction energy and the total pair interaction energy in terms of color and values reflecting the strength range of interactions, charge transfer, and repulsion between fragments. The darkest squares in Figure 3.8a are representations of the most attractive pair interactions, occurring between PMAL®-C_8-OH -SB-PVDF and water molecule fragments such as fragments 11, 10, 6, and 5. The blue color stands for pair interactions between PMAL®-C_8-OH -SB-PVDF and water fragments 8, 12, 18, and 21, which are less strong compared to the ones identified using dark color.

Figure 3.9b and Table 3.4 show that electrostatic interaction energy for PMAL®-C_8-OH-SB-PVDF with water molecules contributes more to PIE and has a determinative role when it comes to the value of the total interaction energy. Although there are similarities between the total pair interaction energy map and electrostatic interaction map, there are specific differences between the strengths of the electrostatic interaction energies of PMAL®-C_8-OH-SB-PVDF–water interactions (Figure 3.9b) with the total interaction energies (Figure 3.9a). As a result, while the

electrostatic interaction energy is most a critical part of the pair interaction energy decomposition analysis for water-solvated PMAL®-C_8-OH-SB-PVDF model, other variables such as charge transfer and exchange repulsion should not be neglected since they continue to affect the total interaction pair energy as well.

As shown in Figure 3.8 and Figure 3.9d, the value sign of the exchange repulsion interaction energy is positive for water-solvated PMAL®-C_8-OH-SB-PVDF complex model at around 171.97 kcal/mol, which follows the total pair interaction energy trend (Figure 3.9a). Thus, the signs need to be considered as part of the total pair interaction energy trend. The energy contributions can be arranged in the order of decreasing importance as ES> CT+mix > EX for the interactions between PMAL®-C_8-OH-SB-PVDF and water molecules.

To examine three zwitterionic head interactions of copolymer zwitterionic structure with water molecules, PIEDA was used to determine highest interactions occurring between sulfobetaine in sulfobetaine zwitterion, carboxybetaine, and phosphobetaine with water molecules as a fragments (Figure 3.10a, 3.10b, and 3.10c).

The greatest difference was noted between the fragment PIEDA maps of carboxybetaine (Figure 3.10a), phosphobetaine (Figure 3.10b), and sulfobetaine (Figure 3.10c) and is related to the electrostatic interaction energy contributions changing from -47, -64, -117 kcal/mol, respectively. The electrostatic interactions from fragments 9, 10, and 11 for PMAL®-C_8-OH-SB-PVDF form three strong hydrogen bonds with SO_3^- group on sulfobetaine head, since electrostatic interactions are used to define hydrogen bond interactions. There is a greater number of attractive interactions for sulfobetaine than for both carboxybetaine and phosphobetaine (Figure 3.10a and 3.10b).

For phosphobetaine, there are two hydrogen bonding interactions between OPO_3^- and fragments 10 and 11, while for carboxybetaine there are also two hydrogen bonding interactions between COO^- and fragments 4 and 5. The charge transfer energy for the interactions between fragments 9, 10, and 11 with sulfobetaine head of PMAL®-C_8-OH-SB showed a large difference of -65 kcal/mol, compared to interactions between fragments 10 and 11 with phosphobetaine head of PMAL®-C_8-PC-PVDF, and 4 and 5 with carboxybetaine head of PMAL®-C_8-CB-PVDF, at -31 and -19 kcal/mol, respectively.

These hydration free energy results agree with the FMO data regarding best performances of sulfobetaine zwitterions compared to carboxybetaine and phosphobetaine, since they offer

stronger and more numerous interactions with water molecules, and consequently increase hydrophilicity of hydrophobic PVDF membranes.

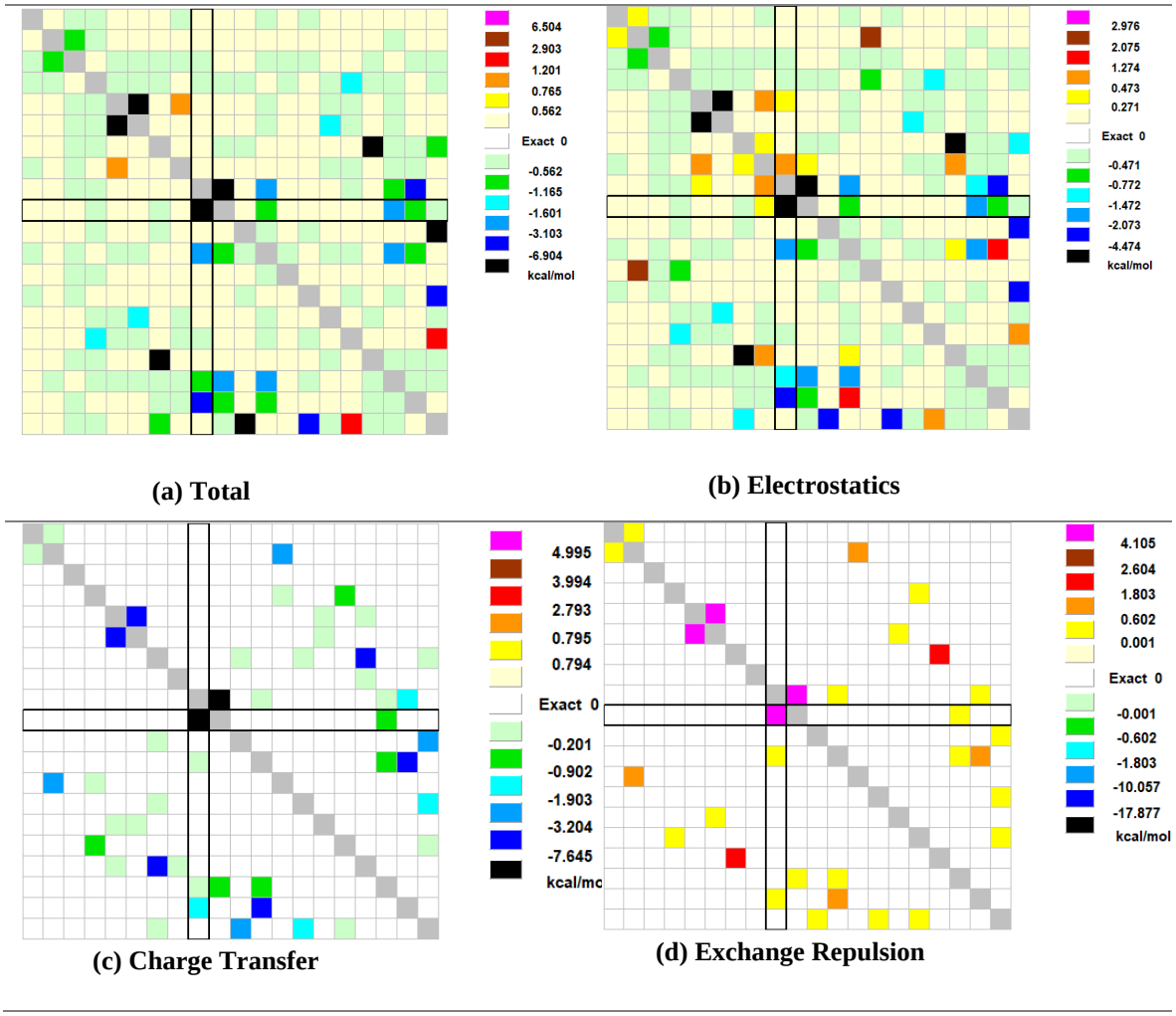

Figure 3.9. (a–d) Color-coded two-dimensional maps of PIE values and components of PIE values are calculated for PMAL®-C_8-OH-SB-PVDF with 20 water molecules (in kcal/mol): (a) total, (b) electrostatics, (c) charge transfer, and (d) exchange repulsion.

3.4.4 Double zwitterion of PMAL®-C_8-OH-SB-PVDF

In this study we designed different zwitterions with changing zwitterionic heads on copolymer PMAL®-C_8 without changing the overall net charge of Zwitterions. In this section, we are examining the structural changes of best performing zwitterion, PMAL®-C_8-OH-SB, by increasing the pH in aqueous environment. The double zwitterionic PMAL®-C_8-OH-SB-PVDF

had formed through protonated carboxyl group on the backbone of copolymer PMAL®-C_8, and protonated the nitrogen atom of amide group, as shown in Figure 3.11b.

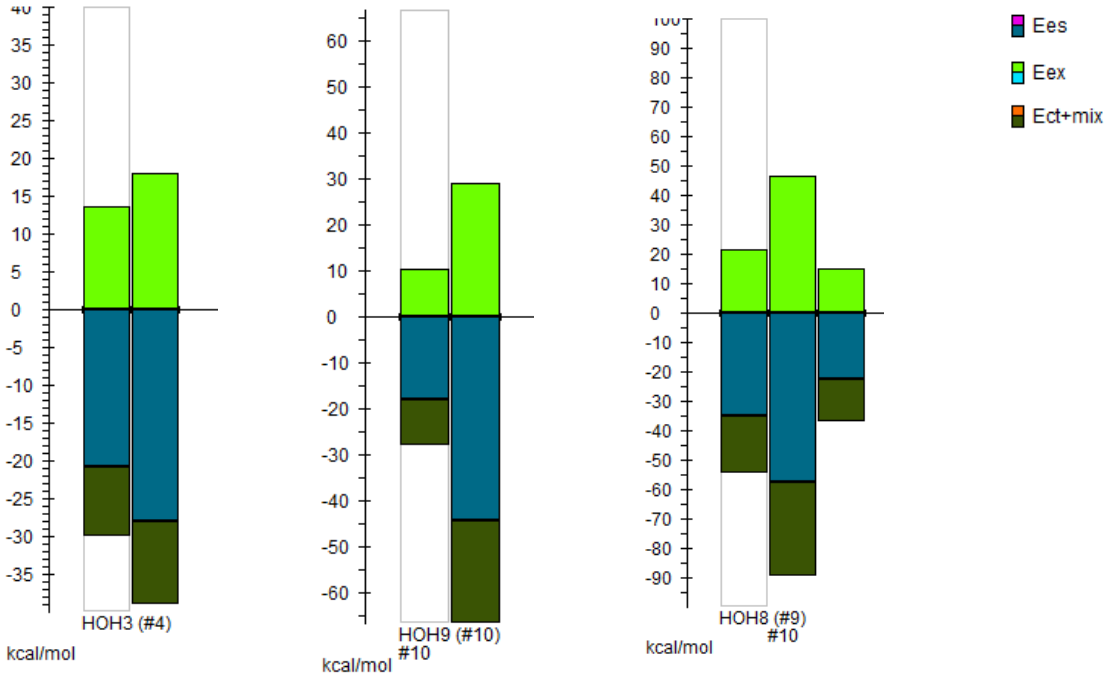

(a)PMAL®-C_8-CB-PVDF **(b)PMAL®-C_8-PC-PVDF** **(c)PMAL®-C_8-OH-SB-PVDF**

Figure 3.10. The fragment PIEDA for a) fragment 4 and 5 showing the interaction between water molecules number 4 and 5 with carboxybetaine head of PMAL®-C_8-CB-PVDF, (b) The fragment PIEDA for fragment 10 and 11, showing the interactions between water molecules number 10 and 11 with phosphobetaine head of PMAL®-C_8-PC-PVDF, and C) The fragment PIEDA for fragment 9, 10, and 11, showing the interactions between water molecules number 9, 10, and 11 with best performing sulfobetaine head of PMAL®-C_8-OH-SB-PVDF from the selection of all sulfobetaine zwitterions in this study. All interactions are in kcal/mol.

Double zwitterion features two anionic groups. such as sulfonate SO_3 and carboxylate COO, which have a net charge of -1, and two cationic groups quaternary ammonium ($(CH_2)_2{-}N^+(CH_3)_2$) and secondary ammonium ($-H_2N^+{-}(CH_2)_2$), which combine to a net charge of +1. The structure was optimized using FMO method and partial charges were catapulted for this double zwitterion.

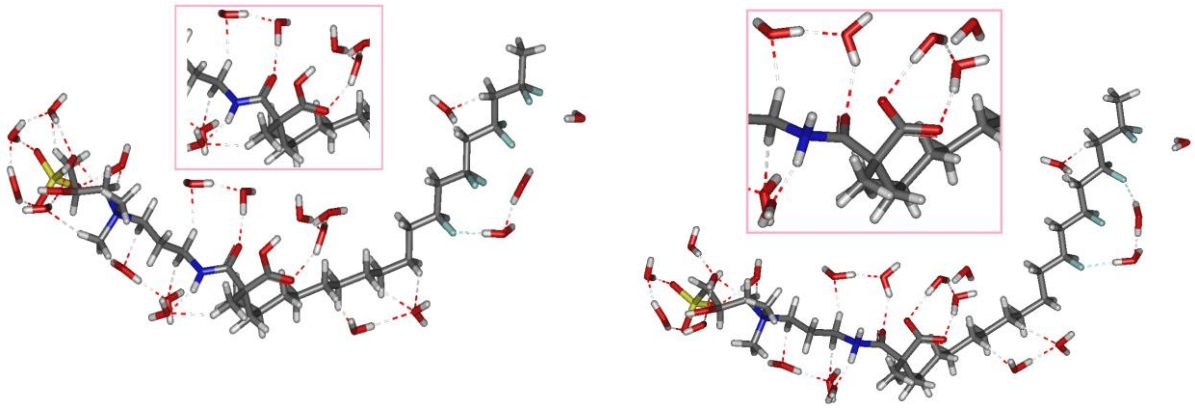

(a) **(b)**

Figure 3.11. FMO optimization of a) PMAL®-C_8-OH-SB-PVDF with 20 water molecules, and b) double zwitterionic PMAL®-C_8-CB-OH-SB-PVDF with 20 water molecules, calculated at FMO-RHF/6-31+G* level of theory.

The obtained result indicated that the sulfonate group has a higher charge density compared to carboxylate group on copolymer of PMAL®-C_8-CB-OH-SB-PVDF. Alternatively, the secondary ammonium ($-H_2N^+-(CH_2)_2$) showed greater charge density compared to quaternary ammonium ($(CH_2)_2-N^+(CH_3)_2$). Therefore, this copolymer has two zwitterionic moieties, with one of them includes as a secondary ammonium group ($-H_2N^+-(CH_2)_2$) and a carboxylate group (CO_2^-), while another zwitterionic moiety has a quaternary ammonium ($(CH_2)_2-N^+(CH_3)_2$) and a sulfonate group (SO_3^-).

Figure 3.11b shows that by forming additional zwitterion moiety, carboxybetaine on PMAL®-C_8-CB-OH-SB-PVDF, the number of water molecules around anionic sulfobetaine with quaternary ammonium group and carboxybetaine with secondary ammonium are nearly same with PMAL®-C_8-OH-SB-PVDF model and without producing a substantial change. It can be derived that the number of water molecules around zwitterionic moieties on copolymer is not influenced by changing cationic groups, a correlation that is consistent with the results previously reported in literature (Shao *et al*., 2014). In preceding section, we discussed that the fact that carboxybetaine on copolymer PMAL®-C_8-CB-PVDF is surrounded by a lower number of water molecules, compared to other sulfobetaine copolymers, due to smaller molecular size of carboxylate group. As a double zwitterion, PMAL®-C_8-CB-OH-SB-PVDF, likewise showed the same results as a PMAL®-C_8-CB-PVDF membrane, with only one extra water molecule around carboxylate group compared to the carboxylic group on PMAL®-C_8-OH-SB-PVDF.

Figure 3.11 displays the numbers of water molecules around quaternary ammonium ($(CH_2)_2$–$N^+(CH_3)_2$) of sulfobetaine moiety on double zwitterionic copolymer PMAL®-C_8-CB-OH-SB, which is nearly identical to the one for cationic group on PMAL®-C_8-OH-SB-PVDF due to the fact that it is not depend on a different anionic charged group. However, the number of water molecules around quaternary ammonium ($(CH_2)_2$–$N^+(CH_3)_2$) of sulfobetaine moiety on double zwitterionic copolymer PMAL®-C_8-CB-OH-SB is more than that of the secondary ammonium ($-H_2N^+$–$(CH_2)_2$) of carboxybetaine on double zwitterionic copolymer due to larger molecular volumes of quaternary ammonium compared to secondary ammonium (Shao *et al*., 2014).

Figure 3.11 also outlines that cationic secondary ammonium group on double zwitterionic copolymer has two hydrogen atoms attached to the nitrogen atom. It shows strong hydrogen bonding, compared to one hydrogen attached to nitrogen on amide group of PMAL®-C_8-OH-SB-PVDF or hydrogen atoms of methyl group attached to nitrogen of quaternary ammonium on double zwitterion. The main reason for this advantage in cationic secondary ammonium group is the dependence of its hydration on the anionic carboxylate group (Shao *et al*., 2014). Therefore, it was able to show greater bond length and, consequently more electrostatic and charge transfer energies compared to PMAL®-C_8-OH-SB-PVDF.

The moiety $–H_2N^+–CO–CH_2–CH_2–COO^-$ has the highest charge densities and had reduced the charge density of other charged groups such as $-N^+(CH_2\text{-}CH_2(OH)\text{-}CH_2)\ SO_3^-$, as shown in Figure 3.12 (a, b). Based on PIEDA diagram included in Figure 11b, carboxybetaine moiety, $–H_2N^+–CO–CH_2–CH_2–COO^-$, produced strong electrostatic interactions with water molecules (fragments 2, 3, and 21). Fragments 2 and 3 presented stronger electrostatic interaction with COO- and fragment 21, thus suggesting attractive electrostatics with secondary ammonium. Conversely, fragments reduced electrostatic interactions between water fragments and sulfobetaine head in double zwitterion when compared to PMAL®-C_8-OH-SB-PVDF. As a result, different cationic groups do not have a substantial effect on the number of water molecules around anionic groups, however they can change hydration properties of the anionic groups by changing their charge densities (Shao *et al*., 2014, Azzaroni *et al*., 2006).

The electrostatic interaction energy of this hydrogen bond is –28 kcal/mol, that is more than hydrogen bond of quaternary ammonium group and with hydrogen attached to nitrogen of amide group on PMAL®-C_8-OH-SB-PVDF, that are -12 kcal/mol and -1.77 kcal/mol, respectively.

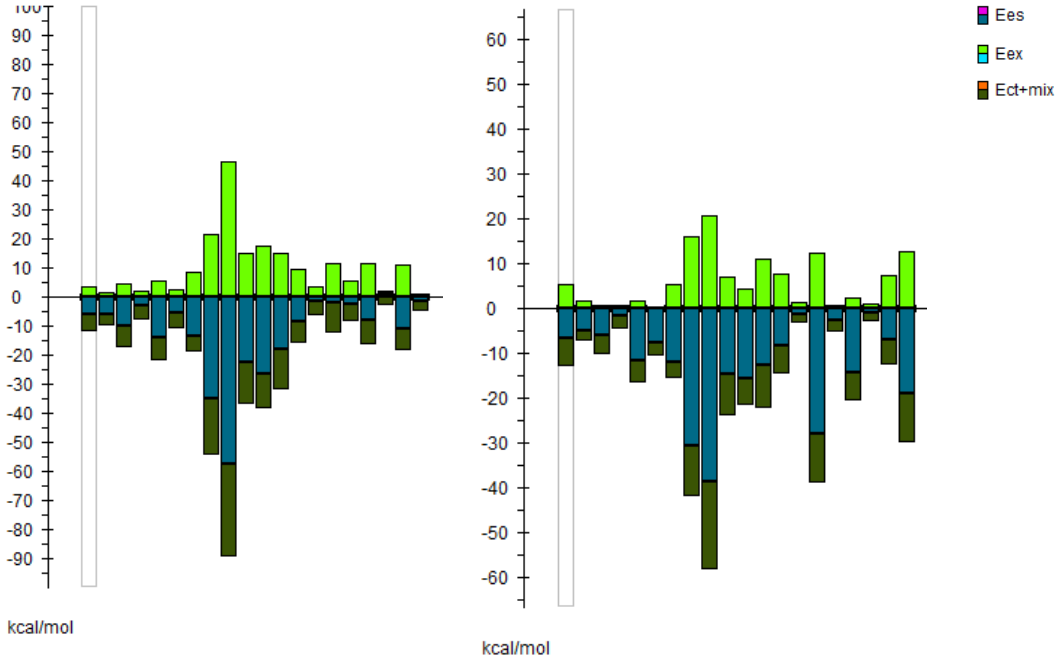

(a) **(b)**

Figure 3.12. The fragment PIEDA for a) fragment 4 and 5 showing the interaction between water molecules number 4 and 5, with sulfobetaine head of PMAL®-C_8-OH-SB-PVDF, and (b) The fragment PIEDA for fragment 16 and 21 outlining the interaction between water molecules number 10 and 11, with sulfobetaine head of double zwitterion, PMAL®-C_8-OH-SB-PVDF. All interactions are in kcal/mol.

3.5 Conclusion

In this work we designed four copolymers of a Poly (maleic anhydride-alt-1-decene), 3-(dimethylamino)-1-propylamine (PMAL®-C_8) with different zwitterionic monomers (sulfobetaine, Phosphorylcholine, and carboxybetaine) that have not been previously reported as a way of enhancing hydrophilicity of hydrophobic PVDF membrane. By using a set of computational methods we investigated the effects of the chemical structure of three zwitterionic monomers, chemical groups between charged groups of sulfobetaine, and the hydrophilic groups on the backbone of copolymer (between charged functional groups of the zwitterions and PVDF polymer as a linker) on the hydrophilicity and water uptake of their copolymers with PVDF membranes.

A combination of the Pair Interaction Energy Decomposition Analysis (PIEDA) within the framework of the fragment molecular orbital (FMO) method were applied to investigate hydration and non-covalent interactions between zwitterionic PVDF membranes derived from

same cationic quaternary ammonium group and three anionic groups sulfobetaine, carboxybetaine, and phosphobetaine with water molecules. All water-solvated zwitterionic PVDF complex models indicated strong hydration, however the strength of hydration around them depended on the types of anionic groups involved. During our comparative analysis of different zwitterionic moieties on copolymer of PMAL®-C_8 and other commercial zwitterions, we found that the sulfobetaine zwitterionic heads have a higher number of water molecules than carboxybetaine and phosphobetaine. This increase in the number of water molecules around the negatively charged group of sulfobetaine moiety can be attributed to its additional oxygen atom when compared to carboxybetaine, as well as a lack of steric hindrance of methyl group when compared to phosphobetaine moiety. Although sulfobetaine groups have a greater number of water molecules around them, carboxybetaine and phosphobetaine moieties showed strong hydrogen bonding with individual water molecules due to higher charge density and larger number of oxygen atoms. The water molecule numbers occurring in the positively charged groups of these three zwitterionic moieties are almost the same for all zwitterionic copolymers and are greater than in the negatively charged groups. It was determined that water molecules have stronger interactions with the negatively charged groups of carboxybetaine, phosphobetaine, and sulfobetaine than the positively charged group due to their higher partial charges. Therefore, partial charge contributes to the strength of hydrogen bonding between betaine moieties and water and shell volume around negative and positive charges. This in turn leads to higher number of water molecules around them and more hydrogen bonding.

All of the novel zwitterions discussed in this study showed dramatically improved performances compared to two commercial zwitterions SBMA and SB2VP used as references. Water-solvated PMAL®-C_8-OH-SB-PVDF complex model offered super hydrophilicity and higher tendency to absorb water molecules when compared to other new zwitterions and commercial zwitterionic PVDF membranes.

In this paper, we performed a systematic study of the double zwitterionic PMAL®-C_8-CB-OH-SB-PVDF derived from cationic quaternary ammonium, secondary ammonium group, and two anionic groups (CO_2, SO_3) without changing the overall net charge of the copolymer in PVDF membrane. The moiety $–H_2N^+–CO–CH_2–CH_2–COO^–$ exhibited high charge density that reduced the charge density of $(CH_3)_2–N^+(CH_2\text{-}CH_2(OH)\text{-}CH_2)\ SO_3^–$. Its PIEDA reflected strong electrostatic interactions between nitrogen of $–H_2N^+–CO–CH_2–CH_2–COO^–$ and water molecules

compared to quaternary ammonium and Hydrogen attached to Nitrogen on amide group of PMAL®-C_8-OH-SB-PVDF. As a consequence, it was determined that although different cationic groups do not have a significant effect on the number of water molecules around anionic groups, they can alter the hydration properties of the anionic groups by changing their charge densities.

This is the first study addressing the design of new zwitterionic copolymers with three diverse anionic groups and double zwitterion with different anionic and cationic groups, and then comparing their respective capacities to enhance hydrophilicity of hydrophobic PVDF membranes with FMO and PIEDA methods. This research study can help design and develop innovative zwitterions for different applications in the future.

3.6 Acknowledgements

The authors would like to acknowledge the Department of Chemical and Biological Engineering at the University of Saskatchewan for the generous support provided. The authors would also like to thank the High Performance Computing Research Facility (HPCRF) at the University of Saskatchewan for the services and facilities provided.

CHAPTER 4

Conclusions and Recommendations

4.1. Summary of Results

This study provides an innovative direction, for a more complete, multi-scaling modelling that can open up new avenues for a closer structural examination of PVDF and its characteristics in terms of hydrophobicity during interactions with water molecules. This approach was used in order to investigate the selectivity and binding of PVDF with water, in comparison to hydrophilic PAN membranes at the molecular level. Within the scope of this study, the PIEDA-FMO used GAMESS and the Facio Viewer. This is first time to implement FMO-PIEDA computational study for the investigation of non-covalent interactions of water molecules with PVDF, compared to PAN. The application of the FMO and PIEDA analyses have allowed for two key advantages: (a) multifaceted QM theories were comprised into four straightforward quantities, and (b) specific calculations were made substantially more accurate and quicker than traditional QM approaches. Such an improvement allowed to better describing non-covalent interactions, when it comes to terms of electrostatic, charge-transfer, exchange-repulsion, dispersion, and optional polarization. This approach also helps to comparatively analyze the interaction energies of hydrophobic PVDF and hydrophilic PAN membranes engaging with water molecules.

The PIEDA results suggest that PAN fragment offers greater charge transfer, exchange repulsion, electrostatic, and interaction energy when interacting with six water molecules. The PVDF likewise indicated a substantial charge transfer that can be linked to a greater polar group and PVDF dipole moment. The FMO optimization revealed that the PVDF allows for hydrogen bonding, however, this bonding cannot function to electrostatic interactions. This study determined that the interactions of water with a hydrophobic solute or surface is directly correlated to the van der Waals interactions, while at the same time independent of the effects of electrostatic interactions. This relative independence is primarily facilitated by higher propensity

of water at room temperatures to maintain its hydrogen bonding network configuration, without enough hydrophilic sites. In this study, the interactions between PVDF, PAN, and water molecules were experimentally analyzed with the aid of Raman and confocal microscopic spectroscopies, the data indicating that there are more interactions between the CN group compared to CF and hydrophobicity of PVDF. Overall, there was a reasonable correlation 83 between theoretical and experimental data. In addition, the interactions between PVDF, PAN, and water molecules were experimentally analyzed, which were in agreement with the theoretical results using Fourier-transform infrared spectroscopy (FTIR- ATR), Raman, and SSNMR spectroscopies. Although Fluorine has a much higher electronegativity than nitrogen, however, the covalent bond of C-F is stronger than C-N, and is harder to break during interactions with water molecules. The energy of the polar covalent bond of C-F is higher than the C-N to be broken for interaction with water. Therefore, water molecules prefer to cluster together with hydrogen bonding instead of breaking the C-F polar covalent bond.

In this work, to overcome hydrophobicity of PVDF membranes, we designed four copolymers of a Poly(maleic anhydride-alt-1-decene), 3-(dimethylamino)-1-propylamine (PMAL®-C8) with different zwitterionic monomers (sulfobetaine, phosphorylcholine, and carboxybetaine) that have not been previously reported. We investigated the effects of the chemical structure of three zwitterionic monomers, chemical groups between charged groups of sulfobetaine, and the hydrophilic groups on the backbone of copolymer (between charged functional groups of the zwitterions and PVDF polymer as a linker) on the hydrophilicity and water uptake of their copolymers with PVDF membranes.

A combination of the Pair Interaction Energy Decomposition Analysis (PIEDA) within the framework of the fragment molecular orbital (FMO) method was applied to investigate hydration and non-covalent interactions between zwitterionic PVDF membranes derived from same cationic quaternary ammonium group and three anionic groups sulfobetaine, carboxybetaine, and phosphobetaine with water molecules. All water-solvated zwitterionic PVDF complex models indicated strong hydration; however, the strength of hydration around them depended on the types of anionic groups involved. During our comparative analysis of different zwitterionic moieties on copolymer of PMAL®-C8 and other commercial zwitterions, we found that the sulfobetaine zwitterionic heads have a higher number of water molecules than carboxybetaine and phosphobetaine. This increase in the number of water molecules around the negatively

charged group of sulfobetaine moiety can be attributed to its additional oxygen atom when compared to carboxybetaine, as well as a lack of steric hindrance of methyl group when compared to phosphobetaine moiety. Although sulfobetaine groups have a greater number of water molecules around them, carboxybetaine and phosphobetaine moieties showed strong hydrogen bonding with individual water molecules due to higher charge density and larger 84 number of oxygen atoms. The water molecule numbers occurring in the positively charged groups of these three zwitterionic moieties are almost the same for all zwitterionic copolymers and are greater than in the negatively charged groups. It was determined that water molecules have stronger interactions with the negatively charged groups of carboxybetaine, phosphobetaine, and sulfobetaine than the positively charged group due to their higher partial charges. Therefore, partial charge contributes to the strength of hydrogen bonding between betaine moieties and water and shell volume around negative and positive charges. This in turn leads to a higher number of water molecules around them and more hydrogen bonding.

The novel zwitterions discussed in this study showed dramatically improved performances compared to two commercial zwitterions SBMA and SB2VP used as references. Water-solvated PMAL®-C_8-OH-SB-PVDF complex model offered super hydrophilicity and a higher tendency to absorb water molecules when compared to other new zwitterions and commercial zwitterionic PVDF membranes.

Furthermore, we performed a systematic study of the double zwitterionic PMAL®-C_8-CBOH-SB-PVDF derived from cationic quaternary ammonium, secondary ammonium group, and two anionic groups (CO_2, SO_3) without changing the overall net charge of the copolymer in PVDF membrane. The moiety $–H_2N^+–CO–CH_2–CH_2–COO^-$ exhibited high charge density that reduced the charge density of $(CH3)_2–N^+(CH_2\text{-}CH_2(OH)\text{-}CH_2)SO_3^-$. Its PIEDA results reflected strong electrostatic interactions between nitrogen of $–H_2N^+–CO–CH_2–CH_2–COO^-$ and water molecules compared to quaternary ammonium and Hydrogen attached to Nitrogen on an amide group of PMAL®-C_8-OH-SB-PVDF. As a consequence, it was determined that although different cationic groups do not have a significant effect on the number of water molecules around anionic groups, they can alter the hydration properties of the anionic groups by changing their charge densities.

This is the first study addressing the design of new zwitterionic copolymers with three diverse anionic groups and double zwitterion with different anionic and cationic groups, and then

comparing their respective capacities to enhance hydrophilicity of PVDF membranes with FMO and PIEDA methods. This research study can help to design and develop innovative zwitterions for different applications in the future.

4.2 Conclusions

1- These results showed the reason behind the hydrophobicity of PVDF membranes. The interactions of PVDF with water molecules are directly correlated to the van der Waals interactions, while at the same time independent of the effects of electrostatic interactions.

2- The experimental interactions between PVDF, PAN, and water molecules were in a good agreement with the theoretical results using Fourier-transform infrared spectroscopy (FTIR- ATR), Raman, and SSNMR spectroscopies, suggesting that more interactions between the CN group compared to CF.

3- The energy of the polar covalent bond of C-F is higher than the C-N to be broken when interacting with water molecules. Therefore, water molecules prefer to cluster together with hydrogen bonding instead of breaking the C-F polar covalent bond.

4- FMO and PIEDA results confirmed that the water-solvated PMAL®-C_8-OH-SB-PVDF complex model is offering a super hydrophilicity and a higher tendency to absorb water molecules when compared to PVDF membranes treated with other commercial zwitterions, such as SBMA and SB2VP.

5- The double zwitterionic PMAL®-C_8-CB-OH-SB-PVDF was designed through the addition of a protonated carboxyl group on the backbone of copolymer PMAL®-C_8, and protonated nitrogen atom of amide group. This double zwitterion showed strong electrostatic interactions between water molecules with the secondary ammonium and oxygen of carboxybetaine, compared to PMAL®-C_8-OH-SB-PVDF model.

4.3 Recommendations

A comprehensive computational study is proposed to predict the hydrophilicity of novel zwitterions on PVDF membranes. The best novel zwitterion can be synthesized experimentally and its performance can be tested with different analysis methods, to be applied in large scale in

industrial. Therefore, the effect of hydrophilicity zwitterions on hydrophobic PVDF membranes should be investigated experimentally in the future work.

In this study, a comprehensive computational study is proposed to predict the hydrophilicity of novel zwitterions on PVDF membranes. The best novel zwitterion can be synthesized experimentally and its performance can be tested with different analysis methods, to be applied in large scale in industrial. Therefore, the effect of hydrophilicity zwitterions on hydrophobic PVDF membranes should be investigated experimentally in the future work. In this work our results showed that novel zwitterion on the PVDF membranes can be helpful to reduce fouling divalent ions such as Ca^{2+} and SO_4^{2-} ions on the membrane surface. According to previous studies the salt rejection increases for divalent ions compared to monovalent ions because there is a stronger electrostatic interaction between divalent ions and the membrane bound charged groups in comparison to the monovalent groups, which should be explored in the future studies experimentally for salt rejection.

This work provided an important structural-based design principle to understand about the structure−property relationship for the role of zwitterionic materials. A subtle change in the Carbon Space Length (CSL) of zwitterion polymers affects the surface hydration and antifouling properties of the membranes. However, in this work the CSL-induced combination effects on surface hydration and the antifouling behavior remain unclear and unexamined when incorporating zwitterionic materials into a hydrophobic PVDF membrane system. Hence, the effect of alkyl chain spacer length between the charged groups (CSL) in zwitterionic poly(sulfobetaine) (PSB) chains in the hydrated state can be studied by computational methods in the future.

REFERENCES

Abboud, J.-L. M., Motario, R., Botella, V., Quantitative treatments of solute/solvent interactions. *Theor. Comput. Chem*., 1, **1994**,135.

Alexeev, Y., Mazanetz, M.P., Ichihara, O. Fedorov, D.G. GAMESS as a free quantum-mechanical platform for drug research. *Curr. Top. Med. Chem*. 12, **2012**, 2013.

Alfrey T.; Morawetz, H. The nature of the active methyl donor formed enzymatically from L-methionine and adenosine triphosphate, *J.Am.Chem.Soc*. 74, **1952**, 43

Antony A, Subhi N, Henderson RK, Khan SJ, Stuetz RM, Le-Clech P, et al. Comparison of reverse osmosis membrane fouling profiles from Australian water recycling plants. *J Member Sci*;407–408, **2012**, 8.

Azzaroni, O.; Brown, A. A.; Huck, W. T. S. UCST wetting transitions of polyzwitterionic brushes driven by self-association. *Angew. Chem., Int. Ed*., 45, **2006,**1770.

Baker, R. W. Membrane technology and applications, 2nd edn, John Wiley & Sons, **2004.**

Bokhary, A.; Cui, L.; Lin, H.J.; Liao, B.Q. A Review of membrane technology for integrated forest biorefinery, *J. Membr. Sci. Res*. 3, **2017**, 120.

Bretscher, M. S.; Raff, M. C. Mammalian plasma-membranes. *Nature*, 258, **1975**,43.

Barone, V., Cossi, M., Tomasi, J. Geometry optimization of molecular structures in solution by the polarizable continuum model. *J. Comp. Chem*. 19, **1998**, 404.

Bengani-Lutz, P.; Converse, E.; Cebe, P.; Asatekin, A. Self-assembling zwitterionic copolymers as membrane selective layers with excellent fouling resistance: effect of zwitterion chemistry. ACS Appl. Mater. Interfaces., 9, **2017,** 20859.

Clark, M.M.; Heneghan, K.S. Ultrafiltration of lake water for potable water production. *Desalination* 80, **1991**, 243.

Chen, W., Gordon, M. S., Energy decomposition analyses for many-body interaction and applications to water complexes, *J. Phys. Chem*. 100, **1996**, 14316.

Dechnik, J.; Gascon, J.; Doonan, C.; Janiak, C.; Sumby, C. Mixed-Matrix Membranes. *Angew Chem Int Ed*. 56, **2017**, 9292.

Drioli, E.; Giorno, L. Membrane operation in molecular separations; Elsevier (Singapore) PteLtd. *Singapore*, **2012**.

Dalvi, V.H, Rossky, P.J. Molecular origins of fluorocarbon hydrophobicity. *P.J. Proc Natl Acad Sci U S A.* 107, **2010**, 13603.

Elimelech, M.; Phillip, W.A. The future of seawater desalination: Energy, technology, and the environment. *Science*, 333, **2011**, 712.

Filloux, E.; Gallard, H.; Croue, J.P. Identification of effluent organic matter fractions responsible for low-pressure membrane fouling. *Water Res*. 46, **2012**, 5531.

Fedorov, D.G., Nagata, T., Kitaura, K. Exploring chemistry with the fragment molecular orbital method. *Phys. Chem. Chem. Phys.* 14, **2012**, 7562.

Fedorov, D.G., Kitaura, K. Extending the power of quantum chemistry to large systems with the fragment molecular orbital method. *J. Phys. Chem. A* 111, **2007**, 6904.

Fedorov, D.G. Kitaura, K. Pair interaction energy decomposition analysis. *J. Comput. Chem*. 28, **2007**, 222.

Fujimura, K., Sasabuchi, Y., The Role of fluorine atoms in a fluorinated prostaglandin agonist, *ChemMedChem*, 5, **2010**, 1254.

Fane, A.G.; Tang, C.Y.; Wang, R. Membrane technology for water: microfiltration, ultrafiltration, nanofiltration, and reverse osmosis, in: W. Peter (Ed.), Treatise on Water Science, Elsevier, Oxford. **2011**, 301.

Gleick, P. H.; Water Resources. In encyclopedia of climate and weather; Schneider, S.H., Ed.; Oxford University Press: New York, 2, **1996**, 817.

Gin, D. L.; Noble, R. D.; Chemistry. Designing the next generation of chemical separation membrane, *Science*, 332, **2011**, 674.

Gordon, M.S., Schmidt, M. W. S. Advances in electronic structure theory: GAMESS a decade later. In theory and applications of computational chemistry: The First forty years; Dykstra, C. E., frenking, G., Kim, K.S., Scuseria, G. E., Eds.; *Elsevier*: *Amsterdam*, **2005,** 1167.

Gordon, M. S.; Fedorov, D. G.; Pruitt, S. R.; Slipchenko, L. V. Fragmentation methods: A route to accurate calculations on large systems. Chem. Rev., 112, **2012,** 632.

Gudipati, C.S.; Finlay, J.A.; Callow, J.A.; Callow, M.E.; Wooley, K.L. The antifouling and fouling-release performance of hyperbranched fluoropolymer (HBFP)-poly (ethylene glycol) (PEG) composite coatings evaluated by adsorption of biomacromolecules and the green fouling alga ulva, *Langmuir*, 21, **2005**, 3044.

Galin, M.; Chapoton, A.; Galin, J. C. Dielectric increments, intercharge distances and conformation of Quaternary ammonioalkylsulfonates and alkoxydicyanoethenolates in aqueous and trifluoroethanol solutions. *J. Chem. Soc., Perkin Trans.* 2, **1993,** 545.

Hannon, M.J.; Boerio, F.J.; Koenig, J.L., Vibrational Analysis of Polytetrafluoroethylene, *J. Chem. Phy*, 50, **1969**, 2829.

Herzberg, M.; Elimelech, Biofouling of reverse osmosis membranes: Role of biofilm-enhanced osmotic pressure, M. *J. Membr. Sci*., 295, **2007**, 11.

Hoek E.M.; Allred J.; Knoell T.; Jeong B.H. Modeling the effects of fouling on full-scale reverse osmosis processes. *J Membr Sci.* 314, **2008**, 33.

Hamingerova, M.; L.B.; Beckmann, M. Membrane technologies for water and wastewater treatment on the European and Indian market. Tech. Rep. Fraunhofer center for *International Management and Knowledge Economy*; **2010**, 37.

Haberkamp, J.; Ernst, M.; Bockelmann, U.; Szewzyk, U.; Jekel, M. Complexity of ultrafiltration membrane fouling caused by macromolecular dissolved organic compounds in secondary effluents. *Water Res*. 42, **2008**, 3153.

Han, G.; Tao, J.; Kang, L.; Lu, J.; Chung, T.S. Advanced anti-fouling membranes for osmotic power generation from wastewater via pressure retarded osmosis (PRO), *Environ. Sci. Technol.* 5, **2018**, 6686.

Holmlin, R. E.; Chen, X. X.; Chapman, R. G.; Takayama, S.; Whitesides, G. M. Zwitterionic SAMs that resist nonspecific adsorption of protein from aqueous buffer. *Langmuir*, 17, **2001**, 2841.

Herold, D. A.; Keil, K.; Bruns, D. E. Oxidation of polyethylene glycols by alcohol dehydrogenase, *Biochem. Pharmacol*. 38, **1989**, 73.

Jang, H.; Song, D.-H.; Kim, I.-C.; Kwon, Y.-N. Mechanical/optical behaviors of imogolite hydrogels depending on their compositions and oriented structures, *J. Appl. Polym. Sci*. 132, **2015**, 41712.

Kaner, P.; Rubakh, E.; Kim, D. H.; Asatekin, A. Zwitterion-containing polymer additives for fouling resistant ultrafiltration membranes. *J. Membr. Sci*., 533, **2017,** 141.

Kwon, B.; Lee, S.; Cho, J.; Ahn, H.; Lee, D.; Shin, H.S. Biodegradability, DBP formation and membrane fouling potential of natural organic matter: characterisation and controllability. *Environmental Science and Technology*. 39, **2005**, 732.

Kowalczyk, S.W.; Blosser, T.R.; Dekker, C. Biomimetic nanopores: Learning from and about nature. *Trends Biotechnol*. 29, **2011**, 607.

Kang, G.-D.; Cao, Y.-M. Application and modification of poly (vinylidene fluoride) (PVDF) membranes – A review, J. *Membr. Sci*. 463, **2014**, 145.

Kang, G.D.; Cao, Y.M. Development of antifouling reverse osmosis membranes for water treatment: a review, *Water Res*. 46, **2012**, 584.

Koening, J.L.; Spectroscopy of polymer, Elsevier, New York, **1999**.

Khorshidi, B., Biswas, I., Ghosh, T., Thundat, T., Sadrzadeh, M. "Robust fabrication of thin film polyamide-TiO2 nanocomposite membranes with enhanced thermal stability and anti-biofouling propensity". *Sci Rep*. 8, **2018**, 784.

Kitaura, K., Morokuma, K., "A new energy decomposition scheme for molecular interactions within the Hartree-Fock approximation", *Int. J. Quantum Chem*. 10, **1976**, 325.

Kitaura, K., Ikeo, E., Asada, T., Nakano, T., Uebayasi, M. "Fragment molecular orbital method: an approximate computational method for large molecules". Chem. Phys. Lett. 313, 1999, 701.

Kobayashi, M.; Tashiro, K.; Tadokoro, H. Molecular vibrations of three crystal forms of poly(vinylidene fluoride). *Macromolecules*, 8, **1975**, 158.

Kang, G.D.; Cao, Y.M. Application and modification of poly (vinylidene fluoride) (PVDF) membranes – A review. *J. Membr. Sci*., 463, **2014**, 145.

Komeiji, Y.; Ishikawa, T.; Mochizuki, Y.; Yamataka, H.; Nakano, T. Fragment molecular orbital method-based molecular dynamics (FMO-MD) as a simulator for chemical reactions in explicit salvation. *J. Comput. Chem.*, 30, **2009,** 40.

Li, N.N.; Fane, A.G.; Ho, W.S.; Matsuura, T. Advanced membrane technology and applications, John Wiley & sons Ltd., Hoboken, **2008,** 101.

Long D.; Nghiem Andrea I. Pharmaceutical retention mechanisms by nanofiltration membranes, Schäfer menachem elimelech, *Environ. Sci. Technol*., 19, **2005**, 7698.

Liu, F. N.; Hashim, A.; Liu, Y.; Moghareh Abed, M. R.; Li, K. Progress in the production and modification of PVDF membranes, *J. Membr. Sci*. 375, **2011**, 1.

Laabs, C.N.; Amy, G.L.; Jekel, M. Understanding the size and character of fouling-causing substances from effluent organic matter (EFOM) in low-pressure membrane filtration. *Environ Sci Technol*. 40, **2006**, 4495.

Lang, W.Z.; Xu, Z.L.; Yang, H.; Tong, W. Preparation and characterization of PVDF–PFSA blend hollow fiber UF membrane, *J. Membr. Sci*., 288, **2007,** 123.

Lewis, A.L.; Hughes, P.D.; Kirkwood, L.C.; Leppard, S.W.; Redman, R.P.; Tolhurst, L.A.; Stratford, P.W. Synthesis and characterisation of Phosphorylcholine-based polymers useful for coating blood filtration devices. *Biomaterials.*, 21, **2000,** 1847.

Montgomery, M.A.; Elimelech, M. Water and sanitation in developing countries: Including health in the equation. *Environ. Sci. Technol*., 41, **2007**, 17.

Misdan, N.; Lau, W.J.; Ismail, A.F. Seawater reverse osmosis (SWRO) desalination by thin-film composite membrane-current development, challenges and future prospects, *Desalination*, 287, **2012**, 228.

Martins, P.; Lopes, A. C.; Lanceros-Mendez, S. Electroactive phases of poly (vinylidene fluoride): Determination, processing and applications, *Prog. Polym. Sci*., 39, **2014**, 683.

Malaeb, L.; Ayoub, G.M. Reverse osmosis technology for water treatment: state of the art review. *Desalination* 267, **2011**, 1.

Morokuma, K. "Molecular orbital studies of hydrogen bonds. III. C=O···H–O hydrogen bond in $H_2CO\cdots H_2O$ and $H_2CO\cdots 2H_2O$", *J Chem Phys*. 5, **1971**, 1236.

Mowery, D.; Clough, R.; Assink , R. Identification of oxidation products in selectively labeled polypropylene with solid-state ^{13}C NMR techniques, *Macromolecules*, 40, **2007**, 3615.

Nghiem, D. L.; Manis, A.; Soldenhoff, K.; Scha¨fer, A. I. Estrogenic hormone removal from wastewater using NF/RO membranes. *J. Membr. Sci*. 242, **2004**, 37.

Nohmi, T.; Yamada, T. Polyvinylidene fluoride type resin hollow filament microfilter and process for producing the same, U.S. Pat. 4, **1983**, 035.

Noble, R.D, Agrawal, R. "Effects of Alkaline Environments at Mild Conditions on the Stability of PVDF Membrane: An Experimental Study". *Ind. Eng. Chem. Res.*, 44, **2005**, 2887.

Ohno, K., Mori, K., Orita, M., Takeuchi, M., Computational insights into binding of bisphosphates to farnesyl pyrophosphate synthase, Curr. *Med. Chem*. 18, **2011**, 220.

Parr, R. G.; Yang, W. "Density-functional theory of atoms and molecules". Oxford University Press, New York, Oxford, **1989**, 333.

Puro, L.; Kallioinen, M.; Mänttäri, M.; Nyström, M. Evaluation of behavior and fouling potential of wood extractives in ultrafiltration of pulp and paper mill process water, *J. Membr. Sci.* 368, **2011**, 150.

Persson, T.; Matusiak, M.; Zacchi, G.; Jönsson, A.S. Extraction of hemicelluloses from process water from the production of Masonite, Desalination. 199, **2006**, 411.

Pierre Kwan H.E. State of the science review of membrane fouling: Organic, inorganic, and biological. Tech. Rep. 06-10 (Phase A). *California Department of Water Resources;* **2013**, 250.

Pendergast, M.M, Hoek, E.M, "A review of water treatment membrane nanotechnologies ". *Energy Environ. Sci*., 4, **2011**, 1946.

Qadir, D., Mukhtar, H., Keong, L. Mixed matrix membranes for water purification applications. *Sep & Purif Rev*. 46, **2017**, 62.

Roy, Y.; Warsinger, D.M.; Lienhard, J.H. Effect of temperature on ion transport in nanofiltration membranes: diffusion, convection and electromigration. *Desalination.* 420, **2017**, 241.

Rabuni, M. F.; Nik, N. M.; Sulaiman, M. K.; Aroua, N.; Hashim, A. Effects of alkaline environments at mild conditions on the stability of PVDF membrane: An experimental study. *Ind. Eng. Chem. Res., 52,* **2013**, 15874.

Rezakazemi, M., Ebadi Amooghin, A., Montazer-Rahmati, M.M., Ismail, A.F., Matsuura, T., "State-of-the-art membrane based CO_2 separation using mixed matrix membranes (MMMs): An overview on current status and future directions*". Prog. Polym. Sci*., 39, **2014**, 817.

Shannon, M.A.; Bohn, P.W.; Elimelech, M.; Georgiadis, J.G.; Marinas, B.J.; Mayes, A.M. Science and technology for water purification in the coming decades. *Nature*, 452, **2008**, 301.

Song, L.; Flux decline in crossflow microfiltration and ultrafiltration: mechanisms and modeling of membrane fouling, *J. Membr. Sci*. 139, **1998**, 183.

Shibutani, T.; Kitaura, T.; Ohmukai, Y.; Maruyama, T.; Nakatsuka, S.; Watabe, T.; Matsuyama, H., Membrane fouling properties of hollow fiber membranes prepared from cellulose acetate derivatives. *J. Membr. Sci*. 376, **2011**, 102.

Shirazi, S.; Lin, C.J.; Sumeet, S.; Rao, A.; Rao, P. Comparison of fouling mechanism by $CaSO_4$ and $CaHPO_4$ on nanofiltration membranes, *Separation Science and Technology*, 41, **2006**, 2861.

Saqib, J.; Aljundi, I.H. Membrane fouling and modification using surface treatment and layer-by-layer assembly of polyelectrolytes: state-of-the-art review. *J. Water Process Eng*. 11, **2016**, 68.

Shao, Q.; He, Y.; White, A. D.; Jiang, S. Y. Difference in hydration between carboxybetaine and sulfobetaine, J. Phys. Chem. B., 114, **2010**, 16625.

Schlenoff, J.B. Zwitterion: coating surfaces with zwitterionic functionality to reduce nonspecific adsorption, Langmuir., 30, **2014**, 9625.

Seoane, B., Coronas, J., Gascon, I., Benavides, M.E., Karvan, O., Caro, J., Kapteijn, F., Gascon, "Metal–organic framework based mixed matrix membranes: a solution for highly efficient CO_2 capture? ". *J., Chem. Soc. Rev*., 44, **2015**, 2421.

Stevens, W. J., Fink, W. H., "Frozen fragment reduced variational space analysis of hydrogen bonding interactions. Application to the water dimer ", *Chem. Phys. Lett*. 139, **1987**, 15.

Su, P., Liu, H., Wu, W., "Free energy decomposition analysis of bonding and nonbonding interactions in solution", *J. Chem. Phys*. 137, **2012**, 034111.

Shen, X.; Gao, Y.; He, Y.; Zhao, Y.; Chen, Li. Preparation and anti-fouling property of carboxybetaine-based zwitterionic PVDF membrane. *Sep. Sci. Technol*., 51, **2016,** 1189.

Shen, M. C.; Martinson, L.; Wagner, M. S.; Castner, D. G.; Ratner, B. D.; Horbett, T. A. PEO-like plasma polymerized tetraglyme surface interactions with leukocytes and proteins: in vitro and in vivo studies. *J. Biomater. Sci., Polym. Ed*., 13, **2002,** 367.

Suenaga, M. Facio: new computational chemistry environment for PC GAMESS. *J. Comput. Chem. Jpn*., 4, **2005,** 25.

Shao, Q.; Jiang, S. Influence of charged groups on the properties of zwitterionic moieties: a molecular simulation study *J. Phys. Chem. B*., 118, **2014,** 7630.

Sin, M.C.; Chen, S.H.; Chang, Y. Hemocompatibility of zwitterionic interfaces and membranes. *Polymer. J*., 46, **2014**, 436.

Schmidt, M. W.; Baldridge, K. K.; Boatz, J. A.; Elbert, S. T.; Gordon, M. S.; Jensen, J. H.; Koseki, S.; Matsunaga, N.; Nguyen, K. A.; Su, S.; Windus, T. L.; Dupuis, M.; Montgomery, J. A. General atomic and molecular electronic structure system. *J. Comput. Chem*., 14, **1993,** 1347.

Ulbricht, M. Advanced functional polymer membranes. Polymer. 47, **2006**, 2217.

Vander Bruggen, B.; Vandecasteele, C. Removal of pollutants from surface water and groundwater by nanofiltration: overview of possible applications in the drinking water industry, *Environ. Pollut*. 122, **2003**, 435.

Vander Bruggen, B.; Schaep, J.; Wilms, D.; Vandecasteele, C. Influence of molecular size, polarity and charge on the retention of organic molecules by nanofiltration, *J. Membr. Sci.* 156, **1999**, 29.

Ventresque, C.; Gisclon, V.; Bablon, G.; Chagneau, G. An outstanding feat of modern technology: The Mery-sur-Oise nanofiltration treatment plant (340,000 m3 /d), *Desalination*. 131, **2000**, 1.

Venault. A.; Liu, Y.H.; Wu, J.R.; Yang, H.S.; Chang, Y.; Lai, J.Y.; Aimar, P. Low-biofouling membranes prepared by liquid-induced phase separation of the PVDF/polystyrene-b-poly (ethylene glycol) methacrylate blend, Journal of Membrane Science 450, **2014**, 340.

Venault, A.; Wei, T.C.; Shih, H.L.; Yeh, C.C.; Chinnathambi, A.; Alharbi, S.A.; Carretier, S.; Aimar, P.; Lai, J.Y.; Chang, Y. Antifouling pseudo-zwitterionic poly (vinylidene fluoride) membranes with efficient mixed-charge surface grafting via glow dielectric barrier discharge plasma-induced copolymerization. *J. Membr. Sci*., 516, **2016**, 13.

Watkins, K. Power, poverty and the global water crisis, Human development report, *United Nations development programme* (UNDP), **2006**.

Weis, A.; Bird, M.R.; Nyström, M.; Wright, C. The influence of morphology, hydrophobicity and charge upon the long-term performance of UF membranes fouled with spent sulphite liquor, *Desalination*. 175, **2005**, 73.

Wu, J.; Lin, W.F.; Wang, Z.; Chen, S.F. Investigation of the hydration of nonfouling material poly (sulfobetaine methacrylate) by low-field nuclear magnetic resonance. Langmuir, 28, **2012**, 7436.

White, A.; Jiang, S. Y. Local and bulk Hydration of zwitterionic glycine and its analogues through molecular simulations. *J. Phys. Chem. B*, 115, **2006,** 660.

Yu, S.; Liu, M.; Ma, M.; Qi,M.; Gao, C. Impacts of membrane properties on reactive dye removal from dye/salt mixtures by asymmetric cellulose acetate and composite polyamide nanofiltration membranes, *J. Membr. Sci*. 350, **2010**, 83.

Zhu, J.; Tian, M.; Hou, J.; Wang, J.; Lin, J.; Zhang, Y.; Liu, J.; Van der Bruggen, B. Surface zwitterionic functionalized graphene oxide for a novel loose nanofiltration membrane, *J. Mater. Chem. A*, 4, **2016**, 1980.

Zhang, Z.; Chao, T.; Chen, S. F.; Jiang, S. Y. Super low fouling sulfobetaine and carboxybetaine polymers on glass slides. *Langmuir*. 22, **2006**, 10072.

Zhao, Y.H.; Wee, K.H.; Bai, R. Highly hydrophilic and low-protein-fouling polypropylene membrane prepared by surface modification with sulfobetaine-based zwitterionic polymer through a combined surface polymerization method. J. Membr. Sci.362, **2010**, 326.

Zularisam, A.W, Ismail, A.F, Salim, M.R, "Separations research needs for the 21st century". *Ind. Eng. Chem. Res*, 44, **2005**, 2887.

Zhu, Yu.; Zhang, F.; Wang, D.; Pei, X. F.; Zhang, W.; Jin, J. A novel zwitterionic polyelectrolyte grafted PVDF membrane for thoroughly separating oil from water w, "The role of fluorine atoms in a fluorinated prostaglandin agonist, *ChemMedChem*, 5, **2010**, 1254.ith ultrahigh efficiency. *J. Mater. Chem. A*., 1, **2013,** 5758.

Zhang, Z.; Chen, S. F.; Chang, Y.; Jiang, S. Y. Surface grafted sulfobetaine polymers via atom transfer radical polymerization as super low fouling coatings. J. Phys. Chem. B., 110, **2006,** 10799.

Zhan, C.G.; Nichols, J.A.; Dixon, D.A. Ionization potential, electron affinity, electronegativity, hardness, and electron excitation energy: Molecular properties from density functional theory orbital energies. *J. Phys. Chem. A.,* 107, **2003**, 4184.

Zhang, Z.; Chao, T.; Chen, S.; Jiang, S. Super low fouling sulfobetaine and carboxybetaine polymers on glass slides. Langmuir., 22, **2006,** 10072.

Zheng, J.; Li, L. Y.; Tsao, H. K.; Sheng, Y. J.; Chen, S. F.; Jiang, S. Y. Strong repulsive forces between protein and oligo (Ethylene Glycol) self-assembled monolayers: a molecular simulation study. *Biophys. J*., 89, **2005,** 158.

APENDIX

ELSEVIER LICENSE
TERMS AND CONDITIONS

Aug 09, 2019

This Agreement between University of Saskatchewan -- Mahboobeh Maghami ("You") and Elsevier ("Elsevier") consists of your license details and the terms and conditions provided by Elsevier and Copyright Clearance Center.

License Number	4644531244314
License date	Aug 08, 2019
Licensed Content Publisher	Elsevier
Licensed Content Publication	Journal of Membrane Science
Licensed Content Title	Flux decline in crossflow microfiltration and ultrafiltration: mechanisms and modeling of membrane fouling
Licensed Content Author	Lianfa Song
Licensed Content Date	Feb 18, 1998
Licensed Content Volume	139
Licensed Content Issue	2
Licensed Content Pages	18
Start Page	183
End Page	200
Type of Use	reuse in a thesis/dissertation
Intended publisher of new work	other
Portion	figures/tables/illustrations
Number of figures/tables/illustrations	1
Format	electronic
Are you the author of this Elsevier article?	No
Will you be translating?	No
Original figure numbers	fig.1
Title of your thesis/dissertation	Novel Zwitterionic Copolymers to Enhance Hydrophilicity of PVDF Membranes: A Comprehensive Computational Study
Expected completion date	Aug 2019
Estimated size (number of pages)	113
Requestor Location	University of Saskatchewan 101 Cumberland south avenue 1008 unit, 101 building, Assiniboine saskatoon, SK s7n 1l5 Canada Attn: University of Saskatchewan
Publisher Tax ID	GB 494 6272 12
Total	0.00 CAD

ELSEVIER LICENSE
TERMS AND CONDITIONS

Aug 09, 2019

This Agreement between University of Saskatchewan -- Mahboobeh Maghami ("You") and Elsevier ("Elsevier") consists of your license details and the terms and conditions provided by Elsevier and Copyright Clearance Center.

License Number	4644530891352
License date	Aug 08, 2019
Licensed Content Publisher	Elsevier
Licensed Content Publication	Journal of Membrane Science
Licensed Content Title	Antifouling pseudo-zwitterionic poly(vinylidene fluoride) membranes with efficient mixed-charge surface grafting via glow dielectric barrier discharge plasma-induced copolymerization
Licensed Content Author	Antoine Venault,Ta-Chin Wei,Hsiao-Lin Shih,Chin-Cheng Yeh,Arunachalam Chinnathambi,Sulaiman Ali Alharbi,Séverine Carretier,Pierre Aimar,Juin-Yih Lai,Yung Chang
Licensed Content Date	Oct 15, 2016
Licensed Content Volume	516
Licensed Content Issue	n/a
Licensed Content Pages	13
Start Page	13
End Page	25
Type of Use	reuse in a thesis/dissertation
Portion	figures/tables/illustrations
Number of figures/tables/illustrations	1
Format	electronic
Are you the author of this Elsevier article?	No
Will you be translating?	No
Original figure numbers	Fig.1
Title of your thesis/dissertation	Novel Zwitterionic Copolymers to Enhance Hydrophilicity of PVDF Membranes: A Comprehensive Computational Study
Expected completion date	Aug 2019
Estimated size (number of pages)	113
Requestor Location	University of Saskatchewan 101 Cumberland south avenue 1008 unit, 101 building, Assiniboine saskatoon, SK s7n 1l5 Canada Attn: University of Saskatchewan
Publisher Tax ID	GB 494 6272 12

RightsLink®

Home | Account Info | Help | LIVE CHAT

Title: Investigation of the Hydration of Nonfouling Material Poly(sulfobetaine methacrylate) by Low-Field Nuclear Magnetic Resonance

Author: Jiang Wu, Weifeng Lin, Zhen Wang, et al

Publication: Langmuir

Publisher: American Chemical Society

Date: May 1, 2012

Logged in as:
Mahboobeh Maghami
University of Saskatchewan
LOGOUT

PERMISSION/LICENSE IS GRANTED FOR YOUR ORDER AT NO CHARGE

This type of permission/license, instead of the standard Terms & Conditions, is sent to you because no fee is being charged for your order. Please note the following:

- Permission is granted for your request in both print and electronic formats, and translations.
- If figures and/or tables were requested, they may be adapted or used in part.
- Please print this page for your records and send a copy of it to your publisher/graduate school.
- Appropriate credit for the requested material should be given as follows: "Reprinted (adapted) with permission from (COMPLETE REFERENCE CITATION). Copyright (YEAR) American Chemical Society." Insert appropriate information in place of the capitalized words.
- One-time permission is granted only for the use specified in your request. No additional uses are granted (such as derivative works or other editions). For any other uses, please submit a new request.

If credit is given to another source for the material you requested, permission must be obtained from that source.

BACK | CLOSE WINDOW